THERMO-MECHANICAL BEHAVIOR OF METAL FOAMS IN THERMAL APPLICATIONS: A COMPUTATIONAL AND EXPERIMENTAL APPROACH

BY

SHAHZADA PAMIR ALY

A Thesis Presented to the

DEANSHIP OF GRADUATE STUDIES

KING FAHD UNIVERSITY OF PETROLEUM & MINERALS

DHAHRAN, SAUDI ARABIA

In Partial Fulfillment of the

Requirements for the Degree of

MASTER OF SCIENCE

In

MECHANICAL ENGINEERING

May 2015

KING FAHD UNIVERSITY OF PETROLEUM & MINERALS

DHAHRAN- 31261, SAUDI ARABIA

DEANSHIP OF GRADUATE STUDIES

This thesis, written by **SHAHZADA PAMIR ALY** under the direction of his thesis advisor and approved by his thesis committee, has been presented and accepted by the Dean of Graduate Studies, in partial fulfillment of the requirements for the degree of **MASTER OF SCIENCE IN MECHANICAL ENGINEERING.**

Dr. Khaled Saleh Al-Athel

(Advisor)

Dr. Zuhair M. Asad Gasem

Department Chairman

Dr. Abul Fazal M. Arif

(Member)

Dr. Salam A. Zummo

Dean of Graduate Studies

Dr. Sulaiman Pashah

(Member)

1/6/15

Date

Dedicated to my mother, my father, my siblings and my teachers

ACKNOWLEDGMENTS

First of all I thank Allah, the Almighty and salutations be upon our beloved Prophet (P.B.U.H). It would have never been possible for me to write this acknowledgement today, if it weren't for ALLAH who gave me a chance to work at such a renowned institute.

I feel blessed and am very grateful to my parents, who had always been a source of comfort with their continuous appraisal and unwavering encouragement throughout my life.

King Fahd University of Petroleum and Minerals (K.F.U.P.M) is highly acknowledged for giving me an opportunity to carry out my graduate studies and providing me with an outstanding research environment.

I am much obliged to my advisor and my mentor Dr. Khaled Saleh Al-Athel for his unrelenting support. I highly regard him for his patience with me and for coping up with my shortcomings. My sincere thanks are to Prof. Abul Fazal M. Arif who kept me going persistently. I also highly appreciate Dr. Sulaiman Pashah for giving me useful tidbits regarding my thesis.

In the end I would also deeply like acknowledge Dr. Abbas Hakeem from CENT for allowing unhindered access to his lab, a seasoned lecturer Mr. Inam who shared his technical skills for the experimentation and the undergraduate student Khaled Hamed Al-Hamed for his unrelenting help with CT scanning.

TABLE OF CONTENTS

LIST OF TABLES

LIST OF FIGURES

LIST OF ABBREVIATIONS

DAQ	:	Data Acquisition
PPI	:	Pore per Inch
PPC	:	Pores per Centimeter
FE	:	Finite Element
CAD	:	Computer Aided Design
3D	:	Three-dimensional
h	:	Heat transfer coefficient
CFD	:	Computational Fluid Dynamics

ABSTRACT (ENGLISH)

Full Name : Shahzada Pamir Aly

Thesis Title : Thermo-Mechanical Behavior Of Metal Foams in Thermal Applications : A Computational And Experimental Approach

Major Field : Mechanical Engineering

Date of Degree : May 2015

Metal foams are porous materials that have a very high percentage of void spaces at the macroscopic level. Depending on the manufacturing technique, they are either produced as open or closed cells. Metallic foams have taken over significant amount of applications due to their improved thermal and mechanical properties. In this study, both experimental and computational work has been undertaken to better understand the thermo-mechanical behavior of metal foams in thermal applications with a focus on heat sinks.

In the experimental work, study was undertaken on aluminum metal foams of 93% porosity, while pore density was of 4 PPC (10 PPI) and 8 PPC (20 PPI), where PPC (PPI) stands for pores per cm (pores per inch). The whole experimental setup and the samples were fabricated in-house. The forced convection results show that heat sinks with thermal spray coating outperformed the thermally glued and solid heat sink samples. Air flow speed variations reveal that heat transfer rate changes almost linearly with increase/decrease of air speed. Further study with multiple fin samples states that 45º is the best orientation between heat sink and the air flow for maximum heat dissipation, while it is 90º for the single fin. This is due to better interaction between fluid and the heat sinks matrix at these respective orientations.

As metal foams' have complex geometry, so for numerical analysis as an easy alternative, researchers usually prefer simplified computational models based on various assumptions. An innovative approach has been undertaken to capture the three-dimensional (3D) detailed geometry of open-cell metal foam sample and make a finite element model out of this. Computed tomography (CT) has been utilized to extract extreme precise 3D surface model and Computer Aided Design (CAD) software have been employed to "clean" the surface model for finite element (FE) analysis. The viability of this model has been demonstrated here as its use in heat sinks and is calibrated against experimental results. The accuracy of the acquired model has been validated with a comparative study with experimental findings. The validated and calibrated model is then used for assessing different scenarios via simulations.

ABSTRACT (ARABIC)

ملخص الرسال

الاسم الكامل :شاهزاده بامير علي

عنوان الرسالة :دراسة تجريبية وتحسيبية للخصائص الميكانيكية والحرارية للرغوة المعدنية

التخصص :الهندسة الميكانيكية

تاريخ الدرجة العلمية :مايو 2015

يمكن تعريف الرغوة المعدنية علي أنها كتلة من معدن تحتوي علي نسبة عالية من الفراغات علي المستوي القياس الدقيق، بحسب طريقة التصنيع يتم إنتاج نوعين، الخلايا المفتوحة والخلايا المغلقة. يتم إستخدام الرغوة المعدنية بكثرة في كثير من التطبيقات نسبة لخصايصها الميكانيكية والحرارية الجيدة. في هذا البحث أجريت دراسة تجريبية وتحسيبية بغرض فهم السلوك الحراري والميكانيكي للرغوة المعدنية في التطبيقات الحرارية مع التركيز علي الزعانف الحرارية.

أجريت الدراسة التجريبية علي رغوة معدنية من الالمونيوم بنسبة فراغية تصل الي 93 % ، و أجريت التجارب علي نسبتين مختلفتين من الكثافة الفراغية التي تقاس بعدد الفراغات في وحدة الطول، النسبة الاولي 4 فراغات في السنتميتر الواحد (10 في البوصة الواحدة)، والنسبة الثانية 8 فراغات في السنتميتر الواحد (20 في البوصة الواحدة). تمت صناعة العينات بغرض التجارب في معامل جامعة الملك فهد. أوضحت نتائج إنتقال الحرارة للهواء أن العينات المغطية بإستخدام الترذيذ الحراري تؤدي بطريقة أفضل من عينات التفريغ الحراري الصلبة و الملصقة حراريا. تغيير سرعة سريان الهواء أوضح أن معدل إنتقال الحرارة يتغير بعلاقة خطية مع زيادة أو نقصان سرعة الهواء. دراسة أخرى أجريت علي عينة تحتوي علي مجموعة من الزعانف أثبتت أن الزاوية 45 درجة هي أفضل توجية بين الزعانف الحرارية وإتجاه سريان الهواء وتعطي أفضل تفريغ حراري، بينما كانت الزاية 90 في

حالة العينة التي تحتوي علي زعنفة واحدة. نتجت هذة الأفضلية بسبب وجود نسبة أحتكاك كبيرة بين الهواء والرغوة المعدنية في هذة الزوايا.

بما أن الرغوة المعدنية لها شكل معقد جدا لذلك التحليل العددي يمثل طريقة جيدة لدراستها، عادة يفضل الباحثون إستخدام نماذج تحسبية مبسطة تعتمد علي مجموعة من الإفتراضات. تم إستخدام طريقة مبتكرة تسهل عملية إنتاج الشكل ثلاثي الأبعاد للعينة من أجل إستخدامه في التحليل بطريقة العناصر المنتهية لتحليل عينة رغوة معدنية من نوع الخلية المفتوحة. تم إستخدام طريقة الرسم السطحي المحسوب لإستخراج رسم سطحي ثلاثي الأبعاد عالي الدقة ثم بأستخدام برنامج تصميم بمساعدة الحاسوب تمت عملية تنقيح الرسم ليصبح جاهزا للإستخدام في التحليل العددي بطريقة العناصر المنهية. تم توضيح أهمية النموذج التحليلي المنتج من خلال أمكانية إستخدامه في تحليل وتصميم المفرغات الحرارية. وتم تأكيد النتائج من خلال التجارب العملية. دقة النموذج التحليلي أكدت بالمقارنة مع نتائج التجارب. في الأخير تم إستخدام النموذج التحليلي في تقييم وتحليل حالات مختلفة عن طريق المحاكاة.

CHAPTER 1

INTRODUCTION

The terminology “porous media” is used to describe any material that has void spaces (or pores) in a solid matrix (or frame). The skeletal part is normally a solid, while pores typically accommodate fluid (liquid or gas). Their naturally occurring examples like rocks, soils, petroleum reservoirs, human lungs, biological tissues, wood etc. have irregular distribution of pore size and shape. Conversely, there are man-made porous materials that can have a regular or irregular structure depending on the type of manufacturing process used for their production. These man-made materials are generally known as metal foams (also called metal sponges).

1.1 Metal Foams

Metal foams are cellular structures that have solid base material, with prominent portion of gas filled pores. The base material can be made up of metals (aluminum, copper, nickel, alloys etc.), polymers, or carbon. Their most prominent feature is their high porosity (void spaces), typically in range of 75- 95%, making them ultra-light materials. Porosity of porous materials is given by following relation [1]:

$$\phi(\%_{age}) = \left\lfloor \frac{V_p}{V_p + V_s} \times 100 \right\rfloor \% \qquad (1.1)$$

Where, V_p and V_s are volume of pores and solid. Experimentally it is found by [1]:

$$\phi(\%_{age}) = \left[1 - \frac{\rho}{\rho_s} \times 100\right]\% \qquad (1.2)$$

Where, ρ and ρ_s are effective and solid densities respectively.

These foams have two broader categories and are classified in accordance with their pore architecture:

1. Closed Cell (pores are sealed).
2. Open Cell (pores form an interconnected network).
    a) Stochastic (irregular pores distribution).
    b) Honeycomb (regular pores distribution).

Figure 1 and Figure 2 show pictures of an open cell and close cell foams respectively [2].

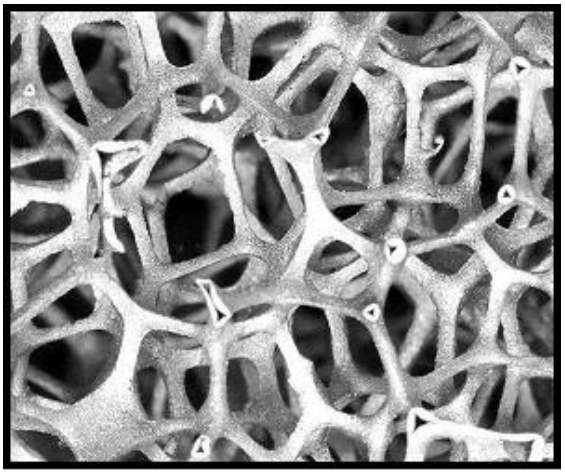

Figure 1 Open Cell Metal Foam

Figure 2 Closed Cell Metal Foam

Two parameters are generally used to describe metal foams: 1) Porosity – expressed in percentage (%) and 2) Pore density - expressed in PPI (pores per inch) or PPC (pores per

cm). Foams generally retain most of the physical properties of their base metal. The characteristics of all metal foams are summed up by their proportional density "ρ /ρ_s".Where ρ and ρ_s denote foam and solid density, respectively; i.e. 10% dense foam will have double the strength as compared to 5% dense foam – this is known as the power law relation. Foams made from non-flammable materials will persist to be non-flammable. Coefficient of expansion remains same while thermal conductivity is reduced. Their most unique mechanical characteristics include high strength to the low weight ratio and a complete isotropic load response (for stochastic type) [3], whereas, on the contrary, honeycomb metals foam have an anisotropic behavior [4]. They are also recyclable and nontoxic due to the type of base metal.

Table 1 [1] shows how physical properties are affected in closed and open cell metal foams when compared to their solid base metal. It can be seen from the table that some properties are retained to that of solid metal while other vary following a generalized relationship. Also unlike most solids, the compressive and tensile strength of metal foams are not same.

Table 1 Thermo-mechanical properties of metal foam [1]

Thermo-Mechanical Properties	Open Cells	Closed Cells
Melting Point (K)	Similar to solid	Similar to solid
Specific Heat (J/Kg.K)	Similar to solid	Similar to solid
Thermal Expansion (10e-6/K)	Similar to solid	Similar to solid
Latent Heat (kJ/Kg)	Similar to solid	Similar to solid
Young's Modulus (G.Pa), E	$E= (0.2\text{-}4)E_s(\frac{\rho}{\rho_s})2.2$	$E= (0.2\text{-}1)E_s * [0.4(\frac{\rho}{\rho_s})2.2+0.3(\frac{\rho}{\rho_s})]$
Compressive Strength (M.Pa), σ_c	$\sigma_c= (0.2\text{-}1)\ \sigma_{c,s}(\frac{\rho}{\rho_s})1.49$	$\sigma_c= (0.2\text{-}1) * \sigma_{c,s}[0.4(\frac{\rho}{\rho_s})0.6+0.3(\frac{\rho}{\rho_s})]$
Tensile Strength (M.Pa), σ_t	$\sigma_t= (1.1—1.4)\ \sigma_c$	$\sigma_t= (1.1—1.4)\ \sigma_c$
Thermal Conductivity (W/m.K)	$(\frac{\rho}{\rho_s})1.79 < \frac{\lambda}{\lambda_s} < (\frac{\rho}{\rho_s})1.66$	$(\frac{\rho}{\rho_s})1.79 < \frac{\lambda}{\lambda_s} < (\frac{\rho}{\rho_s})1.66$

1.2 Manufacturing and Applications

Almost any material can be foamed [1], and because of that, metal foams have a lot of research going on due to their versatile applications and importance. They are attractive for a variety of engineering applications because their thermal and mechanical properties can be controlled by choosing specific manufacturing processes. These properties are produced by controlling mainly three factors: base metal, foaming process and heat treatment conditions [5]. Thus, there are wide variety of metal foams available in market, based on their production techniques [2,6,7].

Closed cell metal foams are mainly used in applications like noise reduction, energy absorption, light and stiff sandwich beams, prosthetics (replacing broken bones), and as impact absorbing agents (e.g. bicycle helmets), etc. On the other hand, open cell foams are used in medical science for joining fractured bones, in chemical industry as catalytic agent, flame arrestors, and with extremely small pores as temperature filters. But the unique features of open cell metal foams, such as their relative low-cost, good permeability, excessive-lower densities, higher surface area to volume fraction, and their astonishing ability to readily mix the flowing fluid, makes them a splendid candidate for thermo-fluid applications such as compact heat exchangers, fuel cells and efficient heat dissipaters in electronic cooling [8-9]. Transport phenomenon of a porous media has been of a great interest to industrial and academic research. For the very same reason, thermal behavior of open cell metal foams has been one of our key focuses in this research.

1.3 Motivation of Proposed Study

The literature review shows that most of the work done so far in metal foams field is experimental and analytical. However, their highly random geometry has only enabled scientists to only approximate their behavior [3,5,10-11]. In most cases, exact solutions do not exist for metal foams, whether it is numerical or analytical. Thus, an objective of this research is to determine the thermo-mechanical behavior that is very close to the exact behavior. Little attention has been paid to the numerical side, so there is a dire need of a working 3D model of metal foams. Most of the models used in the literature are 2D models. And the majority of the 3D models are that of closed cell metal foams. The

reason for this is that they are easy to model. Those that are open cell are usually created using CAD (computer aided design) software. They work on the concept of unit cell approach, like kelvin cell and Weaire–Phelan structure [12–14]. A single unit cell representing a single pore of metal foam is created manually and then multiplied in all principle axes to get a 3D model as an end result. In short, these models are unable to give an accurate prediction about metal foam properties and the overall behavior. Also the literature shows that as the irregularity in the structure of metal foam increases, its isotropic properties also increases [3,15]. This means stochastic type (irregular structure) open cell metal foams are better than honeycomb (regular structure) open cell metals when it comes to isotropic behavior of physical properties. Due to the aforementioned reasons, stochastic type open cell metal foam was chosen for our study.

People in the field of medicine have been using image processing techniques like CT scanning to capture the delicate and complex geometry of human body parts and creating 3D models out of these image bundles. These models are then used for FE analysis to predict the failure of these organs under varying conditions. Similar footsteps were followed to try and capture the highly complex shape of metal foams. The motive was to capture at least twice the PPC unit length (1 cm) of the metal foam, both horizontally and vertically, so studies could be carried out to examine the bulk behavior and not just localized area. The final model acquired can be modified in a number of ways to change the PPC and other parameters of very same model. Thus, there is no need of taking the scan for metal foams with different PPC. This has been explained in detail in the latter chapters. This working model can be used to validate and study the analytical and experimental work that has been done in the literature already.

In the era we live in, every now and then there are ground breaking revolutions in field of electronics. This newer technology demands for more efficient and compact microelectronics. But the newer efficient systems come at the expense of additional heat generated in the circuitry. The more the power, the more it is lethal for the system. This invokes for effective and efficient heat sinks that readily dissipate this heat generated out of the system. Thermal management therefore must be the foremost aim of an electronics design. Life expectancy and the performance of electronic equipment are inversely related to temperature of components in the equipment. New materials and effectual heat sink designs are a focus of study in research sector in order to keep a tight leash on heat generation issues. Metal foams, due to their good heat dissipative properties, promise such a service. Experimental analyses need to be carried out to find out the efficiency and effectiveness of metal foam heat sinks as compared to their conventional counterparts. Along with this, the heat sink design needs to be optimized, both for natural and forced convection scenarios. Furthermore, to reduce the thermal contact resistance between metal foam fins and the base, thermal spray coatings have been applied through a collaboration with the Centre for Advanced Coatings Technologies (CACT) at the University of Toronto [16].

1.4 Objectives of the Proposed Study

1. To develop a real 3D model of metal foams using image processing techniques. Among the Image processing techniques we plan on using CT scan for our purposes. The raw model from CT scan will be cleaned with commercially available software, so it can be imported to any finite element package where it will be used to simulate different metal foam heat sink cases.
2. To check the validity of the model using available experimental data and previously published work. Because the validity of the model is necessary to ensure that this very same model can be used in different scenarios with high accuracy.
3. Use the model to:
    a) Examine metal foam heat sinks under varying environmental and operating conditions.
    b) Study the use of metal foam on the efficiency and effectiveness of heat sinks.
    c) Validate the numerical results with experimental results.
    d) Find the accurate convective heat transfer coefficient.
4. To perform a comprehensive experimental analysis to examine the performance and behavior of metal foam heat sinks for different geometrical parameters and environmental conditions. Geometrical parameters as in changing the orientation of heat sinks with respect to air flow, modifying type of heat sink (solid or metal foam) and changing the number of fins for different cases. While the environmental conditions like varying the power input and altering air flow speeds.
5. Optimize the heat sinks through study of experimental and numerical results.

CHAPTER 2

METAL FOAMS

Metal foams have been investigated a lot by researchers, both experimentally and numerically. The following sections discuss the techniques that are usually undertaken for both of these approaches.

2.1 Experimental

Modern day electronics are opting out for an ever increasing trend of compact components and higher computational power, hence generating an excessive amount of waste heat in the circuitry. In near future, heat flux in integrated circuits (ICs) is predicted to surpass 1000 W/cm^2 [17]. This unavoidable excessive heat needs to be dissipated quickly and efficiently to ensure not only an optimum performance of the system, but its safety as well. Conventional heat sinks are unfortunately not meeting the demands of this rapid progression in instrumentation technology. Thus a lot of dedicated research is being extensively carried out to find other approaches of heat sinking. Most important features of a heat sink influencing its performance are: 1) material, 2) geometry and 3) thermal resistance between the heated surface and heat sink [18].

Heat sinks are sort of heat exchangers used for cooling electronics because of their low cost, simple installation and reliable manufacturing process. Conventional heat sinks are further divided into plate and fin types. Several studies have been published focusing on

the effects of fin types, dimensions and their arrangement [19]. Apart from heat sink shapes, fluid (air or water) flow is another important factor that significantly affects the performance. But in comparison, a little attention has been paid to the effect of flow direction and flow behavior through the heat sinks, which are necessary for efficient cooling of the system. Fluid flow through heat sinks could be bypass or non-bypass. Bypass being where flow is over the heat sink's top only and non-bypass being through the channels of heat sink fins. Though non-bypass is better, it is avoided where pressure drop is critical and also due to space constraints [20].

Metal foams have also been used as extended external surfaces to elevate the heat transfer rate from these surfaces. The two main advantages of using metal foams as effective heat dissipaters are their greater surface area for heat dissipation and the fluid flow inside the pores becomes turbulent in nature, which further causes an uplift of heat transfer coefficient. Air cooled aluminum alloys are most common heat sinks and are simple in general use. With respect to various heat sink fin types, Kang et al. [21] reported that aluminum metal foam fins offered the greatest heat dissipation performance due to enhanced surface area, lesser pressure drop, and complex flow paths that encourage turbulent flow mix up. Forced convection in porous medium has been under study since last century [22]. Since the last two decades study on heat transfer characteristics of metals foams has spurred.

Experimental investigation was carried out by Leong and Jin [23] for forced convection via aluminum metal foam heat sinks. An extensive experimental data for pressure drop and fluid velocity versus Reynolds number was collected. They discovered that the heat transfer rate is improved with increased pore density (PPI), and metal foams with low

pore density require small pumping power to enhance heat transfer. Mancin et al. [24–26] experimented on different samples of aluminum foam for studying heat transfer and pressure loss inside the channel. They highlighted the effect of pore density, porosity and sample height on thermal response of foam. Alongside, semi-empirical models were developed for measuring overall heat transfer and pressure loss. Chiu et al. [27] analyzed the pressure drop of air flow inside aluminum metal foam samples of different porosities and pore densities (PPI). They derived a theoretical correlation which agreed well with their experimental results. They also found that the friction factor of metal foams is low as compared to that of granular porous media. Hseih et al. [28] studied the effect of porosity (void spaces), pore distribution and fluid speed on heat transfer phenomenon in aluminum foams. They concluded that each of the studied parameter had a prominent consequence on heat transfer, and also the Nusselt number was elevated in higher porosity and pore density foams. Through experimentation Dogan et al. [29] found the convective heat transfer of aluminum foam blocks inside a rectangular duct. They discussed the consequences of pore density (PPI) and the foams' aspect ratio, and deduced that the Nusselt number increases as pore density (PPI) and aspect ratio of the block samples increases.

Aluminum foams are not the only foams that are studied for their heat transfer characteristics. Giani et al. [30] performed transient state cooling measurements on iron alloy and copper foams of various pore densities (10-20 PPI). Heat transfer study was carried out for eight different air velocities and respective heat transfer coefficient was determined. Dukhan [31] studied the amount of air pressure drop in different samples of compressed and uncompressed metallic foams, comprising of a variety of porosities and

pore densities (PPI). The pressure drop was found to be proportional to air speed following Forchheimer equation [32] in a quadratic sense and was more in compressed samples. Stefano et al. [33] designed a new experimental setup to study thermal and fluid characteristics of open cell foams. Samples of 5, 10 and 20 PPI were investigated for heat transfer rate and pressure drop under forced humid air flow. The best thermal performance was achieved by 10 PPI (approx. 4 PPC) samples. In experiments by Xu et al. [34] it was shown that rather than porosity, pore density (PPI) more prominently effected the convective heat transfer.

Air is not the only medium that is used for heat dissipation by convective heat transfer. Zhang et al. [35] performed different experiments for finding heat transfer rates of liquid cooled metal foam heat sinks. Different copper metal foam heat sinks were used that were glued to copper heating base. Among 60 PPI samples, the one with least porosity gave the smallest value of thermal resistance with largest pressure drop. Samples of 100 PPI on the contrary had comparatively lowered thermal resistances for same flow conditions, but significantly larger pressure drop than 60 PPI samples. Mahajan et al. [36] examined forced convection in air medium on aluminum metal foam samples ranging from 5-40 PPI and porosity above 87%. The Nusselt number they calculated was Reynolds number of pores. They also obtained volume averaging equations for velocity profiles and heat transfer coefficients. There was a sound agreement between their experimental and numerical findings. The outcomes showed that thermal dispersion is less in air media as compared to that of water media. Odabaee et al. [37] experimental tests showed that air-cooled fuel-cells utilizing metal foams demanded almost half the electric pump power to that of water-cooled fuel-cells. Although dissipating the

equivalent amount of heat at similar test conditions. Zhao et al. [38] inspected the water and air convective heat transfer of highly porous open cell metallic foam tube heat exchangers. They determined that the heat capacity is enhanced with either increasing pore density (PPI) and/or decreasing the porosity. They also anticipated the optimum foam area to volume ratio of aluminum foam inside counter flow heat exchangers.

Chumpia and Hooman [39] estimated the performance of single pipe metallic foam heat exchangers, where aluminum foam were wrapped to the outer surfaces of pipes exposed to cross flowing air. The foam-covered pipes performed significantly better than fin-covered pipes for identical operating conditions. Kim et al. [40] carried out various experiments to study the convective heat transfer and flow characteristics of aluminum foam heat sinks of different pore densities. They determined that the conventional parallel plate heat sinks gave less than 78% thermal performance compared to that of aluminum foam heat sinks of the similar dimensions. Yang et al. [41] undertook a study to see the possible use of aluminum foams in heat sinks for cooling LED lights. Six different types and arrangements of heat sinks were made to test on a LED light bank. Thermal resistance of solid heat sink was dominating the rest of samples. Carbon foam with solid base, simple carbon foams and simple metal foam heat sink came next in number. A further improvement was reduced weight of heat dissipating system of LEDs.

Byon [42] did an experimental study to investigate thermal performance of aluminum metal foams when exposed to an impinging air jet, under fix air flow. The foam heat sinks showed improved heat transfer rate than pin fin heat sinks under same test conditions, for lower Reynolds number. The trend is opposite for higher Reynolds number. Also the shape of cross sectional jet impingement has trivial effect on Nusselt

number. Although jet impingement has better heat transfer rate but it requires pumping that adds to the cost of system [43]. Where pumping is defined as the product of mass flow rate and pressure drop.

Christopher et al. [44] did a numerical study to determine the impact of contact resistance on aluminum metal foam heat sinks performance. They found that as contact resistance is increased the heat transfer gradually becomes asymptote and ceases to increase further due to conduction being completely stopped.

Experimental literature review pertaining to air-flow heat transfer in metal foams in general utilized various metal foam sample sizes, which makes these findings specific to the samples experimented with. Also Zhao [45] did a review article that presented that adequate experimental heat transfer data collection is deficient for open cell metallic foams in particular. Studies of water-flow heat transfer are comparatively much less. Water-flow though provides more heat transfer rate due to its higher thermal conductivity than air, but unfortunately cannot be used for electronic equipment.

A lot of researchers have been undertaking studies on the forced convective heat transfer in metal foams by experimental, numerical and analytical method. Subsequently both heat transfer characteristics and air flow phenomena in foams is adversely related to structural features of the metal foam, like: porosity, PPI (pores density), foam dimensions and type of material too. Operating conditions such as: heat flux, fluid velocity, surrounding pressure and temperature also play another important factor for determining these aforementioned characteristics.

2.2 Computational Modeling

Since the structure of metal foams is very haphazard and intricate, a lot of research has been carried out to idealize the metal foam structure to inquire about the fluid heat transfer and other physical characteristics. Renowned philosophers like Archimedes and Plato, were the first ones in known history who gave the proposition that many structures in nature could be represented by building blocks or unit cells. Although naturally occurring foams (porous materials) and most artificially synthesized foams (metal foams) are not exactly following a regular pattern, many researchers have shown that most foams somewhat follow a repeated geometry matrix [46–49].

More than a century ago Lord Kelvin's gave hypothesis known as "The Kelvin problem", which proposed a three dimensional unit cell theory that described an ideal geometry of foams in general [46]. Kelvin speculated that a tetrakaidecahedron consisting of six squares and eight hexagonal sides satisfies the foam model, with organization of cells of equivalent volume but different surface area. The Kelvin unit cell also imitates the body centered cubic (BCC) which allows it so simultaneously satisfy Plateau's rule for foams [47]. While being adopted as an ideal unit cell by mathematicians, physicist and scientists for more than a century, it has not been able to found in nature – making it only a hypothesis [48]. In 1994 after more than a hundred years of Kelvin's unit cell being unchallenged, D. Weaire and R. Phelan proposed their own unit cell to counter his theory [50]. Unlike Kelvin's monohedral unit cell, this new unit cell consisted of multiple polyhedral of equivalent volumes. This Weaire-Phelan (WP) unit cell was derived from tetrahedral closed packing (TCP), that is found in many naturally occurring chemicals.

Currently no foam model is superior to Weaire-Phelan unit cell. But as discussed earlier Kelvin unit cell has only one pore and Weaire-Phelan unit cell has eight pores per polyhedral. Thus due to simplicity of Kelvin model many researchers still prefer it over Weaire-Phelan model [12–14,51]. Figure 3 and Figure 4 show the difference between geometry of Kelvin's model and Weaire-Phelan (WP) model respectively.

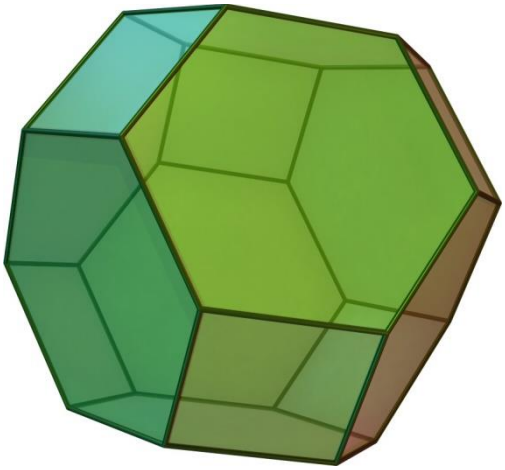

Figure 3 Kelvin Unit Cell [46]

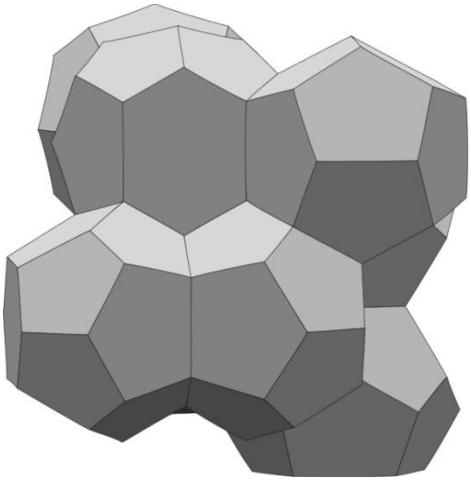

Figure 4 Weaire-Phelan Unit Cell [50]

In order to decipher the true behavior, a clearer understanding of the structure is required. This high level of randomness in the pore size and distribution hinders the researchers to perform analysis of foam bulk properties and behavior in various applications. The structure complexity therefore compels researchers to idealize the structure of metal foam. This significantly jeopardizes the true accuracy in their findings. Some researchers thus used an approach of representing a unit pore of metal foam by subtracting four spheres from all the corners a simple single tetrahedral structure (Figure 5.a) [52].

Playing with the size of spheres the shape, size and dispersion of pores can be altered in the metal foam structure. Others extended this concept by using the same approach of subtraction from a simple cuboid to form a unit cell that represents a single pore of a metal foam (Figure 5.b) [53]. Some still prefer to use Kelvin's tetrakaidecahedron unit cell along with matrix technique of spatial frames as an alternate to a real geometry, because of its acceptance as close to an ideal unit cell of a foam (Figure 5.c) [54]. Researchers have also found the use of body centered cubic (BCC) structures as a good means of idealizing open cell honeycomb metal foam. This is done by extracting nine equivalent balls from a cube (Figure 5.d). They also extended their approach by using vertical and horizontal elliptic egg shaped balls (Figure 5.e) [55].

Most porous solids are random in nature, while all related theoretical models for them assume their periodic structure. This repeating unit cell concept has led many to develop simple analytical relationships between various physical properties. Because if geometry can be defined mathematically (as in case of repeated unit cell pattern) than analytical models could be derived with ease [1,2]. Others have derived analytical results based on just Kelvin's tetrakaidecahedron model (i.e. BCC structure), which has served as a check for finite element results by many [10,56]. Point to ponder is that FE analysis of unit cell approach is not the true depiction of foam behavior but it is computationally very inexpensive Ashby and Banhart with their theory of idealized metal foam structure laid down simple analytical relationship of power law [1,2]. According to this law, most physical properties of metal foams can be approximated by multiplying a constant (different for specific property) with relative density of foam and solid metal (Equation 2.1).

$$Property_{metal\ foam} = Constant_{specific\ property} \times \left[\frac{\rho_f}{\rho_s}\right]^n \quad (2.1)$$

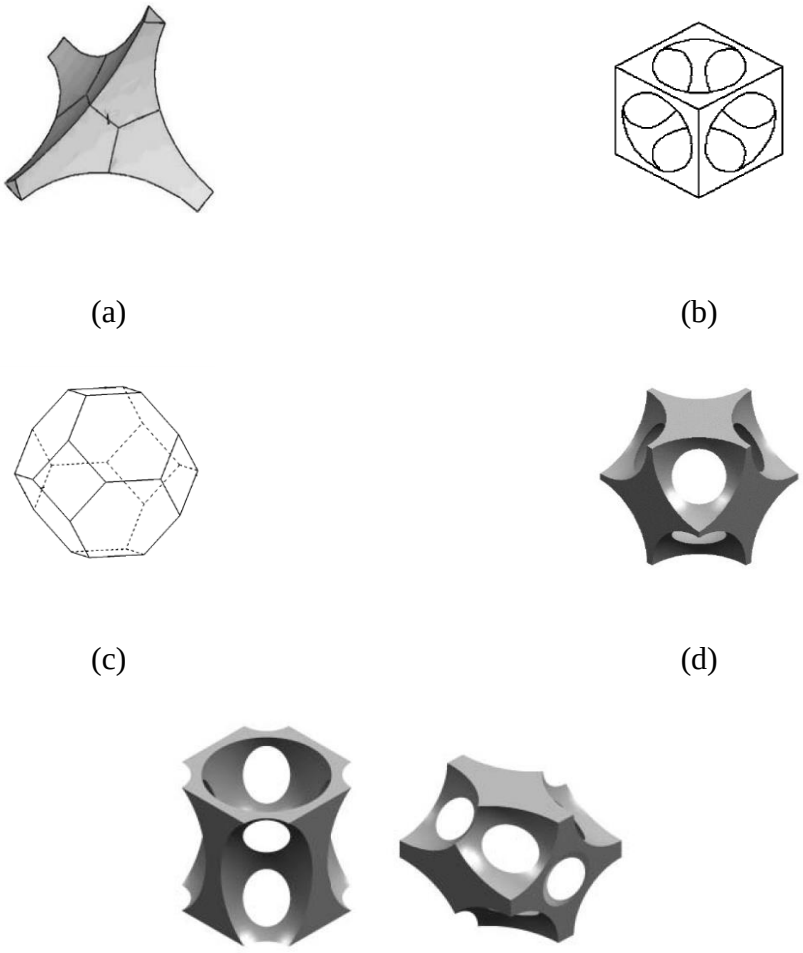

(a) (b)

(c) (d)

(e)

Figure 5 Unit Cells used in Literature for Metal Foam Modeling [52–55]

At global and local (or pore) level cell architecture (open or closed cell), arrangement of cell pores (their relative angle of intersection) and shape of cell struts (or walls) play essential role in study of these complex structures [57]. Most theoretical studies on simple three dimensional metal foams, as discussed, assume cyclic pattern of prismatic cell walls (or struts). These are also known as beam models, as cell walls are of uniform diameter – unlike in real metal foams (Figure 6) [11]. Whereas for closed cell three dimensional modeling generally Voronoi tessellation method and node-bond model is generally used (Figure 7) [58]. Voronoi tessellation method uses point seeds growth in all three dimensions to grow into a random form. A little manipulation is done in these methods to obtain open cell foam but the end results and complexity of approach has not allowed researchers to adopt it much. More or less, these approaches are still in use by researchers today, either using the identical models or only with slight modifications [14,59–61].

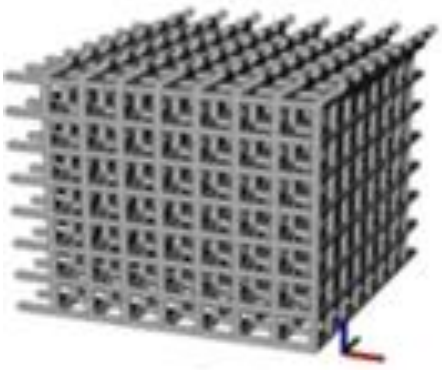

Figure 6 Beam Model [11]

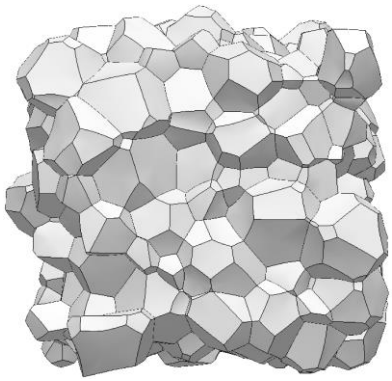

Figure 7 Voronoi tessellation method [58]

Three dimensional (3D) FE analysis in the field of medicine has been used by Doctors, as at micro level human organs exhibit mechanics of materials in day to day regular activities [62–64]. Human organs due to their geometric complexity are not easy to design in FE or CAD software so Doctors prefer the technique of image rendering with help of serial imaging instruments like computed tomography (CT) scanners [65]. This nondestructive approach enables the researchers to acquire even the finest of details in the sample, thus ensuring the accuracy of finite element analysis.

The aforementioned discussion reveals that perplex random order models are the only solution to predict response of metal foams, since periodic unit cell models do not mimic correctly the real observable response. As no exact solutions exist for highly disordered porous metals, large scale computational approach with the help of CT scanning has been considered here as the only way of extracting the true thermo-mechanical behavior of foams. This form of approach has not been taken much for three dimensional models as it is time both, time consuming and computationally demanding. Although CT scanning technique has been employed by few to get exact information about structure parameters and use them in analytical modeling, but finite element tests were not run [66,67]. The research described here only focuses on Aluminum 6101 open cell metal foams with porosity approximately 93%. The aim here is to pave wave for other researchers for finding true response of metal foams in thermo-mechanical systems, where accuracy matters more than mere approximation.

CHAPTER 3

METHODOLOGY

To better understand the thermo-mechanical behavior of metal foams, both numerical and experimental approaches were undertaken for the task. A brief overview is laid down as follows for the work that was carried out for the fulfillment of the objectives.

3.1 Experimental Approach for Heat Sinks Performance

Heat sinks need to be effective and efficient to dissipate the excessive heat generated in the electronic circuitry. Thus, it is of utmost importance to keep the working temperature of the device within safe limits, not only for keeping it safe but also to get an optimized performance out of the device.

Usually the performance of a heat sink depends on factors like: thermal conductance, geometry, fin shape, coefficient of heat transfer (h), mass flow rate and duct/tunnel size. Generally, to approximate the thermal behavior, simple analytical models can be made for studying the performance. Experimental methods are also employed as an alternative. But in reality the most accurate method is by numerical simulations, because of the highly unpredictable three-dimensional interaction between fins and fluid.

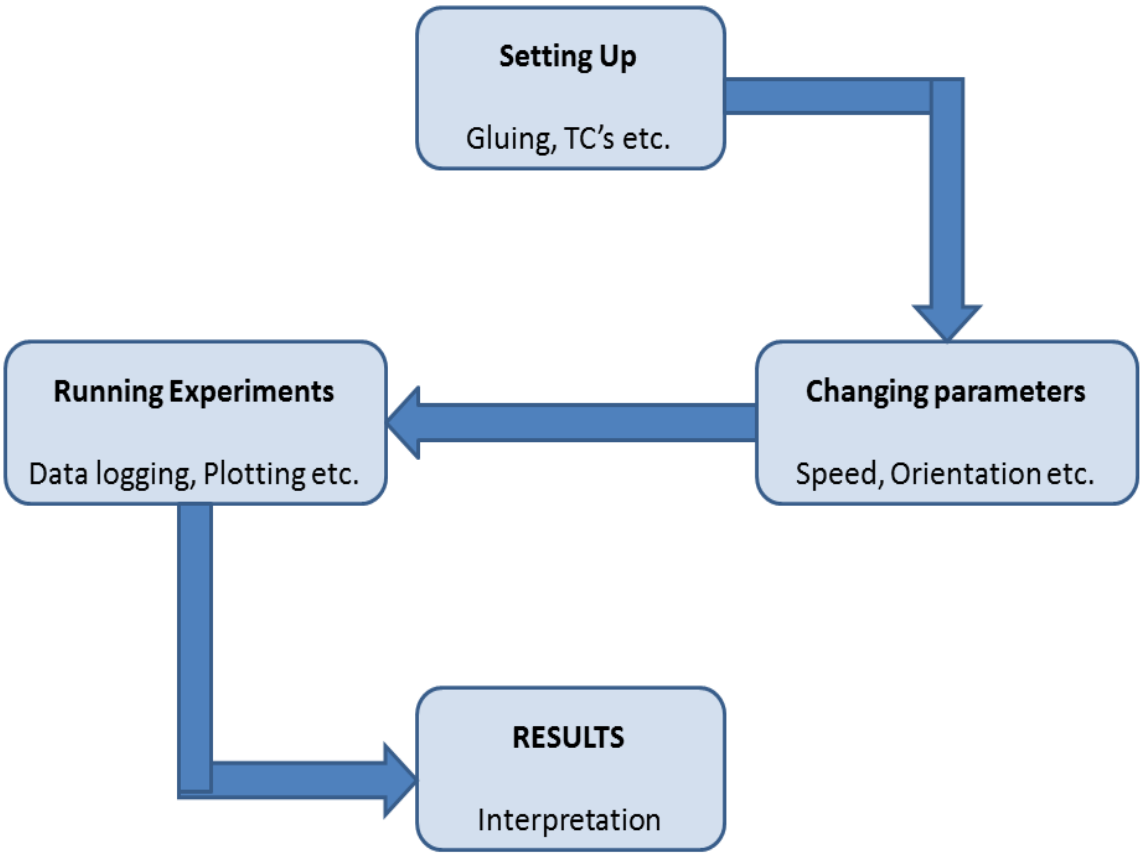

Figure 8 Experimental Methodology

For our case both experimental and numerical approaches were considered. Experimentally determining the thermal performance of heat sinks is among one of the most popular techniques. Figure 8 shows the flow chart of experimental study. And Figure 9 shows the schematic of ducted setup used for experimentation [68]. Performing these experiments in un-ducted environment can lead to unpredictable results; therefore use of ducts is a must to avoid misleading data.

In our experiments the ducted wind tunnel approach was adopted, based on the theoretical knowledge from literature. The assembly is relatively easier to setup and also gives quite reasonable results, without the hassle of using any complicated machinery

[69]. As seen from the schematic, the heat sink is placed inside the middle of wind tunnel. Both natural convection (Fan Off) and forced convection (Fan On) conditions have been exercised. Guide vanes (not shown in the schematic) have been installed just after the blowing fan and before the heat sink to ensure that the air flow reaching the heat sink is laminar. Natural convection conditions were carried out with fan off and both sides of wind tunnel were open to the atmosphere. Alternately, for all experiments of forced convection the fan speed was fixed at 1.6, 2.6 and 3.6 m/s air flow. A rotary type flow meter was installed inside the tunnel to record the speed of air flow.

The first experiment was carried out with single fin solid heat sink and single fin metal foam heat sink. This was done to investigate the difference between thermal behaviors of the two distinct fin type heat sinks. The solid fin has been machined out of pure aluminum, whereas metal foam is an alloy of aluminum (Al-6101) with the base sprayed by similar properties material. For the subsequent experiments multiple fin metal foam heat sinks were also investigated with porosity range of 4 and 8 PPC. Fin dimensions of 20x15x6.35 mm and base thickness of 3 mm was chosen in all experiments, to depict the size of an average commercial heat sink used for this purpose.

A D.C power supply along with heat source used for the first experiment was 1.30 W (approx.) and 5 W (approx.) for the rest. This small wattage heat source has been used to mimic the heat generated from an actual electronic chip – like personal computers. Thermal adhesive was used to attach the heat sink to the heating pad. Heating pad was securely and tightly packed with insulated foam to minimize heat losses.

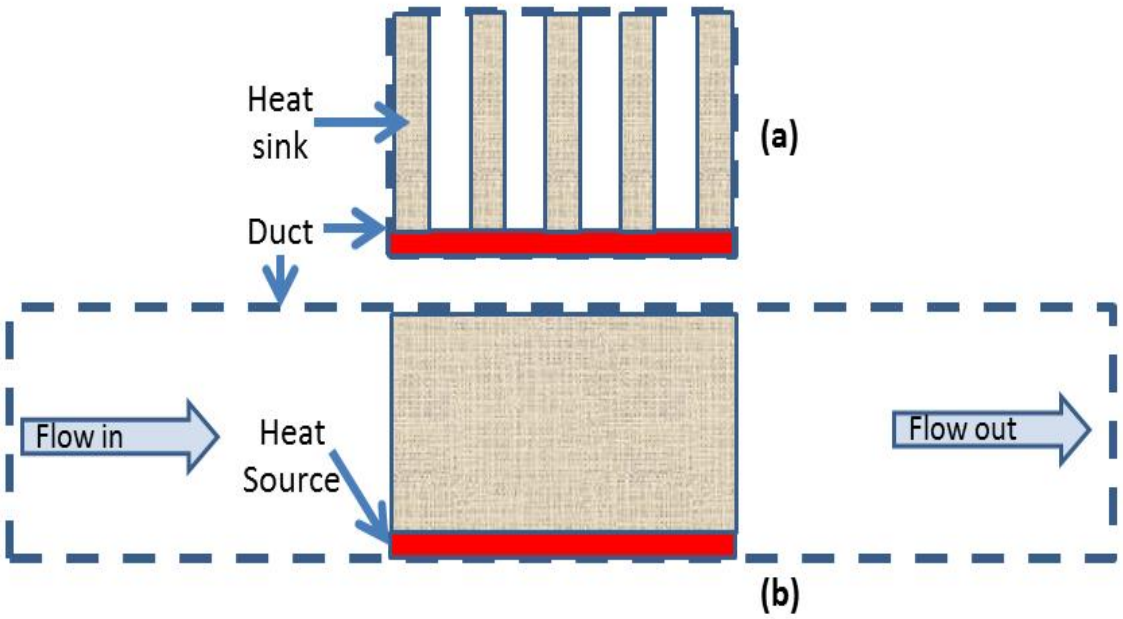

Figure 9 Schematic of Experimental Setup: (a) Front View and (b) Side View [68]

As the work being carried out is in low temperature ranges, T-type thermocouples were employed for better accuracy and response. For real time data logging of temperature with time, NI 9211 DAQ (Data AcQuisition) card was used with LabView. Thermocouples were attached at different points of interest to continuously update about the temperature variations. These points of interest were temperature of fins along the height, base, heating pad, inside tunnel temperature and finally outside room temperature.

To check for optimum performance, variable air flow speeds and different orientation of heat sinks were used with respect to air flow i.e. parallel, perpendicular and at 45 degree respectively. The details of the findings have been elaborated in results and discussion section.

3.2 3D Modeling for Metal Foam Heat Sink Model

As already emphasized in the introduction and literature review, complex and free form shapes like that of metal foams, pose a challenge for designers to manually make them in commercially available software. It is very difficult to manually create them in CAD or FE software. Moreover, simplified models cannot portray the authenticity of numerical studies for such haphazard shaped structures. Figure 10 shows the flow chart of numerical study.

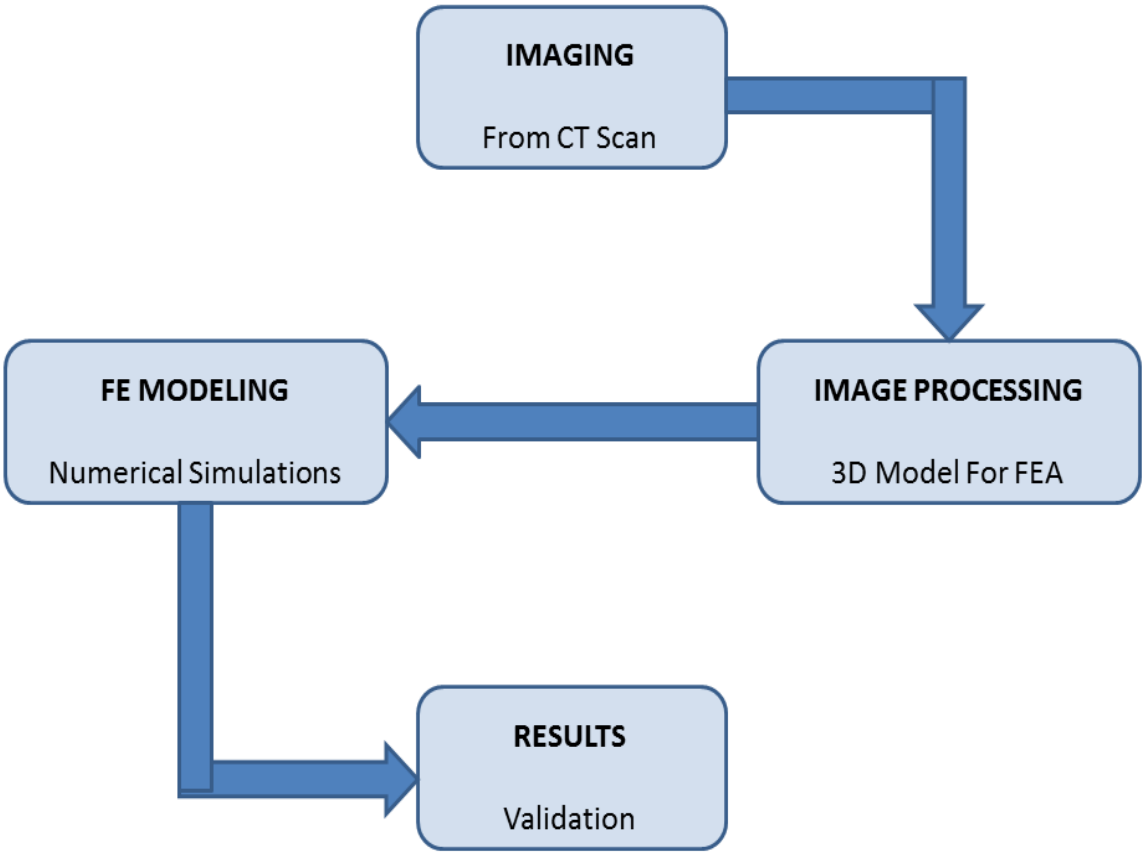

Figure 10 Modeling Methodology

So for this purpose the serial imaging techniques were used to acquire the model of our metal foam. Among several commercially available serial imaging techniques we used Computerized Tomography (CT), as it is a non-destructive technique and the sample is not susceptible to any sort of physical damage. We used the industrial version of Micro CT type - model Skyscan 1172.

Once the Imaging is done, the first phase is to reconstruct a “raw” 3D model from these serial images. The term raw here suggests that this model is only good for visual representation of the sample and cannot be used for 3D printing or any sort of finite element modeling for that matter. The initial software used for this task are “NRecon” and “CTan”. Both these software belong to the CT scan and are available in the CT scan control computer. These images contain all the apparent and hidden details of object being scanned. One then carefully selects the densities of interest that need to be extracted for reconstruction. This image processing setup is the most complicated process of the methodology used.

After deliberate effort of using the most optimized set of parameters for imaging, this raw model is imported in computer aided design software (CAD), that are commercially used for reverse engineering. These software like Geomagic Studio and Meshlab are specifically designed for helping the designers to “clean” and “stitch” the raw model. The terminology cleaning means getting rid of all the noise and extra unwanted details from the model, whereas stitch means closing all the gaps and holes inside the model to prepare a water-tight mesh. This water-tight mesh is a mere surface/skin model, which means its hollow from the inside. To convert this surface/skin model into a solid (or filled) model the file is exported to SolidWorks engineering CAD tool.

The final solid model then can be imported to any finite element software for simulation analysis. Ansys Workbench has been used for this particular study. In Ansys, after assigning the material properties to our model, a mesh of the model was prepared and simple mechanical and thermal tests were run to check the proper working of the final model. Once its validity was acknowledged, the model was used for analysis of our experimental work. Later through our numerical simulations of the model we also proposed a technique of finding heat transfer coefficient of complex shaped objects. Through scaling (upsizing/downsizing) of the model with a specific ratio it has been shown that the same model can also be used to modify the pore density (PPC or PPI) for different simulations, and therefore, completely omitting the need of rescanning a new sample of different pore density. The details of numerical study and their finding have been discoursed in subsequent chapters.

CHAPTER 4

EXPERIMENTAL STUDY

A lot of researchers have undertaken studies on the forced convective heat transfer in metal foams by experimental, numerical and analytical method. Subsequently both heat transfer characteristics and air flow phenomena in foams are adversely related to structural features of the metal foam, like: porosity, PPI, foam dimensions and type of material too. Operating conditions such as: heat flux, fluid velocity, surrounding pressure and temperature also play another important factor for determining these aforementioned characteristics.

The aim of this research is to find optimum heat sink performance based on porosity, air speed, heat sink orientation and most importantly the type of interface (between heat sink's fin and base). Cooling performance can be increased using higher fan speeds and impinging jet stream. But parametric study should also be carried out with respect to thermal performance of heat sinks under fixed fan speed and normal air flow, while varying the heat sink orientation and the number of fins. The porosity has been chosen to be constant at 93% for all samples as its effect on heat transfer are not very prominent [34]. Metal foam heat sinks highlighted in the literature were made by attaching the metal foam fins to solid base via thermal glue/epoxy. Here the most prominent feature of the study is to compare the enhancement of thermal performance of heat sinks with thermal spray coating as an adhesive method for fins and the base, rather than conventional glue/epoxy method because according to simulated results of Christopher et al. [44], the

effect of typical thermal epoxies when compared to ideal bonds had small effect on heat transfer performance.

4.1 Metal Foam Heat Sink Samples Fabrication

Sample fabrication of the heat sinks is an important aspect of this experimental study. Three types of samples were fabricated:

a) Machined solid heat sink.

b) Metal foam heat sink with thermal glue as an adhesive between fin and base.

c) Metal Foam heat sinks with thermal spray coating between fin and base.

4.1.1 Solid heat sink

Solid heat sink has been machined out by milling process as one single unit as shown in Figure 11. Therefore no thermal glue/epoxy has been applied between base and fin interface.

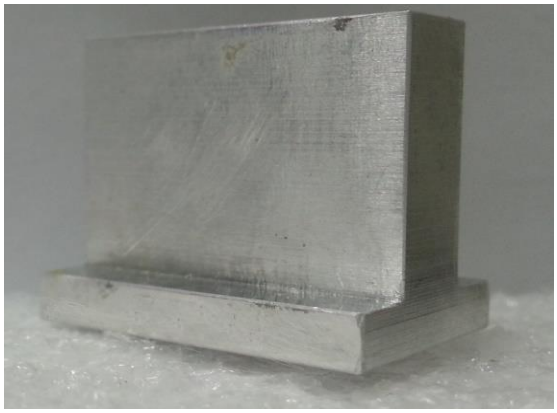

Figure 11 Solid heat sink

4.1.2 Metal foam heat sink with thermal epoxy

The metal foam fins were cut using precision saw while taking care not to damage the structure matrix of the foam. The base plates were machined using milling machine with slots at particular locations for insertion of the fins. After the fins were properly placed in the machined slots of the base, both were couples together by using thermal glue/epoxy for reducing thermal contact resistance. For glued sample conductive epoxy "OMEGATHERM 201" with a thermal conductivity of about 2-3 W/m.K was used and after application it was allowed to set as per vendor's instructions [70].

4.1.3 Metal foam heat sinks with thermal spray

These samples were fabricated using the same technique as that of metal foam heat sink with thermal epoxy. The only difference is that the thermal epoxy/glue was replaced by thermal spray coating technique in collaboration with CACT, University of Toronto [71].

Figure 12 shows the junction point where glue/epoxy or thermal spray was applied. With thermal spray coating one, two and three fins samples were prepared. But only one single fin sample each was prepared for machined solid heat sink and metal foam heat sink with thermal glue. The pictures of one, two and three fins metal foam heat sinks are given in Figure 13.

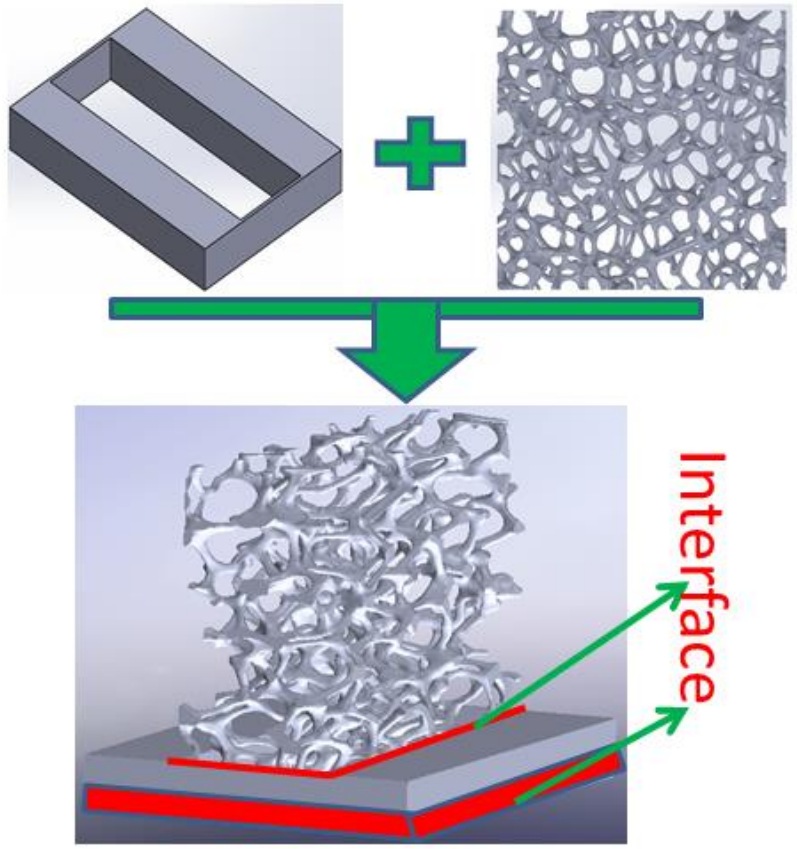

Figure 12 Schematic for joining base and fin with thermal spray or thermal epoxy

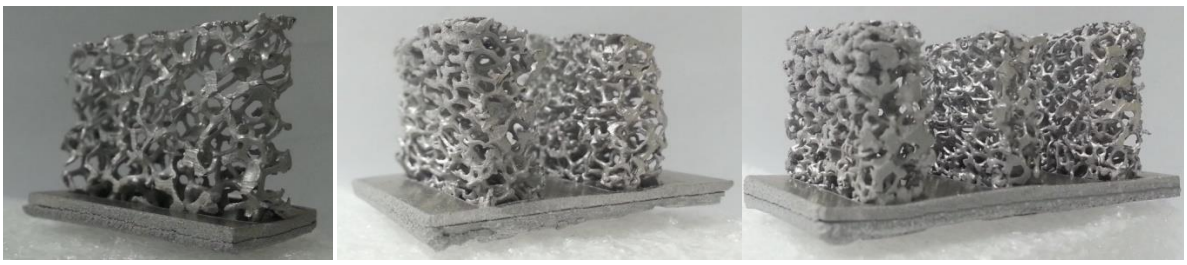

Figure 13 Pictures of one, two, three fin metal foam and one fin solid heat sink

The Metal foam fins were made from Aluminum 6101 alloy with 93% porosity for all samples and were obtained from "Goodfellow" [72]. Pore density (PPC) of single fin sample is 4 PPC (approx. 10 PPI), whereas it is 8 PPC (approx. 20 PPI) for two and three fin samples. Base material for all heat sinks and the solid heat sink are made from same alloy as well. Table 2 shows the thermal properties of metal foam fins, base material and solid heat sink.

Table 2 Material thermal properties [72]

Material	Aluminum 6101
Density (Kg/m^3)	2700
Thermal conductivity (W/m ºC)	218
Coefficient of thermal expansion (1/ºC)	23.58×10^{-6}
Specific heat (J/g ºC)	0.895

All single fin samples have been manufactured at exact same dimensions. The base dimensions for all single fin samples are 20x14.35x3 mm (where 3 mm is the thickness of the base). And the dimensions of fin are 20x15x6.35 mm (where 6.35mm is the thickness and 15 mm is the height of the fin). Furthermore the summary of one, two and three fin heat sinks dimensions is given in Table 3, where all dimensions given are in "mm". And Figure 14 shows the schematic of heat sink dimensions.

Table 3 Dimensions of Heat Sinks (mm)

Heat Sink	**Base Dimensions**			**Fin Dimensions**			**Fin Spacing(g)**	**Extra Width on both sides of fin**
	L_b	**W_b**	**T_b**	**L_f**	**H_f**	**T_f**		
1_Fin	20	14.35	3.0	20	15	6.35	1 x T_f	4
2_Fin	20	27.05	3.0	20	15	6.35	1 x T_f	4
3_Fin	20	39.75	3.0	20	15	6.35	1 x T_f	4

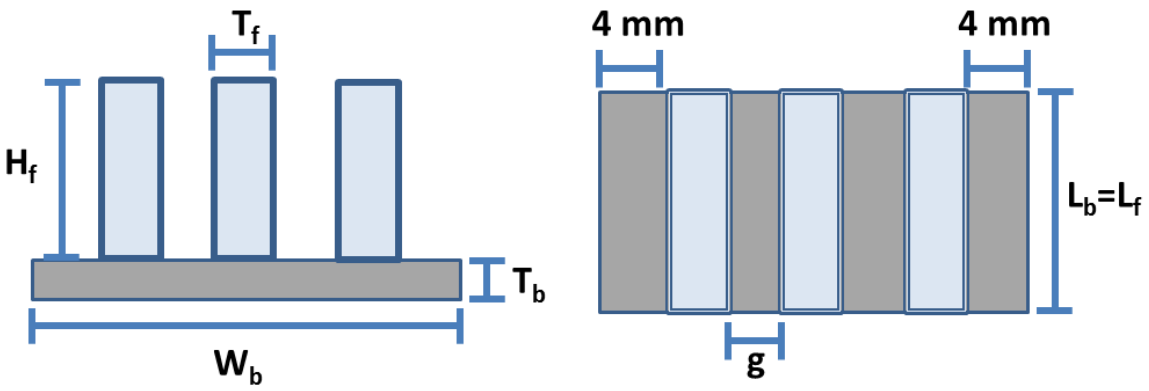

Figure 14 Heat sinks dimensions

Figure 15 shows interface studied from CT scan for thermal glue and thermal spray. The color contours in thermal glue sample are due to density difference of glue and material in the sample. For thermal spray we don't see any color contours at all. This indicates a uniform density throughout, due to sprayed coating being of same material.

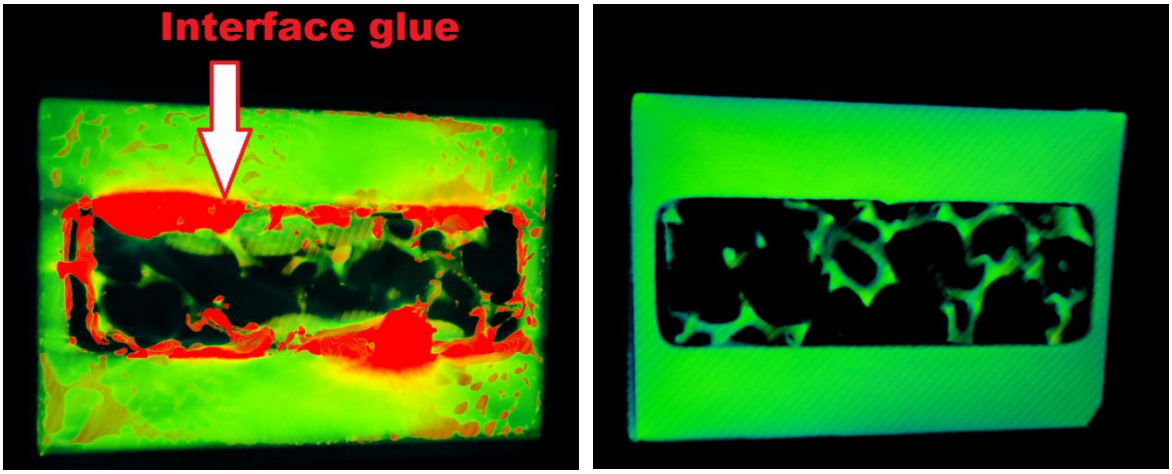

(a)With Glue (b)With Thermal spray coating

Figure 15 CT Scan Images of interface

4.2 Experimental Setup

Figure 16 shows the schematic of the experimental setup, where the whole wind tunnel setup has been manufactured in-house. The heat sink samples were placed in the apparatus one by one and an A.C powered fan with a regulator was used for wind blowing inside the tunnel with variable velocities. Wind direction was from right to left and the wind tunnel was open from both ends for natural convection flow in case of fan-off condition. A D.C powered heater was used as the heat source for heat sinks. For the experiments this heater mimics the heat generation of an electronic circuitry. The heater was approximately 5W (i.e. 12 V and 0.42 A) with heat generation area of 25 x 50 mm. The heater was heavily padded using Styrofoam to ensure minimum heat loss. Only an area equal to each heat sink's respective base area was let open to attach the heat sink for heat dissipation of the heater via the heat sink. The straightening vanes were installed in the airflow path to make the turbulent flow of air into a laminar flow and to ensure a before it interacts with the heat sink. A velocity meter was also installed to continuously monitor the air flow speed. Moreover in many electronic devices, it is normal to find heat sinks in open space where forced air by-passes the heat sink. This is one of the motivations to keep our setup in by-pass arrangement as that for real applications.

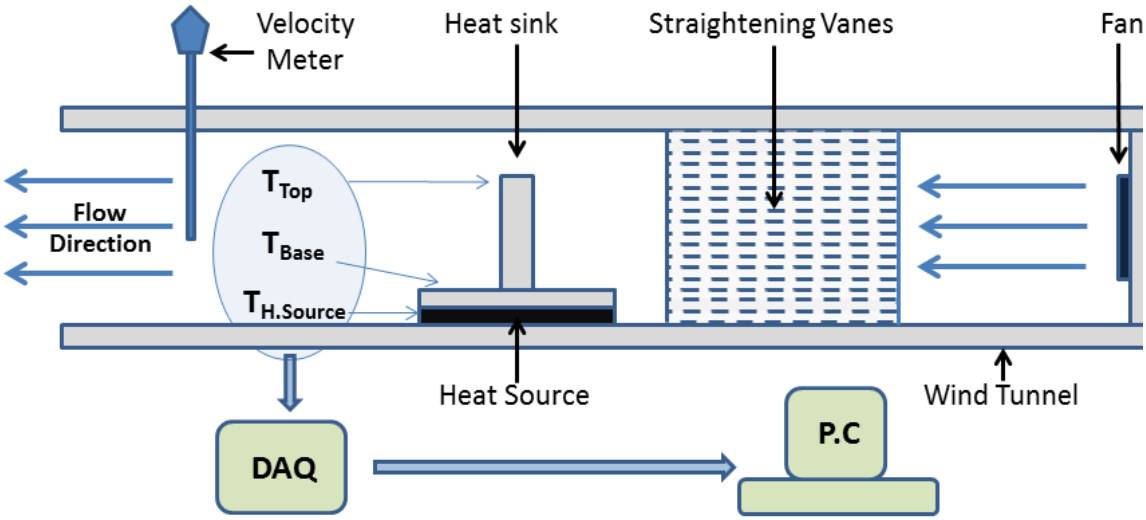

Figure 16 Schematic (NOT DRAWN TO SCALE)

T-type thermocouples were attached at different locations of heat sink to observe the thermal temperature profile of the heat sinks. For continues temperature monitoring and data logging in real-time, "NI 9211 DAQ" (Data AcQuisition) card was used with "LabView" software. Sampling rate in the software was set to 1Hz to ensure that temperature data is logged for each second, for the complete time span of the experiment. As shown in schematic Figure 16, thermocouples were mainly attached to top and bottom of heat sink, along with one directly on the heat source. Also one thermocouple was used to monitor the room temperature outside the tunnel and one thermocouple for temperature inside the tunnel. Figure 17 shows a schematic for the details of thermocouple attachment location for one, two and three fins heat sinks.

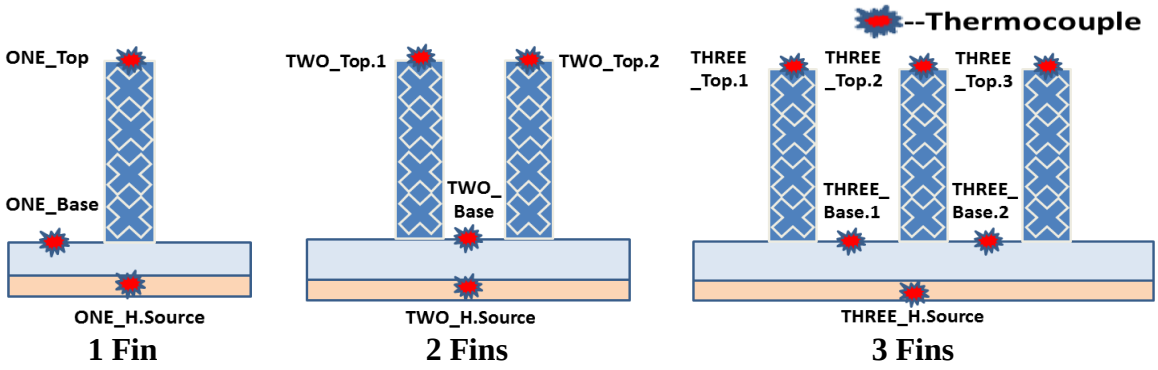

Figure 17 Thermocouples attachment locations on each heat sink

4.3 Experiments

Each of the heat sink was attached to the heating source with a thin layer of thermal grease in between the contacting surfaces of heats sink's base and the heating source. For all experiments the heat sinks were heated from room temperature (almost 24.5ºC) to a fix 60ºC temperature at fan-off (natural convection) condition. The moment the heating source temperature hit 60ºC, the fan was switched on; hereon referred to as fan-on (or forced convection) condition. Thus fan-off and fan-on conditions being same for all the experiments.

Figure 18 shows the picture of experimental setup. Performance test on each sample was done by changing its velocity and orientation. Where three orientations used are 0º (fin length parallel to flow), 45º and 90º (fin length perpendicular to flow). It was reported by Mancin et al. [73] that heat transfer coefficient is independent of heat input so it was not varied in any of the experiments and was fixed at 5W. How the different sets of these parameters have been employed for each experiment has been elaborated and explained

in the results section. For all experiments the thermal resistance found for each heat sink sample is calculated by:

$$R_{th} = \frac{T_b - T_{amb}}{Q}$$

Where T_b is temperature of base, T_{amb} is ambient temperature, and Q is total heat dissipated.

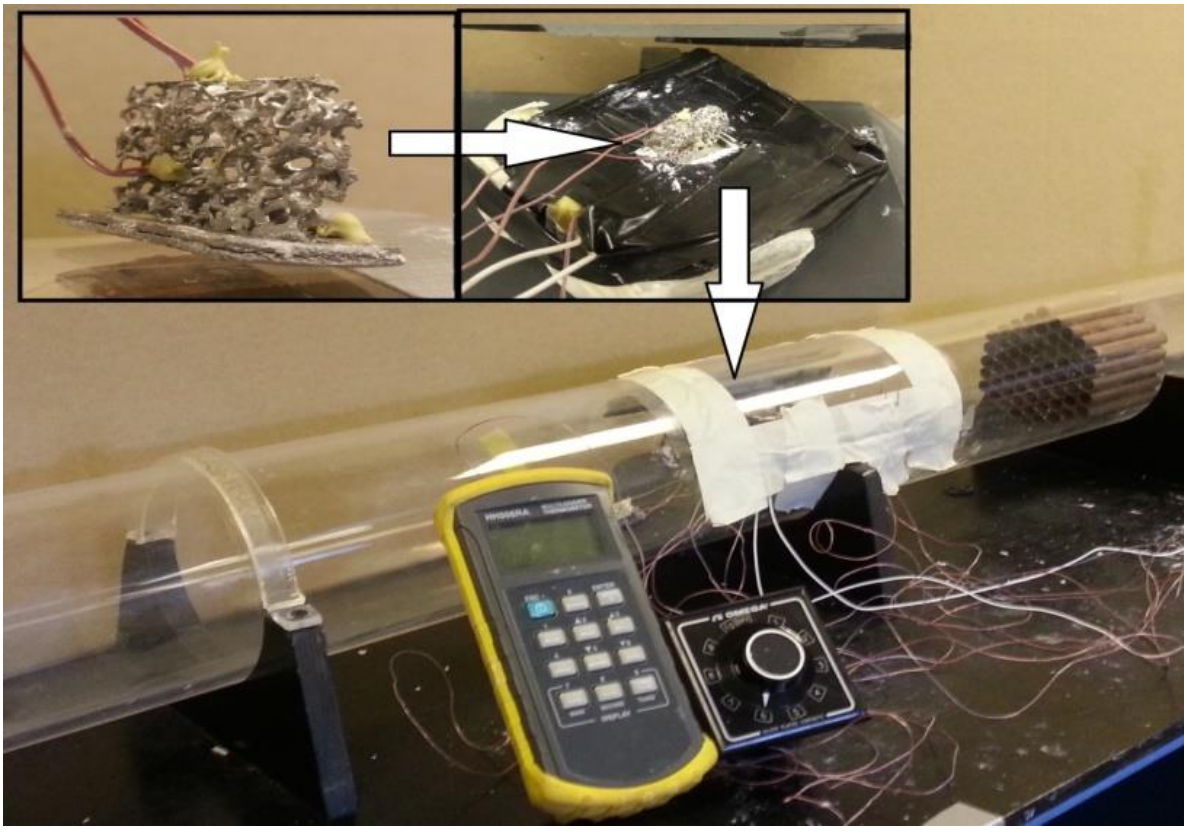

Figure 18 Experimental setup

CHAPTER 5

EXPERIMENTAL FINDINGS

As already explained in the previous chapter, the motive of the study is to find the peculiar behavior of metal foam heat sinks under varying test conditions. Following sub-sections discuss in detail the experiments performed and their results.

5.1 Results and Discussion

Experiments have been carried out in form of different studies. Power input as already explained wasn't varied for the experiments so it remains 5W for each and every experiment. As the heating source providing the heat input to the heat sinks is used to mimic the temperature rise in electronic equipment, so our main concern in each experiment is to monitor how much the total temperature falls when it reaches the steady-state. For all the experiments temperature drop is in reference to 60 ºC, when the fan was switched on.

5.1.1 Study A: Effect of Fin Type and Interface

For study A, (i) single fin metal foam heat sink with thermal spray coating, (ii) single fin metal foam heat sink with thermal glue and lastly (iii) single fin solid heat sink were compared, where both metal foam samples were of pore density equal to 4 PPC. All these three samples were given the same test conditions i.e. orientation of the heat sink samples was 90º and a fixed fan speed of 3.6 m/s for fan-on condition. Figure 19 shows the trend

plotted for a time span of 60 min. Figure 19 (a), (b) and (c) are plots of solid fin, glued fin and thermal spray coated fin respectively, showing temperature variations of different points of the heat sink; fin top, fin base and heat source. Figure 19 (d) is a combined graph comparing the variations of heat source temperature only, for each case respectively.

In Figure 19 (a) solid heat sink's temperature is seen to be almost isothermal from base to the tip at fan-off condition (i.e. there is negligible temperature gradient) and is almost same as that of heating source. Whereas in both Figure 19 (b) and Figure 19 (c), it can be seen that for fan-off condition in the metal foam heat sinks, there is an obvious temperature gradient from base to the tip and is also less than the heating source throughout.

This phenomenon is due to solid heat sink having more effective thermal conductivity compared to metal foam heat sinks (almost 38 times more – as thermal conductivity of solid aluminum is almost 218 W/m K and effective thermal conductivity of metal foam is only 5.8 W/m K [72]). So solid heat sink conducts heat more rapidly and thus has almost same distribution throughout. On the contrary, metal foams having less thermal conductivity not only conduct heat slower, but at the same time their more surface area per unit volume efficiently and rapidly dissipate heat, even at natural convection (fan-off). Thus having a temperature gradient and also having temperature less than that of heat source.

Coming to the fan-on condition, it can be observed from Figure 19 (a) to Figure 19 (c) that the initial temperature drop at the fins top for the heat sinks is very fast for solid heat

sink and is almost abrupt for both metal foam heat sinks. As seen, the top temperature of metal foam samples not only reaches steady-state instantly but it also reaches almost at room temperature. Thus, this huge temperature difference between top and bottom further expedites the cooling process in case of metal foam samples. This higher temperature drop in the metal foams is mainly due to two reasons. First, more surface area per unit volume of metal foams provides more contact area between solid and fluid to improve convective heat transfer. Second, the turbulence of air created inside the irregular matrix mesh of metal foam further enhances the convective heat transfer coefficient which in return increases heat dissipation.

Lastly, Figure 19 (d) shows that solid heat sink takes more time to reach 60 ºC as compared to metal foams heat sinks and further it takes longer period of time to reach steady-state when fan is switched on. The reason for this is solid heat sink has more mass per unit volume compared to metal foams, so it takes more time to heat up and also more time to get rid of that stored thermal energy. Most importantly the comparison highlights that the typical thermal epoxy and an ideal bond (thermal spray in this case) have a prominent difference in the heat transfer performance. Thermal spray interface outperforms the other two samples by up to 9.8% more temperature drop and even after 60 min the temperature is still dropping.

5.1.2 Study B: Single Fin Metal Foam Heat Sink

Effect of Air Velocity

First for study B, single fin metal foam heat sink with thermal spray coating was tested for the variation of performance under three different air speeds of fan-on condition: (i)

1.6 m/s, (ii) 2.6 m/s and (iii) 3.6 m/s. Test conditions like room temperature, heat input and 90º orientation were same as study A, but only speed was altered in these cases. Figure 20 shows the graphs plotted for a time span of first 60 min.

Figure 20 (a), (b) and (c) are plots of 1.6 m/s, 2.6 m/s and 3.6 m/s fan speeds, showing temperature variations of different points on the heat sink; fin top, fin base and heat source. Figure 20 (d) is a combined graph comparing the variations of heat source temperature only, for each case respectively.

Without repeating the reasons for temperature trends of the metal foam fins, it can be seen from Figure 20 (a), (b) and (c) that fin top temperatures of the heat sink for 1.6 m/s, 2.6 m/s and 3.6 m/s are 32.47 ºC, 29.02 ºC and 26.52 ºC, after 60 minutes respectively i.e. almost reaching room temperature for 3.6 m/s. And the comparison in Figure 20 (d) shows that heating source's temperatures after 60 minutes at 1.6 m/s, 2.6 m/s and 3.6 m/s are 57.59 ºC, 53.39 ºC and 49.11 ºC respectively. Also the steady-state is reached in the least time for speed of 3.6 m/s.

The results indicate that heat transfer rate varies linearly in the tested velocity range. The two other reasons for this behavior between solid and metal foam heat sink is that, firstly the effective thermal conductivity of metal foam is almost 38 times less than that of solid heat sink of same aluminum alloy. Thus solid aluminum results in faster heat dissipation through conduction. Secondly, the solid heat sink has more surface area in contact with the heating source as compared to metal foam heat sink [74].

Effect of Orientation

For second part of study B, again single fin metal foam heat sink with thermal spray coating was tested. In this study also, experiments were carried out for time span of 60 min, with air speed at fan-on condition being fixed at 3.6 m/s. The performance was tested under three different orientations: (i) 0º, (ii) 45º and (iii) 90º. Figure 21 (a), (b) and (c) are plots of 0º, 45º and 90º orientation, showing temperature variations of different points on the heat sink; fin top, fin base and heat source. Figure 21 (d) is a combined graph comparing the variations of heat source temperature only, for each case respectively.

Figure 21 (a), (b) and (c) show that fin top temperatures of the heat sink at 0º, 45º and 90º are 29.63 ºC, 27.22 ºC and 26.48 ºC respectively. The comparison combined graph of Figure 21 (d) shows that heating source's temperatures after 60 minutes at 0º, 45º and 90º are 53.78 ºC, 51.06 ºC and 49.10 ºC respectively. And the steady-state of single fin is reached in the least time is for the orientation of 90º. For the single fin it makes perfect sense as the sample is thin in width (only 6.35mm compared to 20mm length), so maximum and even fluid-surface interaction takes place at this orientation.

5.1.3 Study C: Multiple Fin Heat sinks

For study C, experiments were done on two fins and three fins metal foam heat sinks with thermal spray coating. Velocity was kept constant at 3.6 m/s and only orientation was varied for this study. (a), (b) and (c) of Figure 22 and Figure 23 are plots of 0º, 45º and 90º orientation, showing temperature variations of different points on the heat sink; fins

top, fins base and heat source, for time span of 60 min. (d) of Figure 22 and Figure 23 is a combined graph comparing the variations of heat source temperature only, for each case respectively.

For 2 fins heat sink, plots of Figure 22 (a), (b) and (c) show that fins top's temperature of 0º, 45º and 90º are almost same for fan-off up till 60 ºC. This suggests that at natural convection orientation has negligible effect on heat transfer. Unlike 0º and 90º, heat sink with 45º orientation has the same temperature gradient in both fins, for fan-off and fan-on conditions. This is due to thorough and even mixing of air with the metal foam matrix at this orientation,

At 90º for fan-on, Top1 temperature is lower than Top2, as Top1 is the fin facing the air flow directly first. The first fin not only diverts some of the air reaching the second fin but it also heats up the air, which further reduces heat transfer. Therefore an uneven temperature gradient in both fins hinders efficient heat transfer. As expected, Figure 22 (d) for comparison shows that most temperature drop is given by 45º, followed by 0º and 90º. But at 0º, the length of fins being comparatively longer, the air because of haphazard matrix of metal foam, diverts in all directions before reaching the far end of fin and this in return minimizes the proper air-solid interaction as that takes place at 45º. This escape of air from the metal foam structure is due to by-pass arrangement of our wind tunnel.

In Figure 23 are the plots for 3 fins heat sink. Once more in Figure 23 (a), (b) and (c) show the same trend as that of 2 fin samples due to aforementioned reasons. And the combined graph of Figure 23 (d) again shows that temperature drop is most for 45º, followed by 0º and 90º respectively.

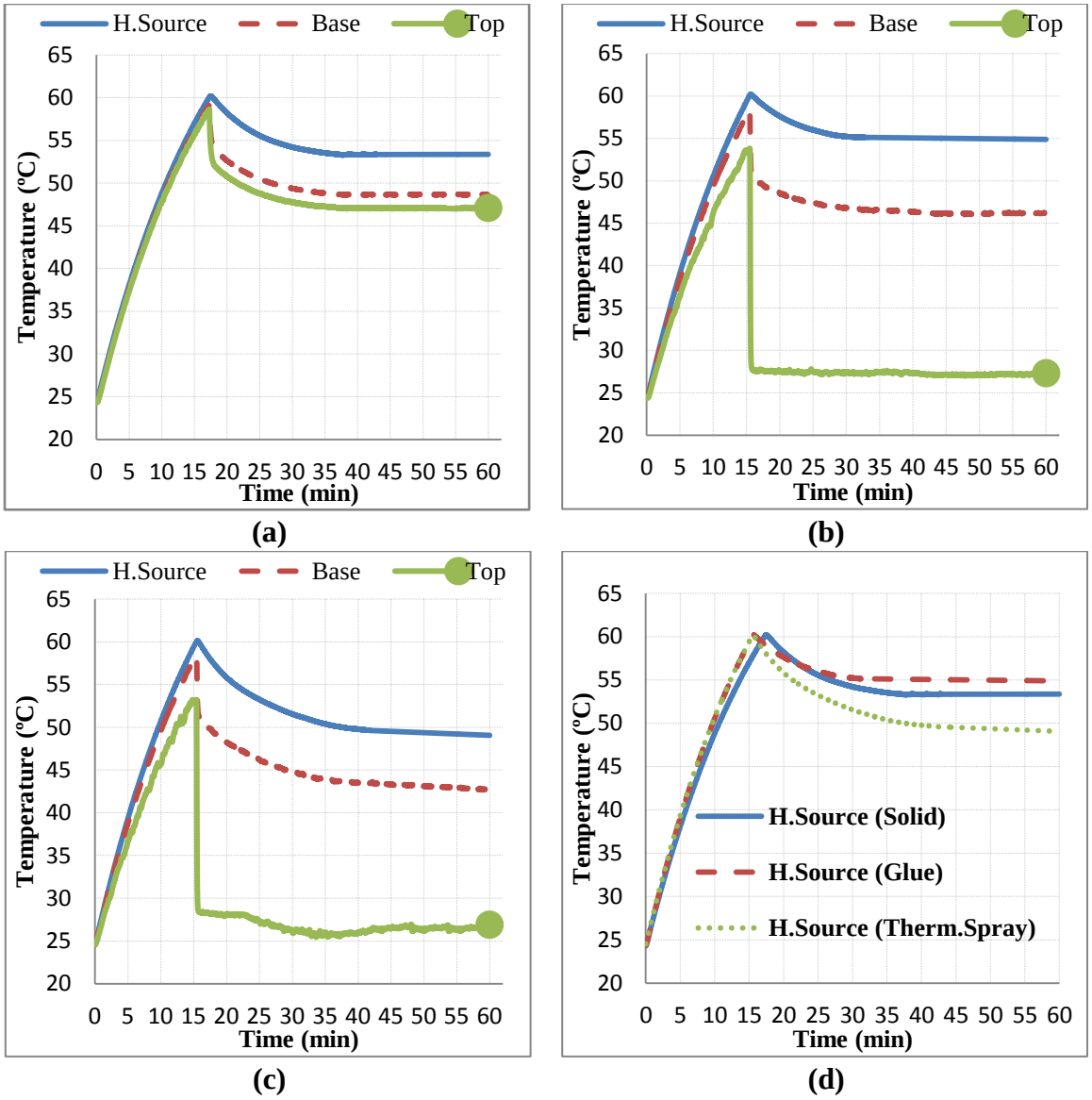

Figure 19 1_Fin Heat Sinks with 5W input, 90º orientation and 3.6 m/s flow; (a) Solid Heat Sink, (b) Glued Heat Sink, (c) Thermal Spray Heat Sink and (d) Comparative Plot

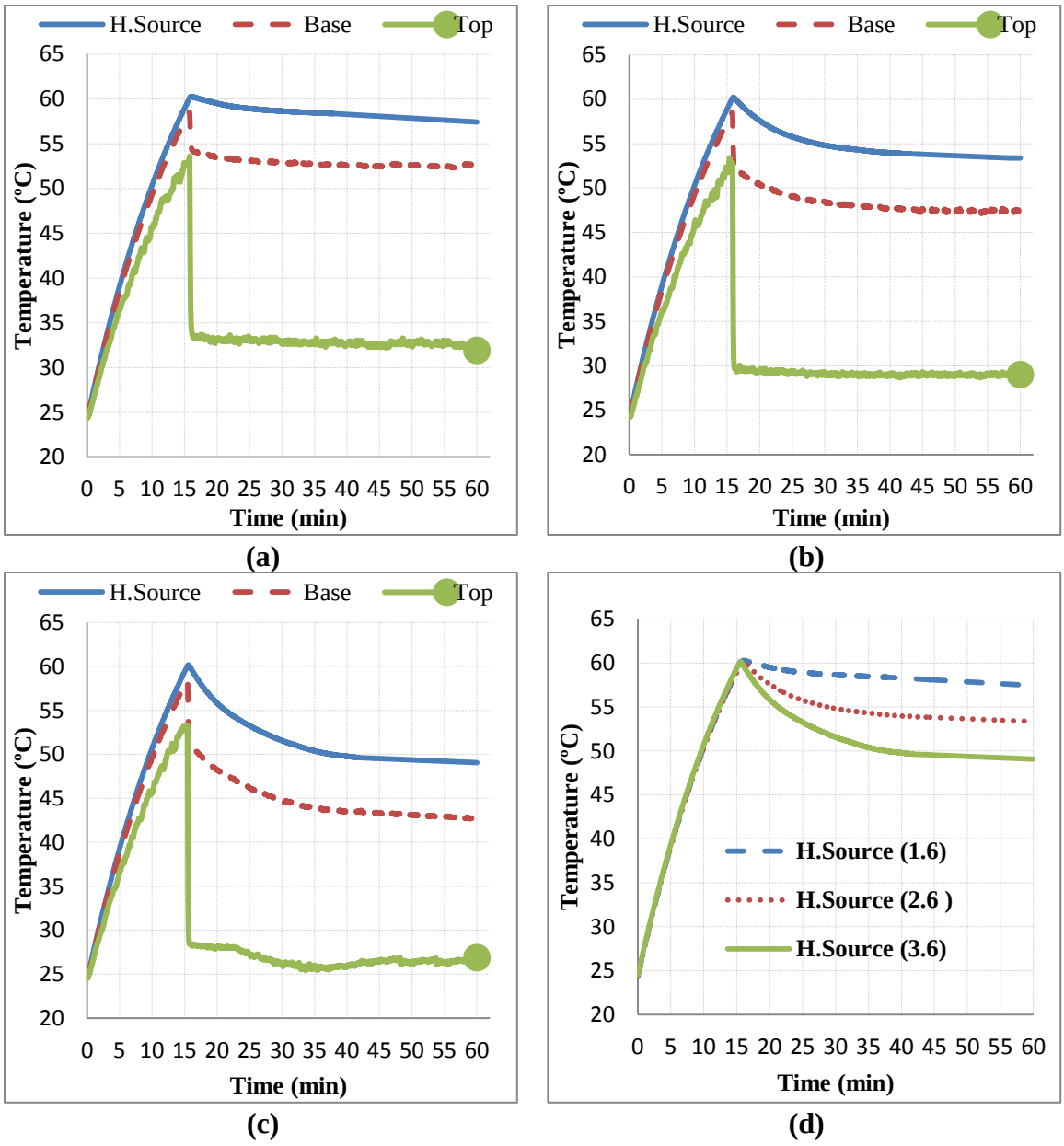

Figure 20 1_Fin thermal sprayed Heat Sinks with 5W input, 90º orientation and variable flow; (a) 1.6 m/s, (b) 2.6 m/s, (c) 3.6 m/s and (d) Comparative Plot

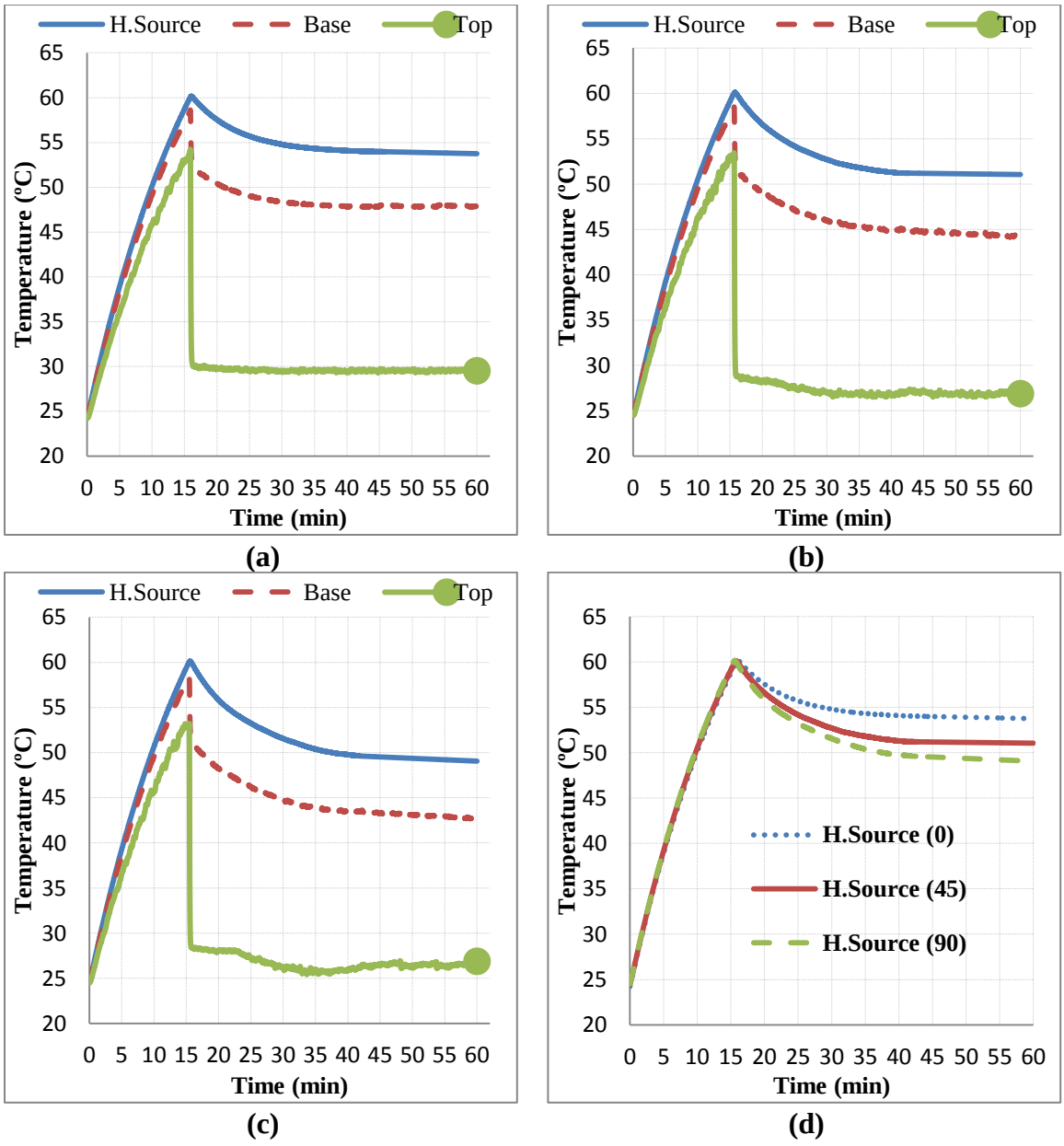

Figure 21 1_ Fin thermal sprayed Heat Sinks with 5W input, 3.6 m/s flow and variable orientation; (a) 0 degree, (b) 45 degree, (c) 90 degree and (d) Comparative Plot

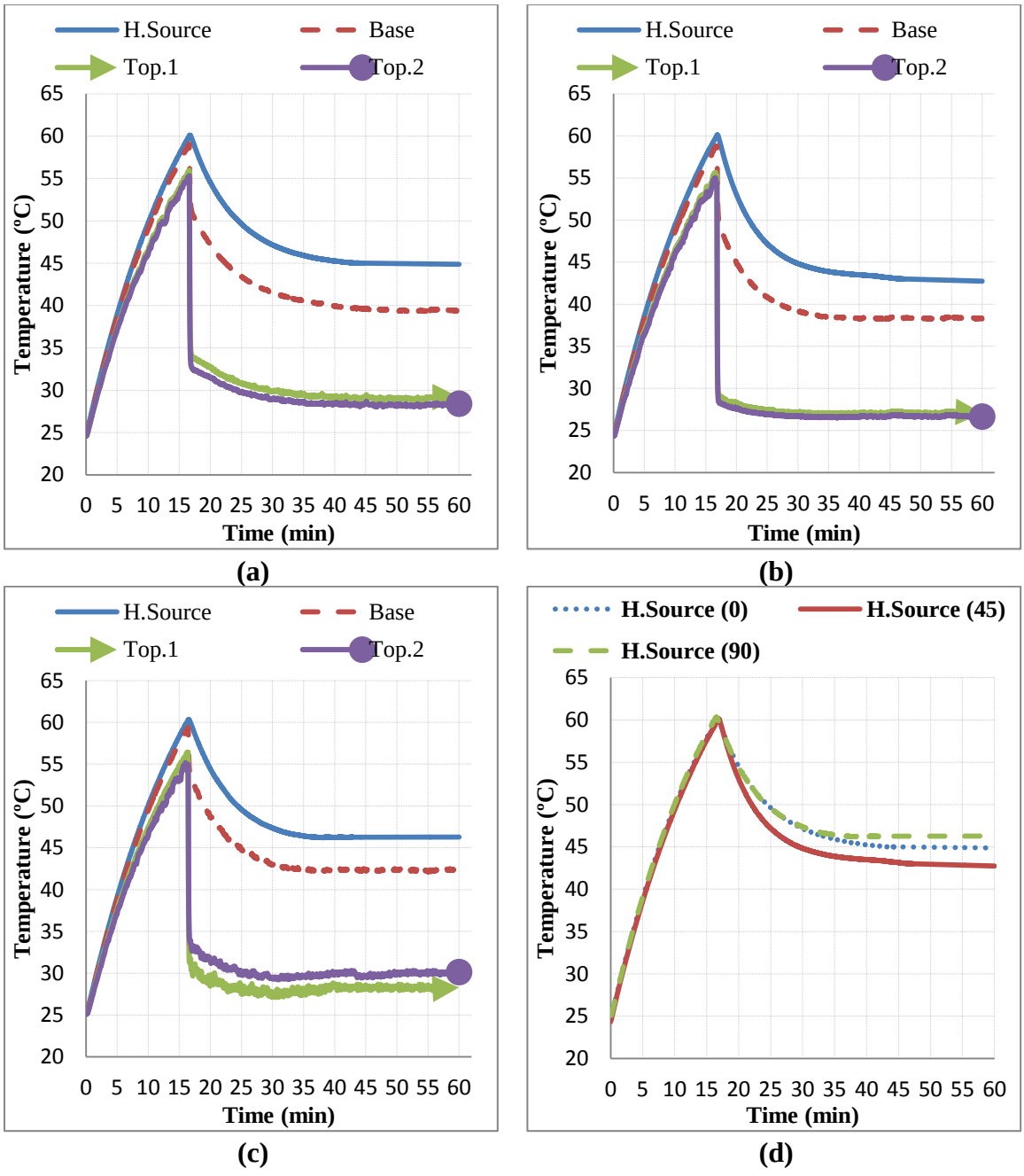

Figure 22 2_Fins thermal sprayed Heat Sinks with 5W input, 3.6 m/s flow and variable orientation; (a) 0 degree, (b) 45 degree, (c) 90 degree and (d) Comparative Plot

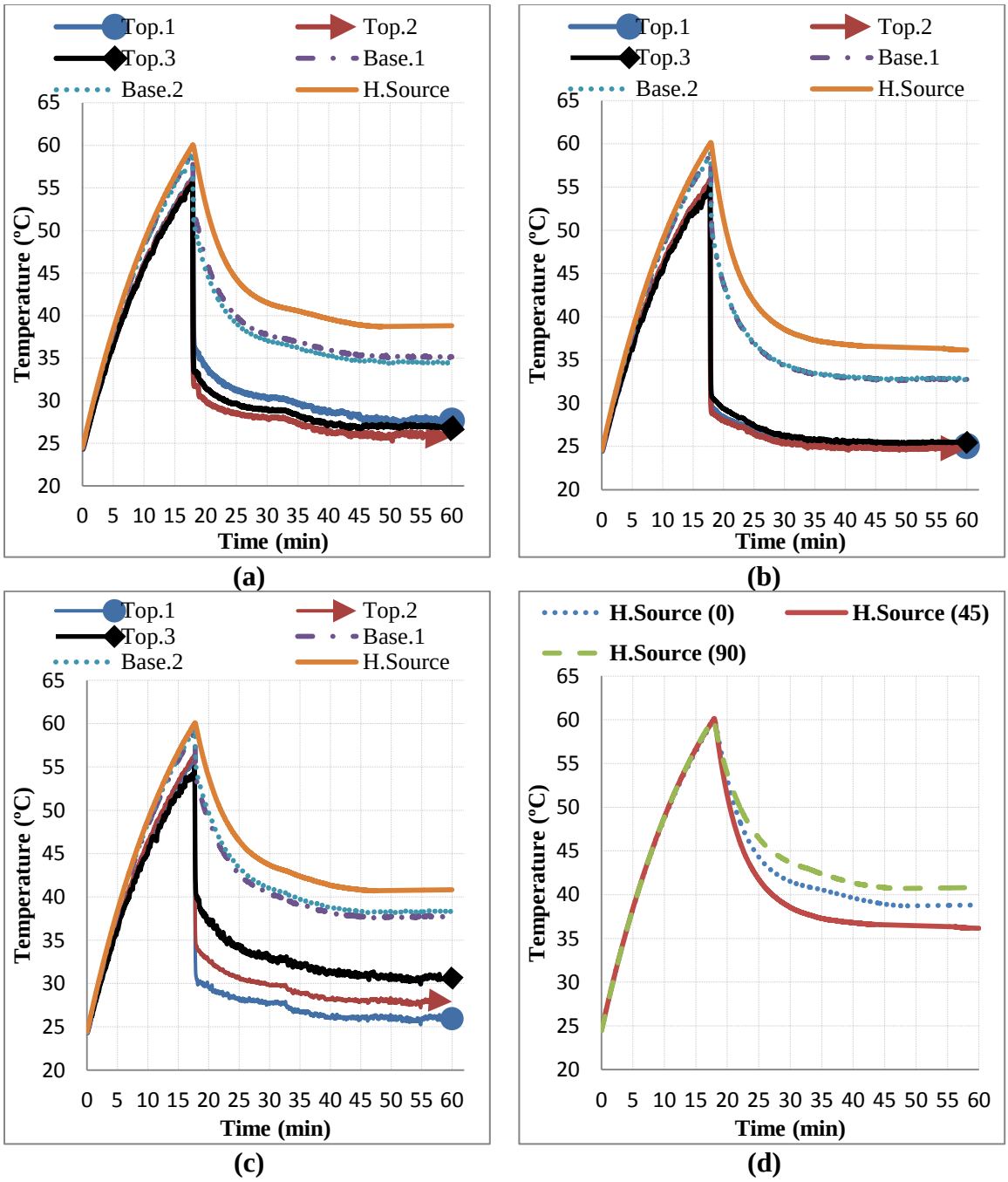

Figure 23 3_Fins thermal sprayed Heat Sinks with 5W input, 3.6 m/s flow and variable orientation; (a) 0 degree, (b) 45 degree, (c) 90 degree and (d) Comparative Plot

5.2 Summary

Figure 24 shows the thermal resistance (R_{th}) calculated for each sample from study A to study C. Whereas, Table 4 gives the summary of the results discussed above.

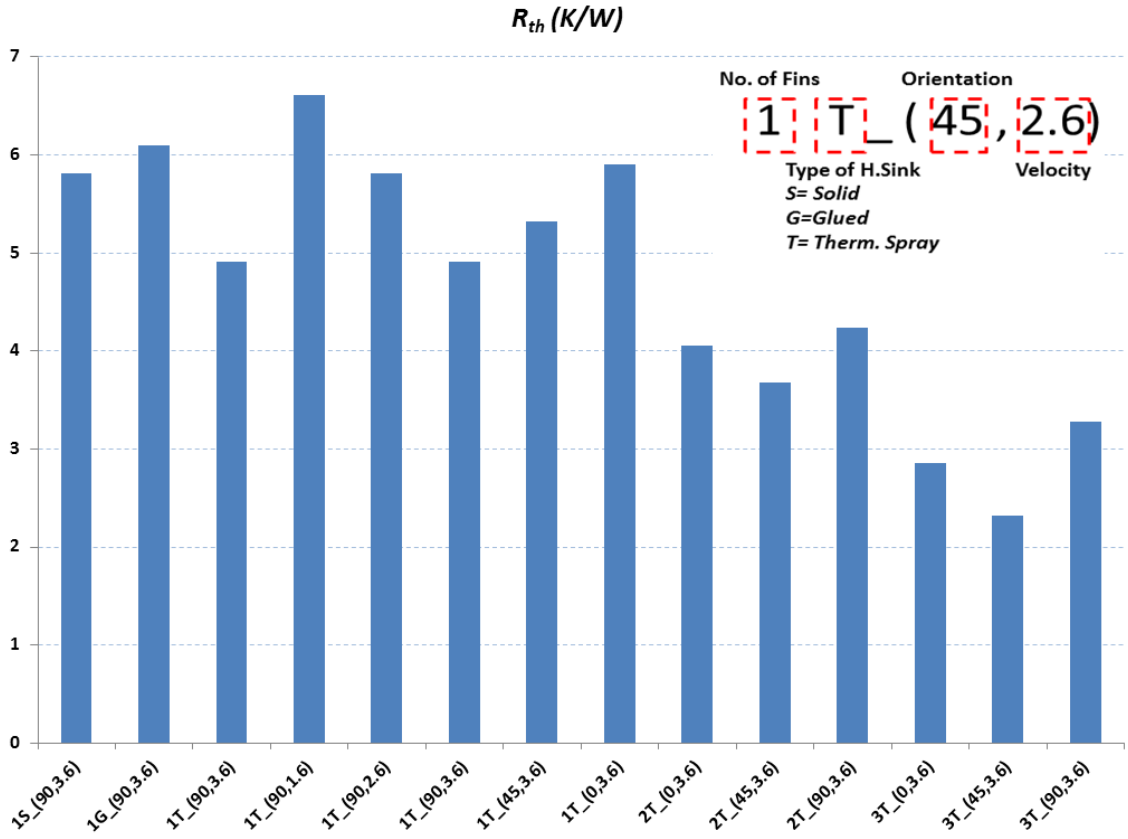

Figure 24 Thermal Resistance

Surprisingly, even though the heat transfer coefficient for multiple fins is less than that of single fins heat sinks, still the total temperature drop is more in two and three fins samples, as shown in Figure 22 and Figure 23. This phenomenon is better understood if we have a look at the thermal resistance bar graph of each sample (Figure 24). Clearly

with increase in number of fins the thermal resistance decreases subsequently, thus easing the faster flow and dissipation of heat from the heat sinks at much larger rate as compared to single fin heat sinks.

Table 4 Summary of the experimental findings

Heat Sink	**No. of Fins**	**Porosity (%age)**	**Pore density (PPC)**	**Flow Speed (m/s)**	**Orientation (degree)**	**Final Temp. (°C)**	**Total Temp. drop (°C)**	**R_{th} (K/W)**
Solid	1	N.A	N.A	3.6	90	53.36	6.72	5.812
M.Foam Glued	1	93	4	3.6	90	54.90	5.12	6.092
M.Foam Thermal Spray Coating	1	93	4	3.6	90	49.08	11.01	4.908
				2.6	90	53.38	6.70	5.812
				1.6	90	57.46	2.54	6.612
				3.6	45	51.05	8.89	5.318
				3.6	0	53.76	6.18	5.9
	2	93	8	3.6	0	44.88	15.17	4.056
					45	42.75	17.25	3.678
					90	46.28	13.80	4.236
	3	93	8	3.6	0	38.81	21.19	2.858
					45	36.17	23.83	2.312
					90	40.81	19.19	3.28

CHAPTER 6

Metal Foam 3D MODELING

In many areas of research and development, it is sometimes desirable to create a geometric model of an already prevalent complex shaped object that is not easy to create manually. For such tasks, researchers usually prefer the recent upcoming technique called reverse engineering. Reverse engineering is a procedure of extracting information or blueprint contents of anything that has been synthesized by humans. The process usually involves the dismantling of the specimen under study, for scrutinizing its components and analyzing them in detail [75].

With the advancement of computational power resources, this practice which was done manually in the old industrial era is now done on computers. Software like Computer Aided Drawing/Design (CAD), Finite Element Analysis (FEA), Computational Fluid Dynamics (CFD), Computer Aided Engineering (CAE) and Computer Aided Manufacturing (CAM), make use of these 3D models that have been captured using various 3D scanners. The reverse engineering technique measures the physical object and then reconstructs it as a 3D virtual model. The physical specimen can be captured by means of 3D scan technologies like Laser scanner, Structured Light Digitized (SLD) scanner, Coordinate Measuring Machines (CMM) and Computer Tomography (CT) scanner.

6.1 CT Scanning

6.1.1 Working Principle

Keeping this background in knowledge, we see that the complex and free-form shape of metal foams poses a challenge in 3D finite element modeling. This has also been verified in the detailed literature review that researchers opt for simple 3D models in analysis; because of the same reasons of perplexity in shape. As already explained, one of the most efficient ways to generate Finite element (FE) models of such objects is by means of serial imaging techniques. These serial images can be obtained by using any of the following methods:

a. Computerized Tomography (CT)
b. Confocal Microscopy
c. Magnetic Resonance Imaging (MRI)

CT technique is utilized for the fulfillment of this task. It is a non-destructive technique used for capturing the internal and external structural geometry of the components using irradiations (usually X-rays). CT scanning is used for both medical and industrial purposes. Further there are different types of CT scanners:

a. Spiral (or Helical) CT
b. HRCT (High resolution)
c. Micro CT (Microwaves)

An industrial desktop version of Micro CT – model Skyscan 1172 was used in this work. Figure 25 shows the picture of the CT scan.

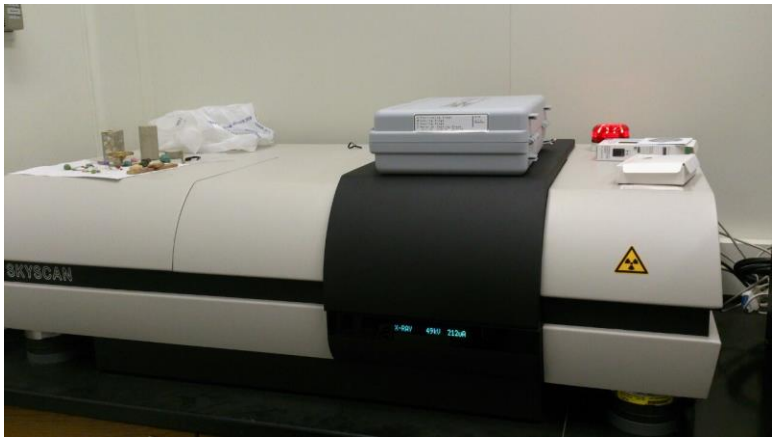

Figure 25 Skyscan 1172 Micro CT

The working principle of all CT scanners is more or less the same, as shown in (Figure 26 A). Usually an X-ray source is used to irradiate the specimen. The X-rays being highly energetic electromagnetic waves easily pass through the test object and finally fall on a fluorescent screen or a detector film to form the respective image. The sample or the X-ray source are than normally rotated a complete 360 degree to ensure that all the object has been thoroughly captured.

A CT image is generally called a slice (Figure 26 B), as it would show how the specimen being scanned would appear if it were sliced open alongside any plane. Similar to a bread loaf slice, a CT slice represents a certain thickness of the specimen that has been scanned. A distinctive digital image is compiled up of pixels (2D picture elements) and on the

contrary a CT slice image is made up of voxels (3D volume elements). Like a bread loaf can be reconstituted by stacking up all of its constituent slices, a complete 3D representation model of an object can be obtained by juxtaposing neighboring sets of CT slices. This complete process of reconstruction by CT slices is called Tomography.

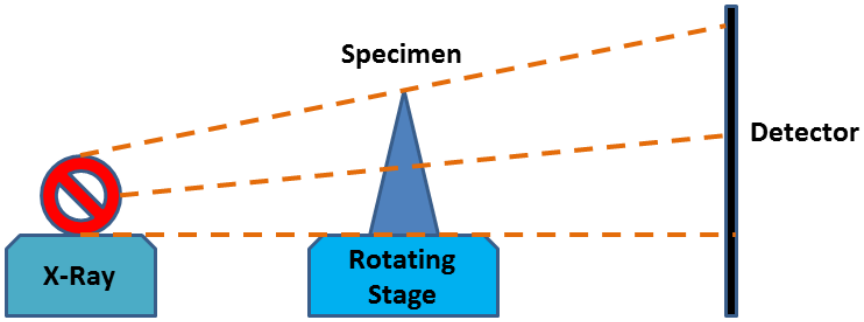

(a)

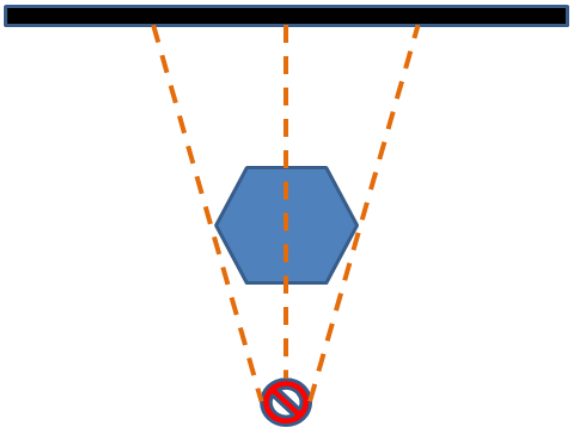

(b)

Figure 26 CT Scan Working Principle: (a) A Schematic of typical assembly and (b) a CT slice

6.1.2 CT Imaging

CT scan was performed on a sample of Aluminum (6101) alloy metal foam in Skyscan 1172 as shown in Figure 27. Porosity of this metal foam sample was 93% and pores density was 4 PPC. Sample size used for the scan was 25 x 25 x 6.35 mm. This size was chosen so that a minimum of two times the PPC of the sample is captured in both length and width directions.

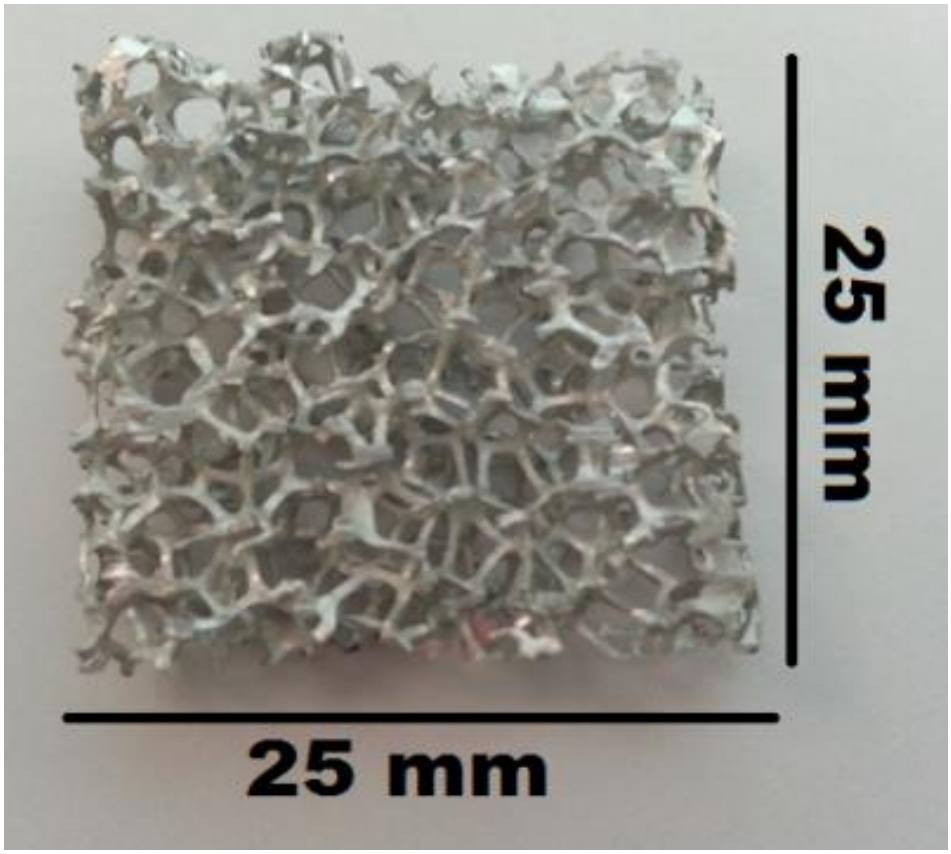

Figure 27 Sample for scan

The sample is first held tightly on a sample holder so that it does not get displaced during the scanning process. As the sample stage is rotating continuously during the scan, even slight vibrations can cause a significant amount of noise in the images. Once the sample is placed inside the scanners' chamber, X-ray source is turned on from "Skyscan" software. It takes a while to heat up the X-ray source and once it's ready the red light on top of the CT scanner starts to blink. This can also be verified from the software. Figure 28 shows the interface of software when it is opened. Refer to the Figure 28 for standard operating procedure (S.O.P) of a typical scan:

1) *Mark 1* in Figure 28 appears when the X-ray source is heated up and ready to commence operation.
2) *Mark 2* in Figure 28 is pressed to illuminate the inside of chamber that gives visual aid for some of the subsequent steps in the process.
3) Sample (*Mark 3*) can be seen clearly in the display window then.
4) The position of the x-ray source and the detector is vital for proper acquisition and can be adjusted by the bar at the bottom center right position of the window (*Mark 4*).
5) Still Pictures or real time view of the sample can be taken by pressing the 'grab image' or 'snap image' options on the top left of the screen on the tool bar (*Mark 5*). These displays appear in the window at *Mark 6*.
6) The sample holder (and hence the sample) can also be rotated by adjusting the bar on the bottom right corner (*Mark 7*).
7) The height of the sample holder can also be changed by pressing the up or down green arrow buttons on the bottom right of the window (*Mark 8*).

8) The filters are required depending on the density of the sample. If it is of low density no filter is used. If the sample is of medium density, “Al” 0.5mm filter is used and saving the “Al+Cu” filters for the densest. The button is located on the extreme right bottom corner of the window (*Mark 9*).

9) Once all the settings are done, data acquisition is started. *Mark 10* shows the status of scan and also the approximate time remaining to finish the job.

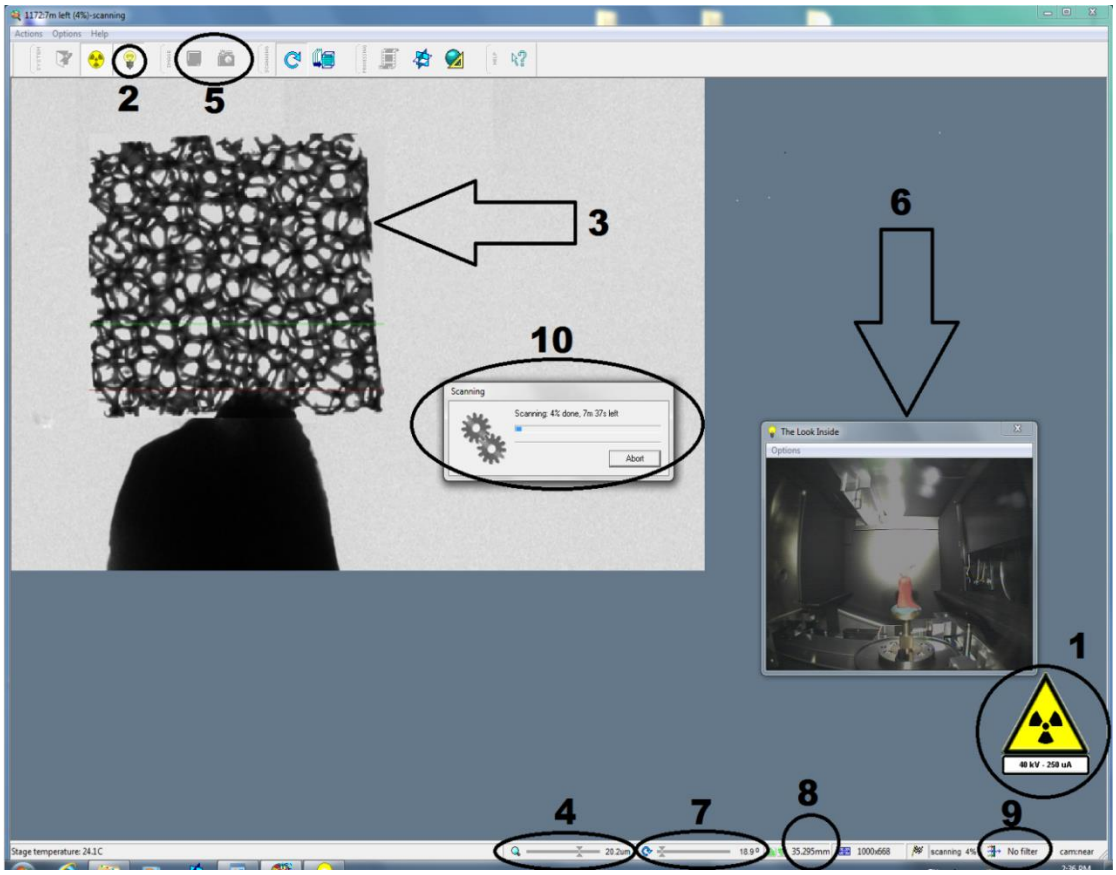

Figure 28 Interface of Skyscan software

After a series careful trials, a set of parameters which gave the most optimum 3D model as the end result was achieved. X-ray source voltage of 40 kV and source current of 250 µA was used. Total numbers of slices captured were 512 by keeping the rotation step to 0.7º (degree). Exposure time was set to 90 ms, with average of 2 frames per angle step. Scanning trajectory was round, so complete 360º rotation was made of the sample to ensure thorough and complete capture of the sample. Total scan duration was approximately 15 minutes. To ensure a good quality of serial slices image pixel size was set as 27.34 µm. As our sample is a low density material so no filter was used (as filters should be preferred for moderate to high density materials). All the slice images were saved in .tiff (16 bit) format – as like other formats it doesn't require much manipulation at later stages of 3D model reconstruction.

This model of CT scanner cannot capture the serial images of a sample whose size exceeds 18 mm. But as already mentioned our sample is 25 mm in height, so a total of 2 scans were taken – keeping the parameters constant (i.e. one for the lower half and one for the upper half). Later these 2 parts were conjoined together in the reconstruction phase of image processing. The parameters used for imaging are summarized in the following Table 5:

Table 5 Imaging parameters

Camera=Hamamatsu C9300	11Mp	**Number of connected scans**	2
Camera Pixel Size (µm)	9.00	**Image Pixel Size (um)**	27.34
Number of Images	512	**Object to Source (mm)**	258.500
Image Format	TIFF	**Camera to Source (mm)**	340.475
Depth (bits)	16	**Vertical Position (mm)**	27.855
Source Voltage (kV)	40	**Rotation Step (degree)**	0.700
Source Current (µA)	250	**Use 360 Rotation**	YES
Filter	No filter	**Scanning Trajectory**	ROUND
Median Filtering	ON	**Rotation Direction**	CC
Frame Averaging	ON(2)	**Exposure per Image (ms)**	90
Random Movement	ON(10)	**Scan duration (minutes)**	14.5

6.1.3 Image Reconstruction

The initial 3D rendering "Skyscan NRecon" package is used at first. This is the CT scanners own software, so it automatically recognizes the native format – though external data from other sources can also be imported for reconstruction. Parameters set at this phase will greatly influence the quality of final 3D model, so a significant emphasis is to be laid on an optimized set of variables.

As previously mentioned, 2 scans were taken due to height of sample exceeding the upper limit of CT scan. For this a standard reconstruction mode was chosen and reconstruction of both scans was connected after applying computer calculated default pre/post alignment values – resulting in a single model file. A Gaussian smoothing kernel with a medium value of 7 is used. Ring artifact reduction and beam hardening correction is also applied to remove any unnecessary background noise, thus resulting in sharp images. It is important to note that no density threshold was set for reconstruction of our sample, as in our case the material distribution is almost constant and interest is in capturing the sample as a whole. Final images are saved in .bmp (8bit) format. Unlike other formats this does not require any compression factor before saving. The parameters used for imaging are summarized in the following Table 6 and Figure 29 shows the interface for "Skyscan NRecon" software:

Table 6 Reconstruction parameters

Reconstruction mode	Standard	**Pixel Size (µm)**	27.34
Post alignment	-3.50	**Smoothing**	7
Sub-scan post alignment	-4.0	**Smoothing kernel**	Gaussian
Total Reconstruction (parts)	2	**Ring Artifact Correction**	20
Result File Type	BMP	**Threshold (%)**	0
Angular Step (degree)	0.70	**Beam Hardening Correction (%)**	68

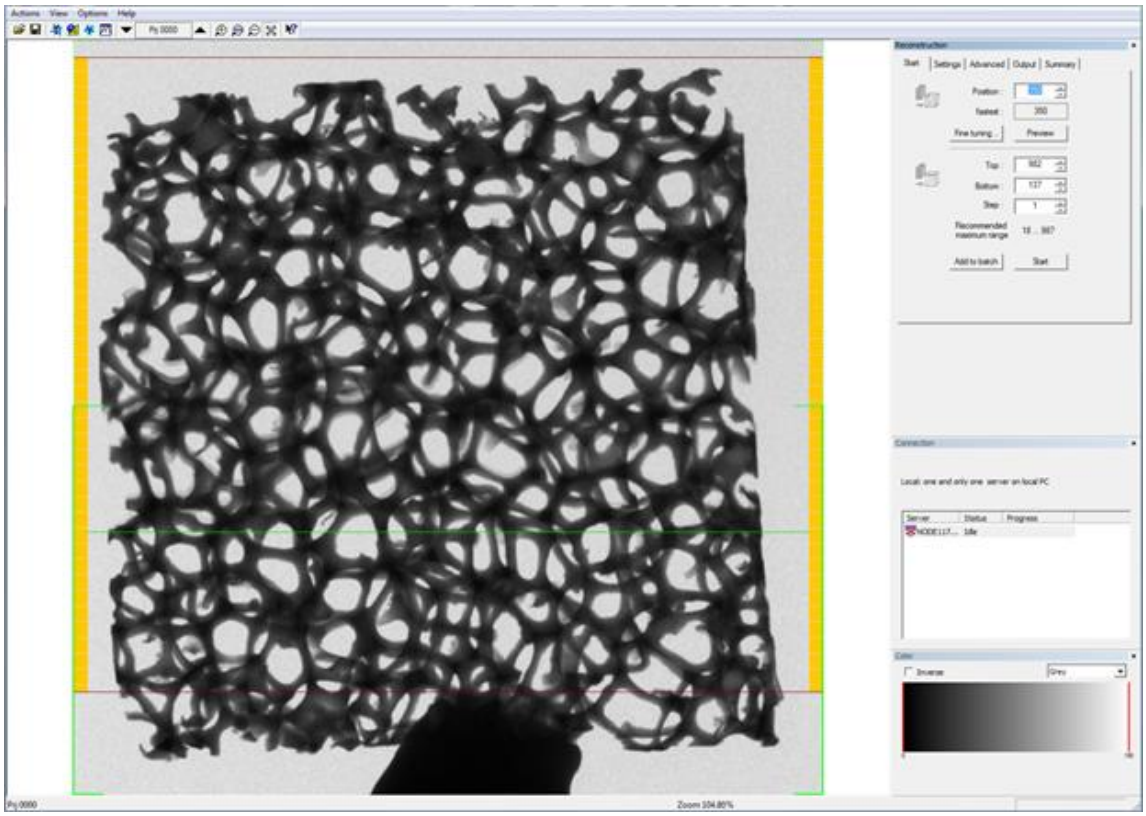

Figure 29 Interface for Skyscan NRecon software

"Skyscan CTan" is the next package that comes with the CT scanner. It is used for constructing visual 3D models from images that were reconstructed by 'Skyscan NRecon'. The 3D surface rendered by Skyscan CTan can be viewed and manipulated in "Skyscan CTvol" (also CT scanner software). CTan provides us with an option of saving the surface model (it's not solid!!!) in variety of formats. In our opinion and from literature, .stl (Stereo Lithography) works best, as it is an industrial standard surface rendered model used as an input for other commercially available software that manipulate 3D models. Stl also gives the option to save the model in terms of units of length (mm, µm, cm etc.), thus depicting the true size of sample in real life.

The image in Figure 30 shows the interface for “Skyscan CTan” software. As seen it only displays one single slice at any particular selection. Here a suitable slice is chosen and parameters are varied to see the changes by visual aid. Once the parameters are finalized the generate button is hit to create first raw 3D model. And the image in Figure 31 shows “Skyscan CTvol” with the final 3D surface model displayed:

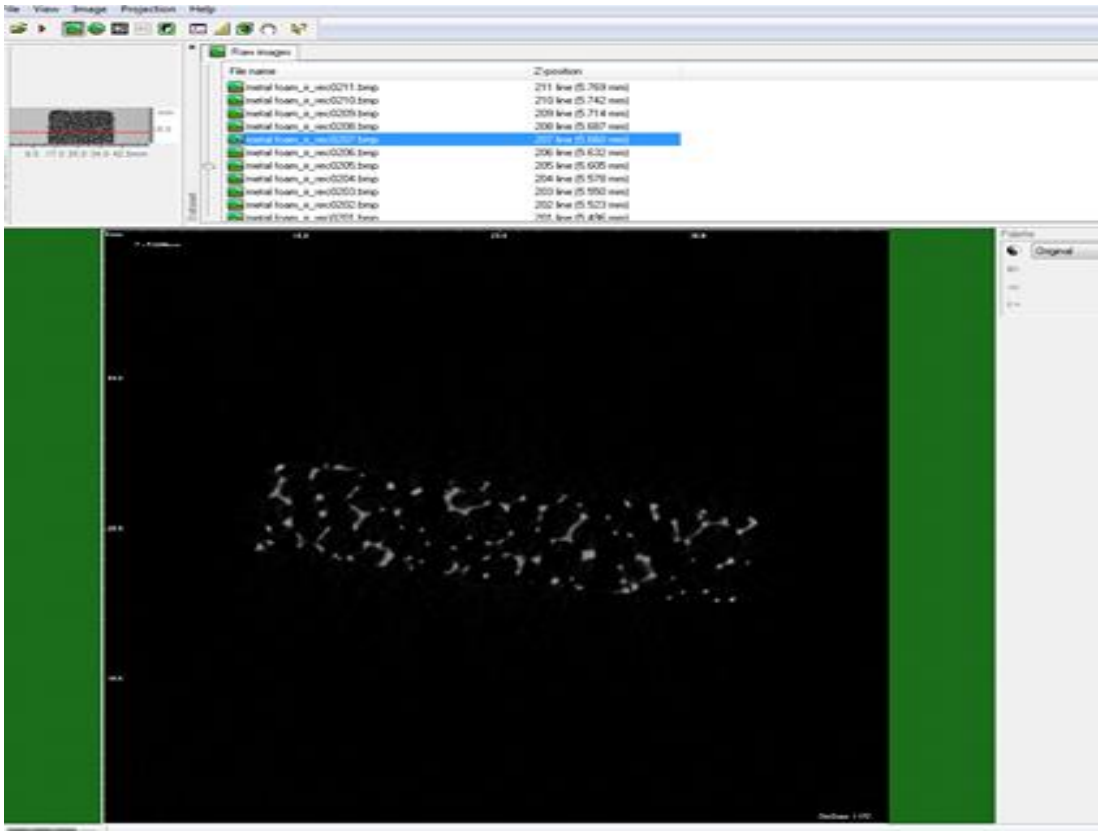

Figure 30 Interface of Skyscan CTan showing a single slice of the scanned object

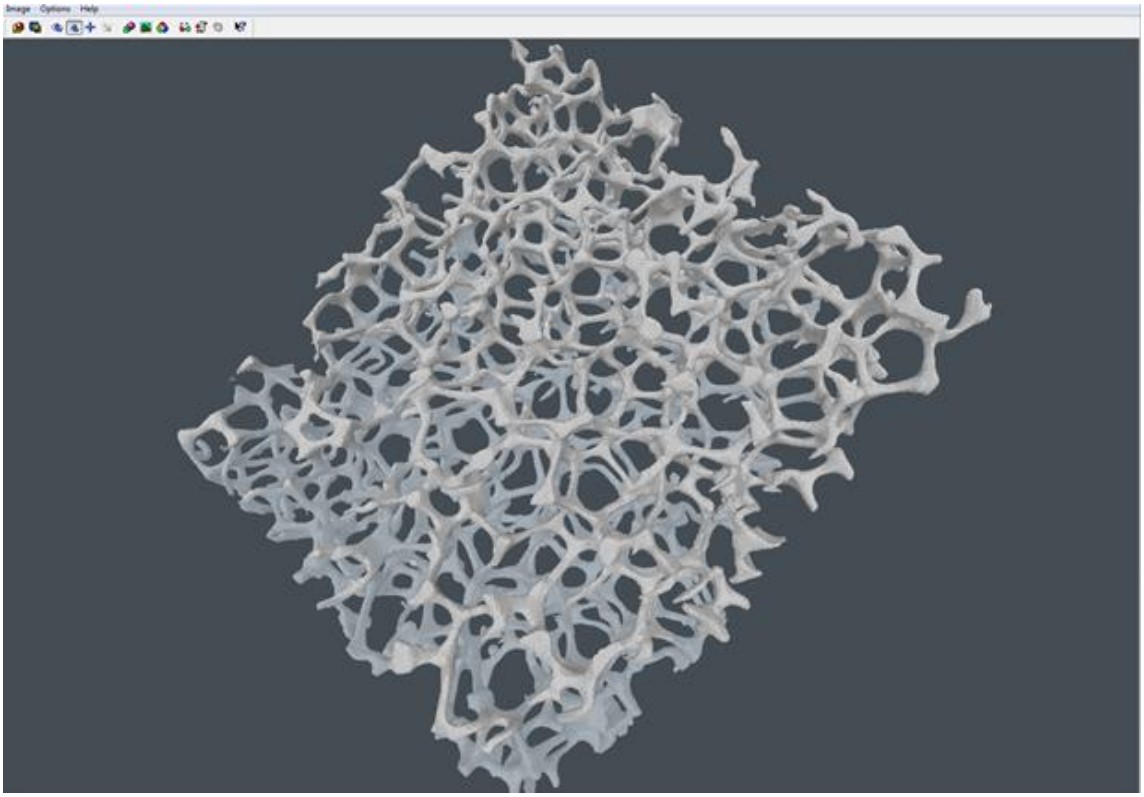

Figure 31 Interface of Skyscan CTvol showing 3D model of the scanned object

6.2 Metal Foam Image Processing

The initial 3D surfaced model is generally quite rough and requires an ample amount of editing before they can be imported into a FE tool and successfully meshed for analysis. So for “cleaning” of these rough surfaces “Geomagic Studio” was opted out of other commercially available editing tools. 3D model created by CTan of Skyscan 1172 is imported in Geomagic. The 3D model as explained earlier is imported in .stl format. Other formats can also be used but .stl makes editing and importing comparatively quite easier related to other ones. Figure 32 shows the imported .stl file in Geomagic Studio.

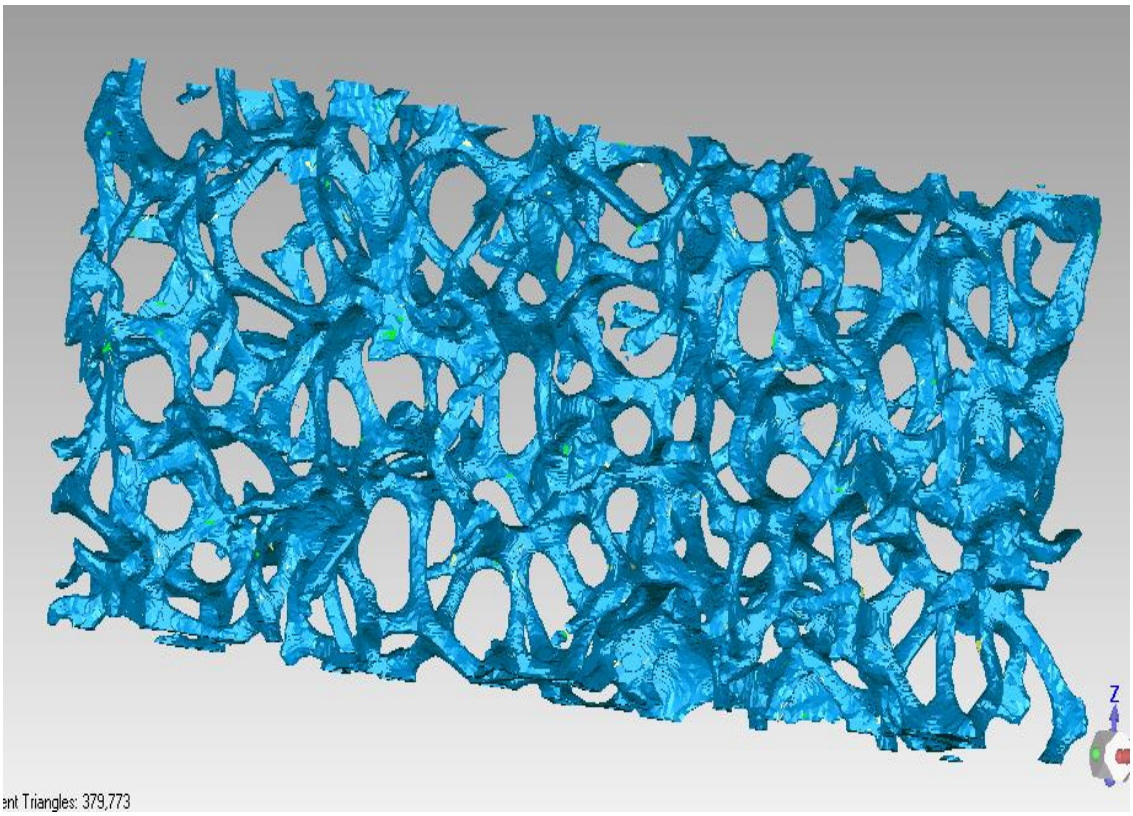

Figure 32 Rough imported model

It is visually evident from Figure 32 that this model cannot be used directly in FE analysis or for that matter in 3D printing too. After import, the geometry check option available in Geomagic Studio reveals hundreds to thousands of errors in the imported geometry and as shown in Figure 33 the software automatically highlights those troubling areas in red color. And Figure 34 shows the list of some of these errors in detail. Cleaning steps for the model are highly dependent on the type of errors present in the imported model.

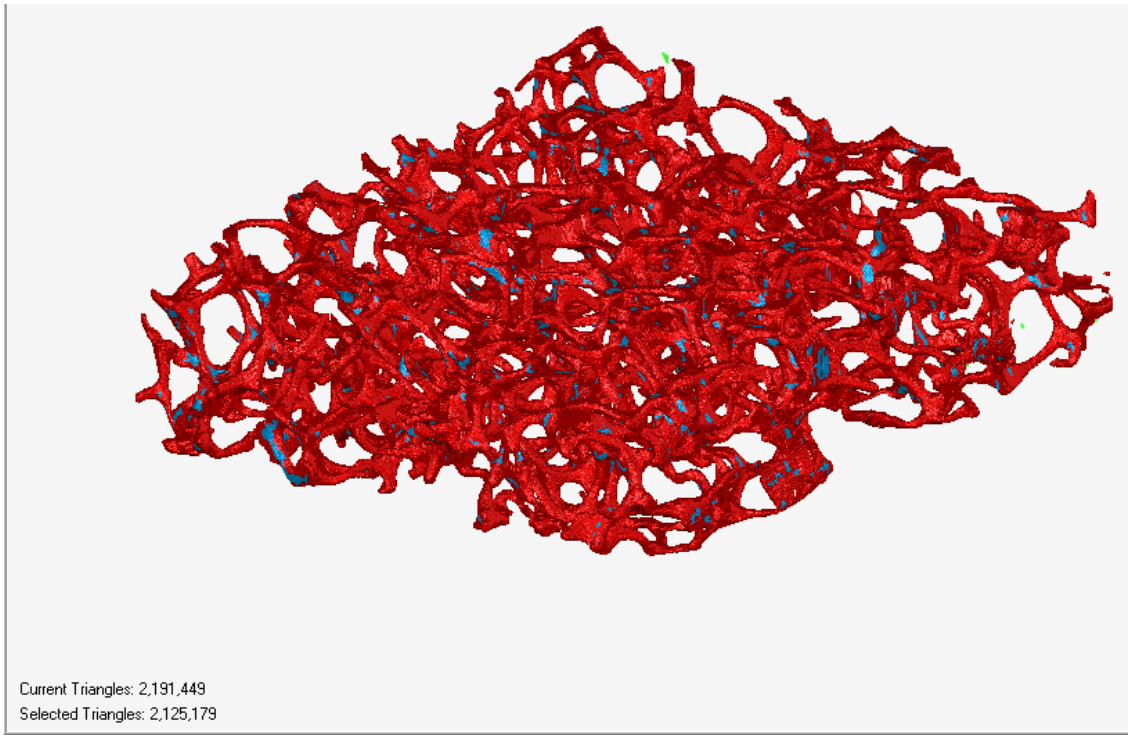

Figure 33 Red regions showing errors in geometry

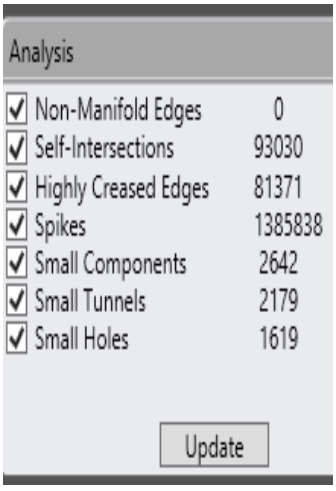

Figure 34 Geometry check revealing several errors in the imported geometry

When the rough imported model is trimmed in half along any plane, it reveals that the model is hollow from the inside. As expected, this way it is made sure that the model is only a surface or skin model and not a solid model. But as shown in Figure 35 there are inner surfaces present too. These appear during image reconstruction in CT scan software and are because of very slight density difference in the material.

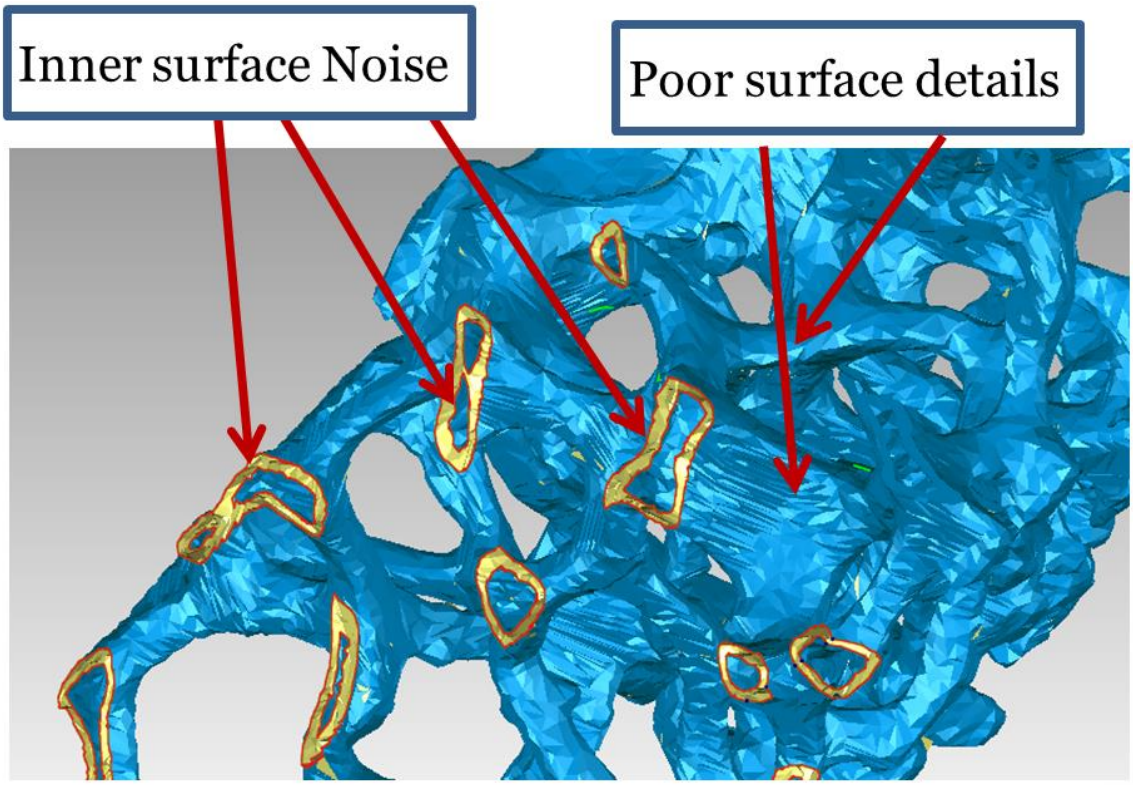

Figure 35 Trimming the cross-section of rough model

All the common occurring errors like self-intersections, highly creased edges, holes, floating components etc. are taken care of with help of problem specific tools available in Geomagic Studio. The inner surfaces are also manually removed alongside the process. The model is frequently geometry checked for seeing how the tools applied are affecting the model's errors. This lengthy procedure is continued until the model is free from all types of errors. Figure 36 shows the trimmed section of cleaned model, exposing the removed inner surfaces too.

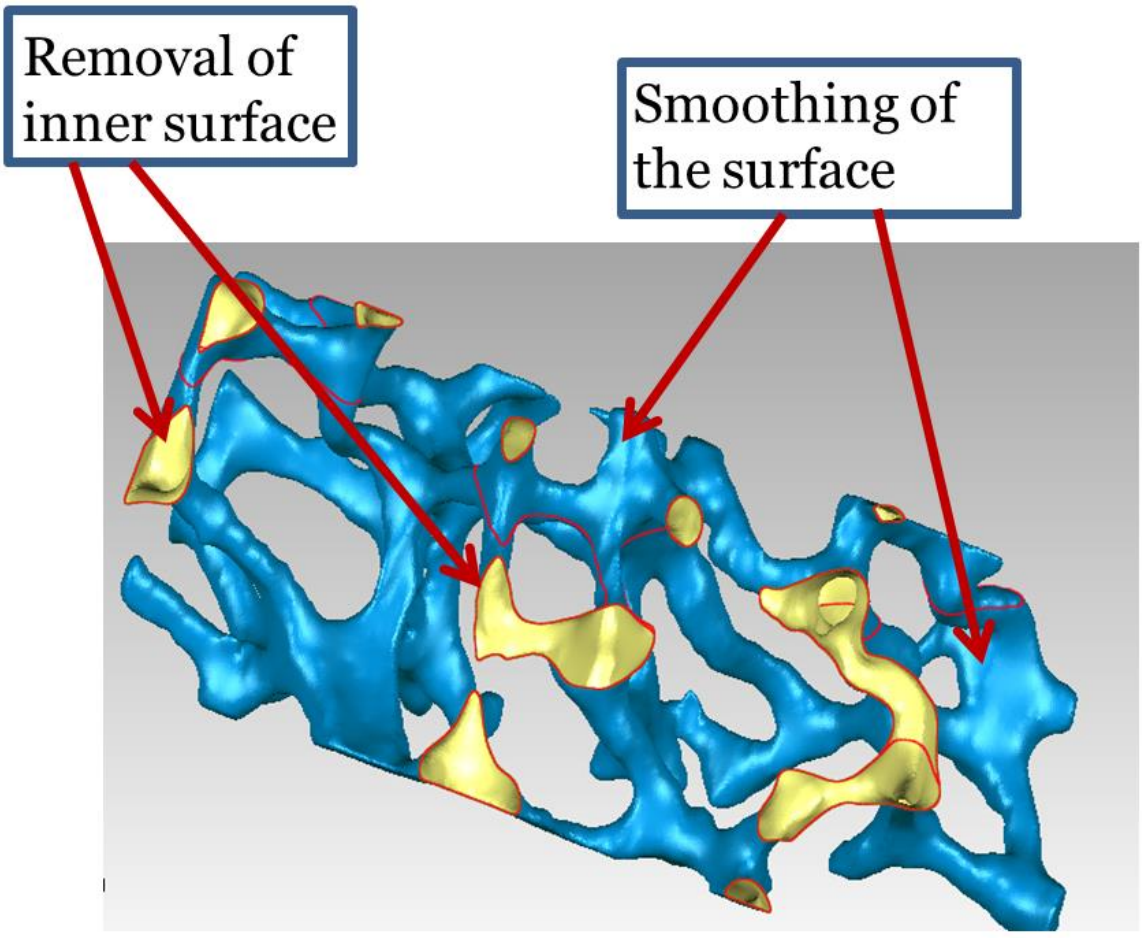

Figure 36 Smoothing of metal foam sample

Figure 37 shows the close up cleaned surface/skin model. If it is compared with initial rough imported model in Figure 32 it is apparent that this model is very smooth on the surface. This type of cleaned model is now suitable for 3D printing or FE analysis as in our case. This cleaned version of the model is also sometimes referred to as “water-tight” model. To envision a water-tight model simply imagine a hollow skinned object. If this object were to be fully immersed in water the insides of the object should remain dry. In other words the model is free of holes/gaps and errors in the model.

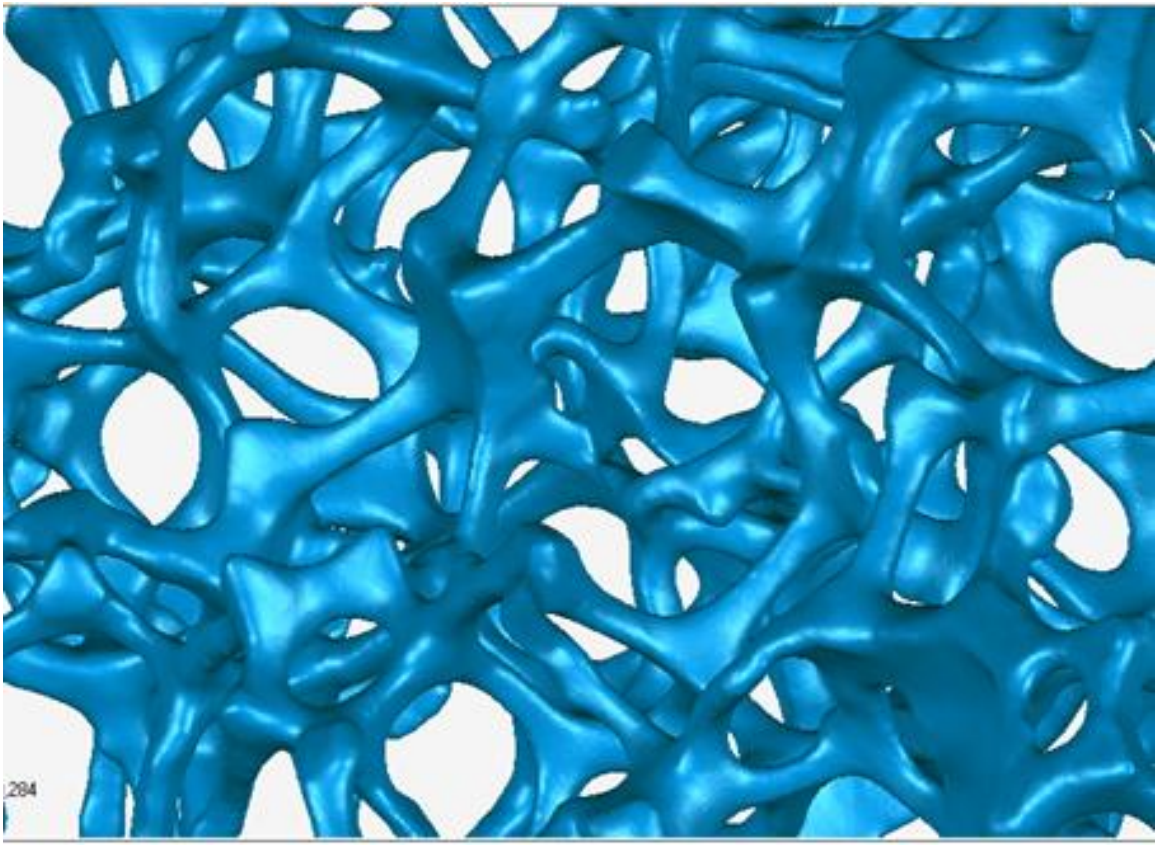

Figure 37 Cleaned model close up

Another very important service rendered by Geomagic Studio is to reduce the overall size of the model in terms of number of triangles (or surfaces). Greater the number of triangles, greater is the size of model and vice versa. Also the large size means more computational resources are required. Figure 38 shows the cleaned surface model with almost 3.8 million surfaces. This is a huge number of surfaces even for a high end computer.

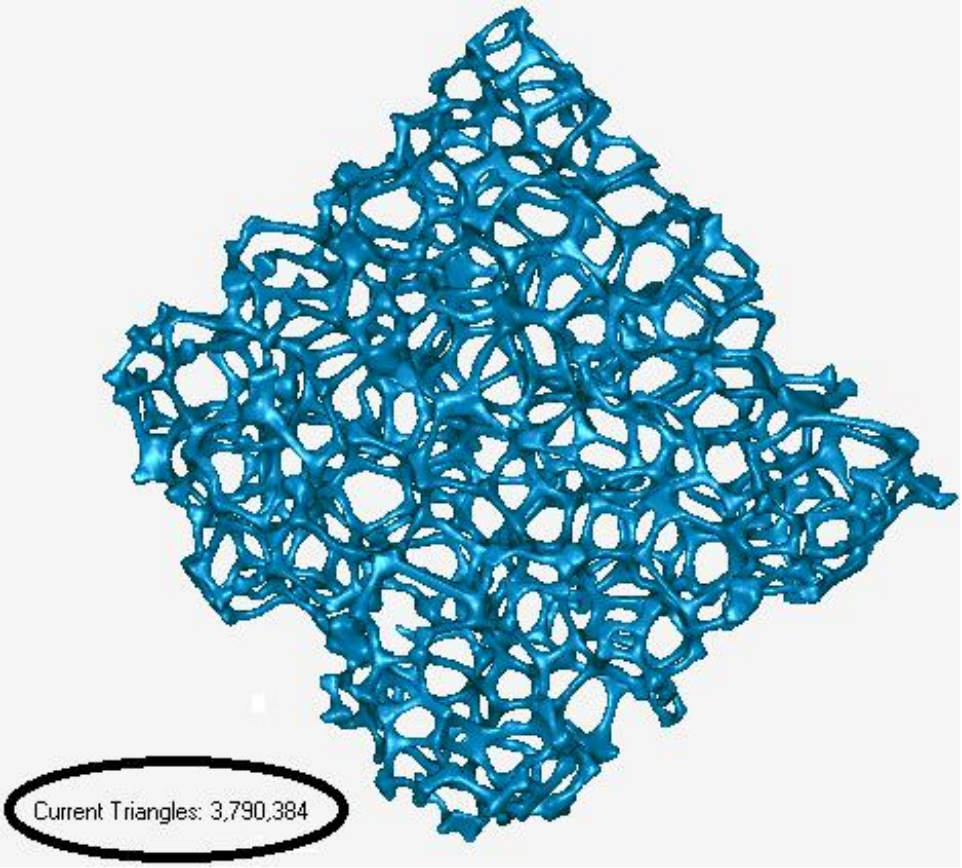

Figure 38 Cleaned Stl model (watertight)

Surfacing tool in the software groups together certain number of triangles and makes them into a single surface, thus reducing the overall number of triangles in the model. Figure 39 shows the model after being surfaced. The new grouped surfaces are now called patches and as seen the number is reduced to almost 16 thousand. Most importantly the model has been optimized, without compromising the original shape. This model is now small in size and will run even on normal PCs.

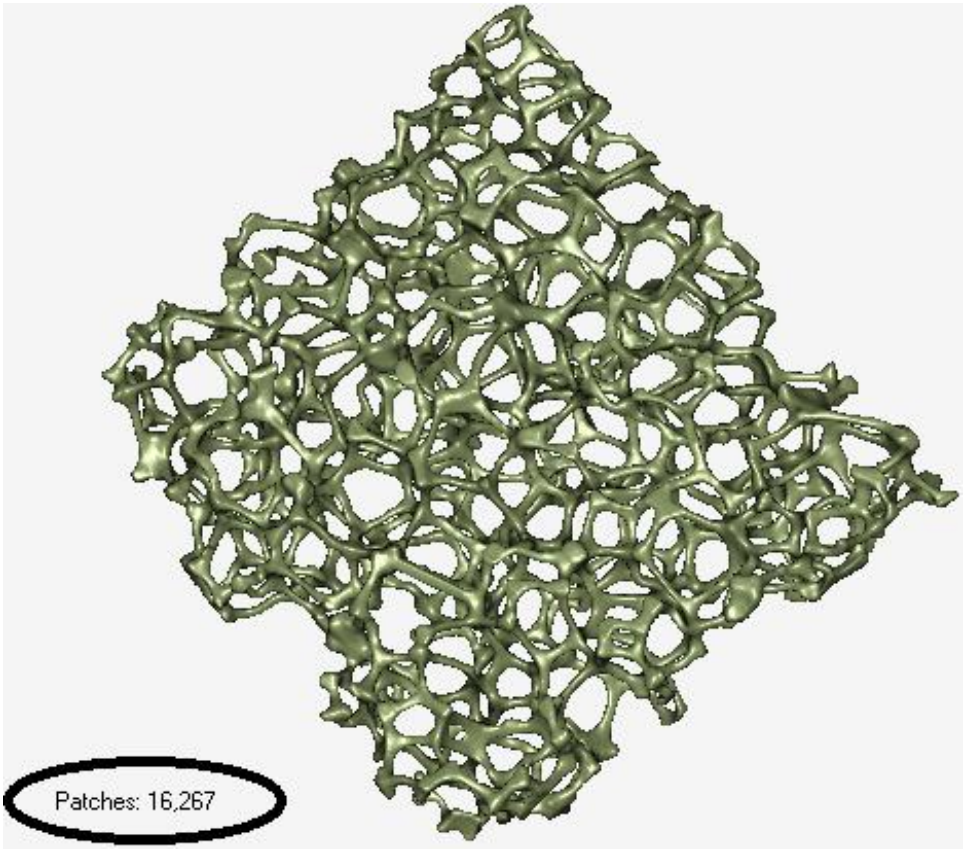

Figure 39 Optimized surfaced model

6.3 Surface to volume/solid model

Once our metal foam model is free from all errors, the surface model can be imported to a FE package in .stl format, a mesh file or any CAD format. Most of the new FE software can deal with .stl directly. But even the thoroughly cleaned .stl surface models usually cause flaws when imported directly to FE software for analysis. So an attempt made by FE software to make a solid mesh out this error containing model is failed. Some FE software provides with an option to again fix these problems causing a successful mesh, but this approach is quite hectic and cumbersome. To overcome this scenario in advance the model is imported in a Computer Aided Design (CAD) format, which is recognized by all prevailing FE software and SolidWorks was used for this purpose. The cleaned surface representation was imported into SolidWorks and with its available powerful tools the ‘surface’ model was converted into a ‘solid’ CAD model. Out of all acquirable CAD formats, ‘parasolid’ format works best with all FE packages. Figure 40 shows final cleaned SolidWorks volume/solid model. For FE analysis we found ANSYS Workbench to be quite useful for our task.

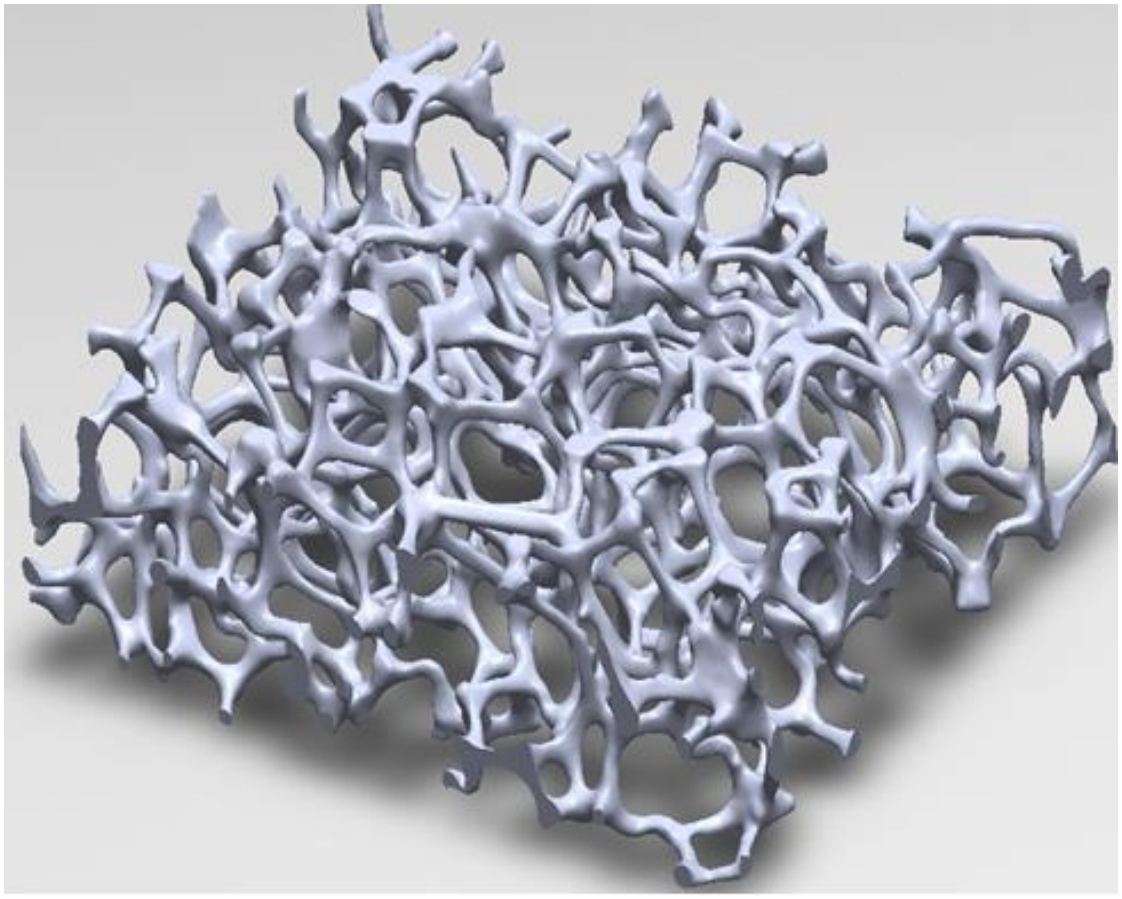

Figure 40 SolidWorks volume/solid model

6.4 Summary

The following flow chart in Figure 41 summarizes the whole procedure from start of scanning to the end of final solid/volume model. Numbering in the figure are: (1) Aluminum alloy metal foam sample, (2) Skyscan NRecon, (3) CTvol, (4) Geomagic unclean raw geometry, (5) Geomagic cleaned raw geometry, (6) Geomagic clean 3D surface model and (7) SolidWorks 3D volume model.

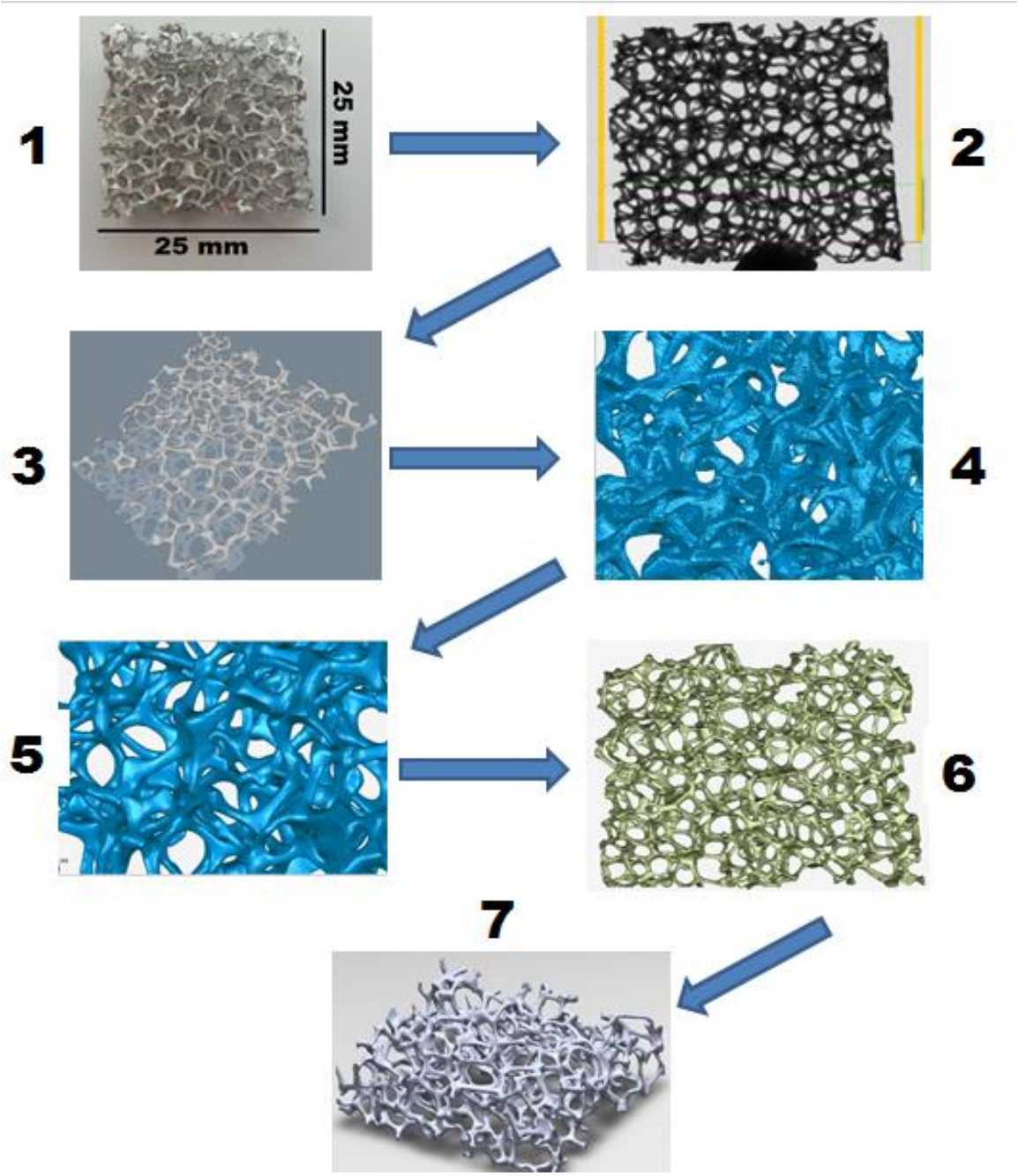

Figure 41 Flowchart steps for creating 3D metal foam model

CHAPTER 7

NUMERICAL STUDY

Most metal foam systems studied are usually simplified to get analytical or closed form solutions for them. But in reality the physical world is way too complex to be modeled to exact precise depth of detail. And most of them cannot be simplified to obtain an analytical solution, or even if obtained, they lack the accuracy to depict the real solution. Thus analytical solutions of such systems cannot be obtained. For such systems, the computer-based techniques such as approach of finite element modeling can be used.

The 3D model rendered using CT scan can be used to run a number of different simulations in different FE packages. The surface model as explained in the previous section was converted to solid/volume model using SolidWorks. SolidWorks was also used to make the heat sink models used in the simulations. Following section discuss in detail the modeling of Heat sink and their different simulations.

7.1 Computational Modeling of Heat Sinks

SolidWorks has been employed for FE model generation of the heat sinks used in the experimental setup. Dimension of the FE models have been kept exact same as that of the real heat sinks. In the experimental sample fabrication it was explained in detail that the metal foam heat sink's fin and base were two different units which were joined together using either glue or thermal spray coating. Same technique has been opted for the

computational FE model generation, i.e. the metal foam and the base were modeled separately and then glued together in the SolidWorks software. Size of each respective heat sink has been fixed to that of its experimental counterpart. Dimensions of the heat sinks are explained already in table X and inn the schematic of figure X. Figure 38 shows the drawing generated by SolidWorks for a single fin heat sink.

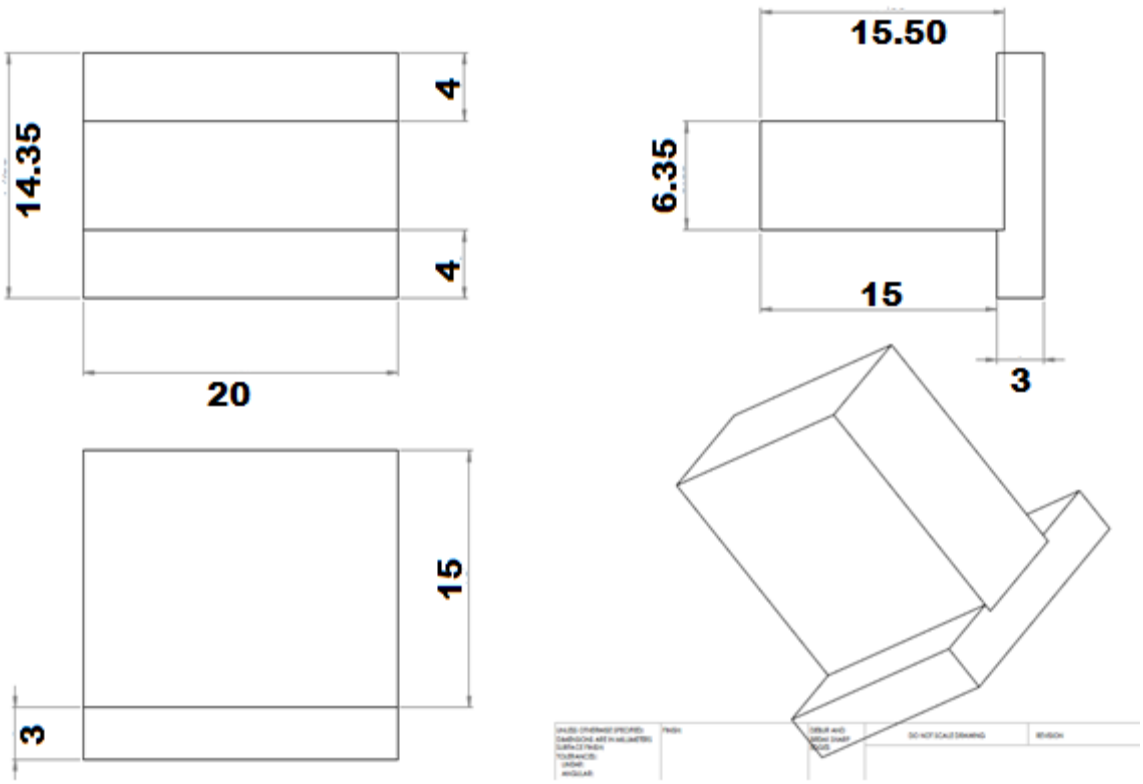

Figure 42 SolidWorks drawing of single fin dimensions

The metal foam part of the FE model has been made and imported into the SolidWorks from the detailed procedure explained in 3D modeling section. On the contrary, the base

was prepared in SolidWorks using its own CAD tools. Following types of heat sinks were made in SolidWorks for their use in the simulation based FE study.

i. 2PPC__1 Fin
ii. 4PPC__1 Fin
iii. 4PPC__2 Fins
iv. 4PPC__3 Fins

It was mentioned in the computational modeling section that the sample for our scan had 93% porosity and a pore density of 4 (i.e. 4PPC). In SolidWorks, by using the scale feature, the pore density can easily be altered to meet our requirements for the simulation, while porosity of 93% was kept the same as it is just a mere ratio. For example if we "SCALE UP" the model by 50% then its pore density will now be reduced to 2PPC. Similarly if we "SCALE DOWN" the model by 50% then as its pore density will now be increased to 8PPC. Although we did not use the 8PPC sample in our simulations presently but its model has been prepared to show how the scaling procedure works and it could then also be used in future work.

Figure 43 shows the three models that were made by direct scanning (i.e. 4 PPC) and by SCALING (i.e. 2 and 8 PPC) in SolidWorks. And whereas, Figure 44 shows the bases made in SolidWorks for gluing them with the above imported and scaled metal foam fin models. These bases were attached to different metal foam models by gluing to make heat sinks required for our simulation, as shown in Figure 45. These models have been glued so they are two different CAD objects rather than being one single unit as a whole. So their material properties can be controlled independent of each other.

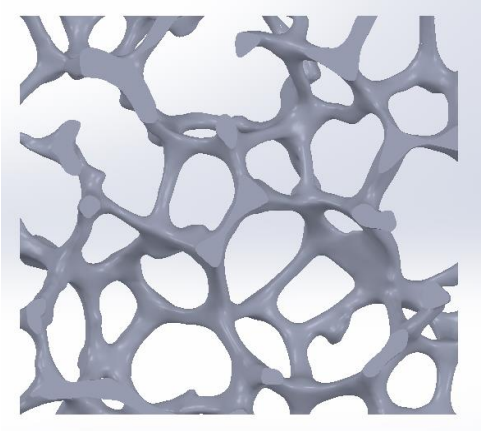

(a)

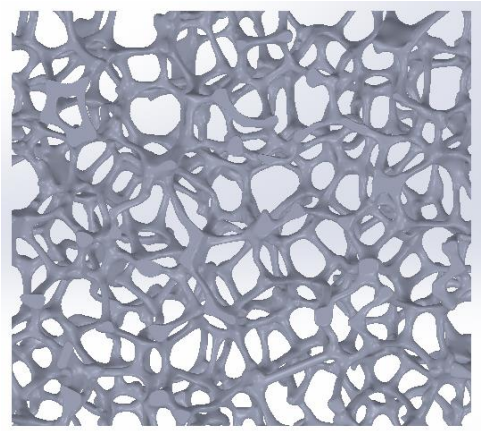

(b)

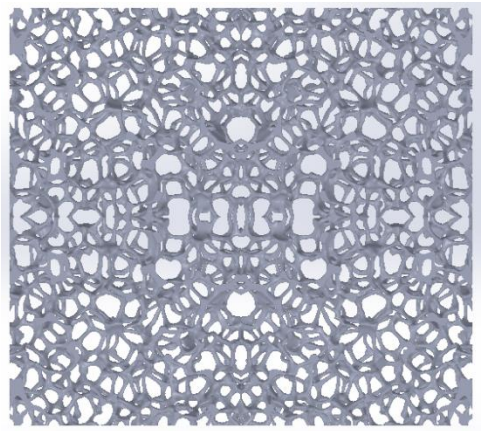

(c)

Figure 43 Different models made by SCALING: (a) 2PPC, (b) 4PPC and (c) 8PPC

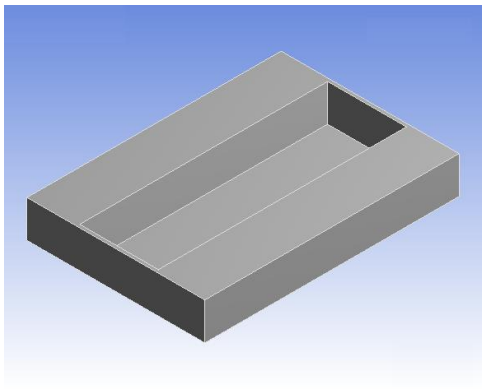

(a)

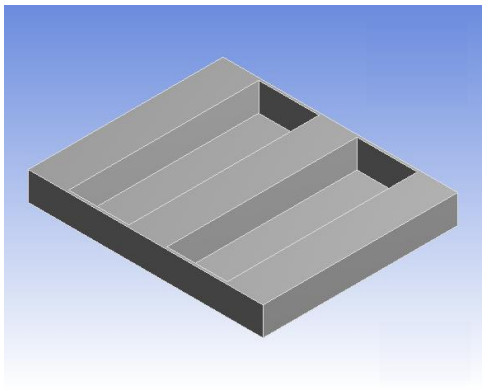

(b)

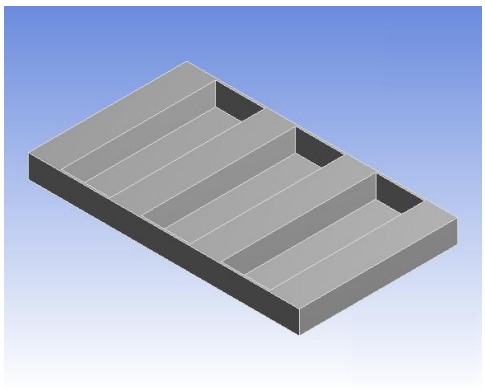

(c)

Figure 44 Different Base models:(a)1 Fin Base, (b) 2 Fins Base and (c) 3 Fins Base

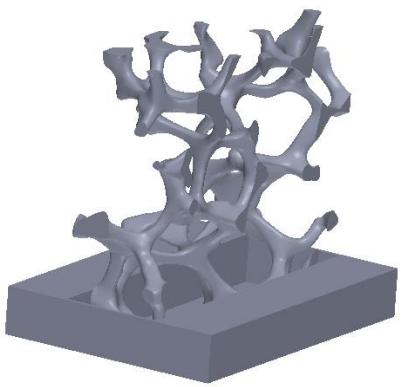

(a)

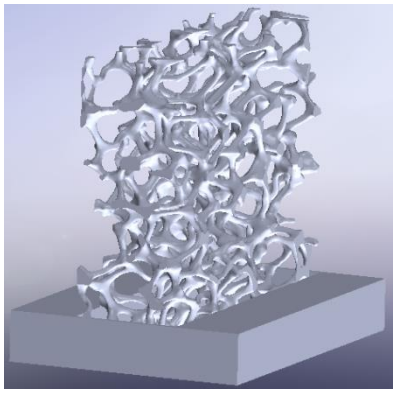

(b)

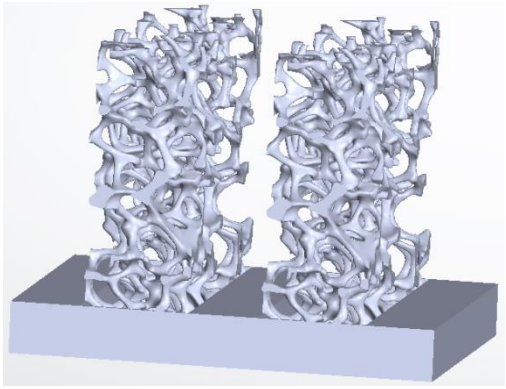

(c)

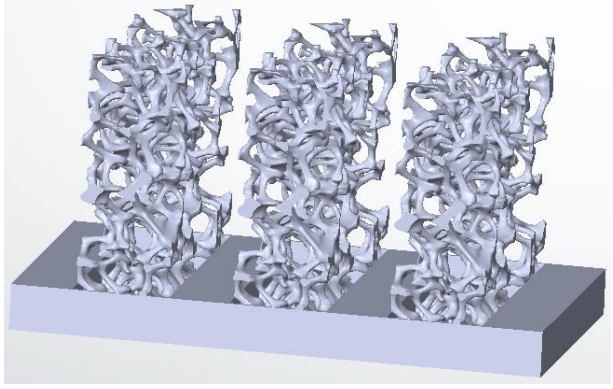

(d)

Figure 45 (a) 2PPC_1 Fin, (b) 4PPC_1 Fin, (c) 4PPC_2 Fins and (d) 4PPC_3 Fins

7.2 3D Metal Foam Heat Sinks FE Simulations

After successfully building the respective models in SolidWorks, they were imported into ANSYS Workbench for utilizing them in FE simulations. The import file format was "parasolid", as it doesn't need any manipulation and cleaning after its import in the FE tool. As explained in the introduction section, metal foams retain most of their physical properties of the parent metal. Metal foam used in our study is Aluminum 6101 alloy, whereas base material is pure Aluminum. As they are alloys of same metal their most thermal and physical properties are common. Table 7 shows the physical and thermal properties of each, which were used for FE simulations.

Table 7 Heat Sink material properties

	METAL FOAM FIN	**SOLID BASE**
Property	**Aluminum 6101**	**Aluminum (pure)**
Density (kg/m^3)	2700	2700
Young's Modulus (Pa)	7.2×10^{10}	7.0×10^{10}
Poisson's ratio	0.33	0.35
Coefficient of Thermal Exp. (C^{-1})	2.30×10^{-5}	2.31×10^{-5}
Thermal conductivity (W/m.K)	218	230
Specific heat (J/g.K)	0.895	0.910

7.2.1 Convective heat transfer coefficient (*h*) calibration

The properties shown in the above Table 7 were available from the vendor. The other unavailable parameters needed for our simulations like heat transfer coefficient (*h*), room temperature, heat source temperature etc. are obtained from experiments. In this section an experiment to explain the calibration of *h* for model's simulation is discussed.

Figure 46 shows the experimental setup. The single fin heat sink sample was placed inside a wind tunnel with room temperature of 24ºC and power input of 1.3W (approx.). For first 60 min temperature was recorded for fan-off conditions (natural convection) and after that for further 30 min, temperature readings were taken for fan-on (forced convection), with wind speed of 1.6 m/s inside tunnel. Temperature was monitored by T-type thermocouples and "Omega HH506RA" was used for temperature data logging. Temperature variations for heat sink over a span of 90 min are shown in Figure 47. As shown, temperature readings were taken of heat source, fin top and fin base.

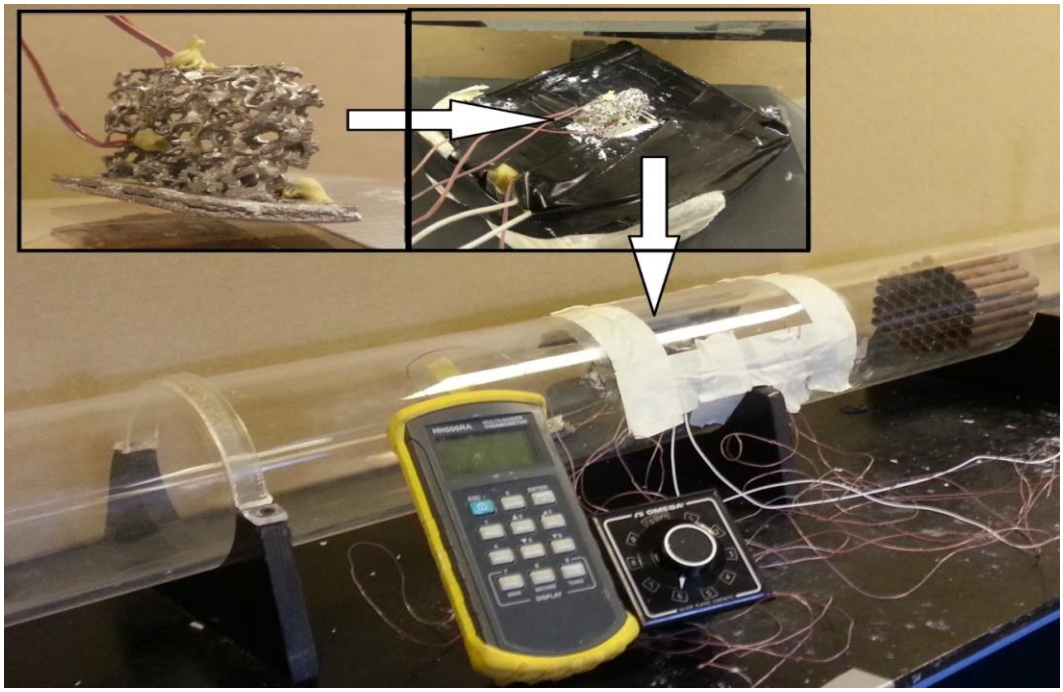

Figure 46 Heat sink experimental setup for h calibration

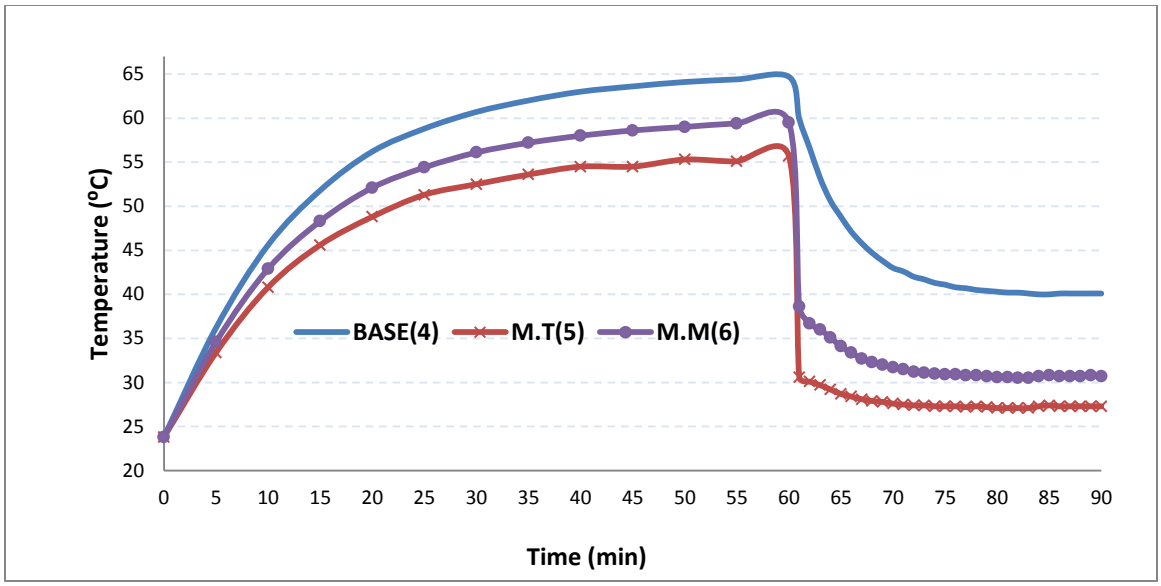

Figure 47 Heat Temperature variation of metal foam heat sink

From experimental data (Figure 47) we can obtain temperature distribution of the heat sink at any time interval. The model is exact replica of the real sample, so base temperature from any instance in Figure 47 was imposed as an input to the base of heat sink model. Thermal analysis was run and *h* was calibrated such that temperature distribution in the simulation matches that of the experiment for that particular instant. This way the *h* value has been acquired for that specific moment only. The procedure was repeated for different time intervals of entire time span of fan-off and fan-on phase. For example Figure 48 and Figure 49 show the temperature distribution of heat sink at steady-state of fan-off and fan-on respectively.

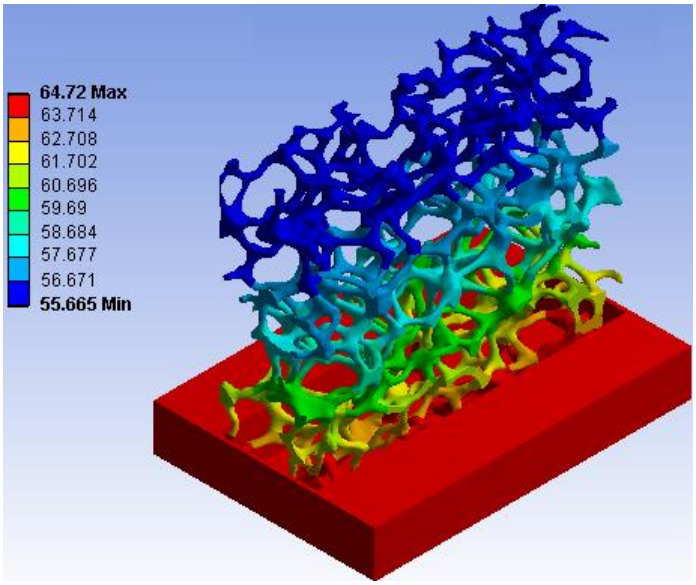

Figure 48 Steady-state temperature distribution at fan-off

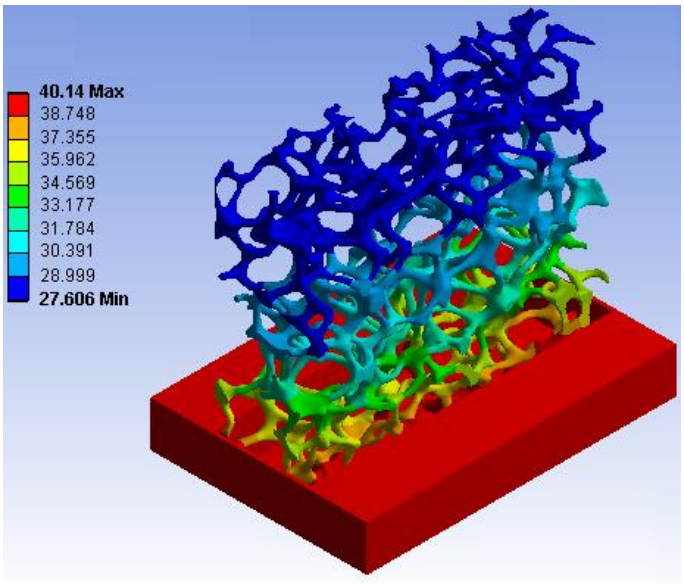

Figure 49 Steady-state temperature distribution at fan-on

Figure 50 shows the calibrated value of *h* as a function of time during fan-on and fan-off. The figure also enlightens the fact that *h* value for fan off is approximately 12.5 W/m2K and that of fan-on is approximately 109.5 W/m2K.

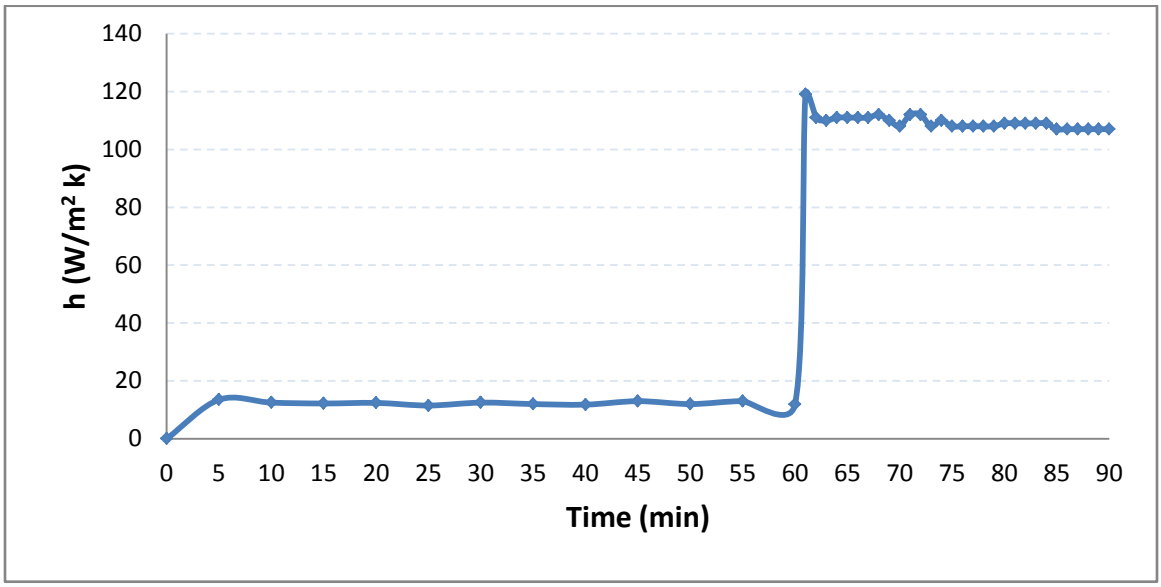

Figure 50 Heat transfer coefficient (h) for single fin metal foam –fan-off and fan-on conditions (4PPC with fan speed of 1.6 m/s)

Similarly, another experimental data was obtained to find heat transfer coefficient (*h*) for fan speed of 3.6 m/s Figure 51. In this experiment the heat sink was heated to 60 ºC by an input of 5W and then the fan was switched on till steady state was reached. Same procedure as in case of Figure 50 was followed to get a new *h* value for this case, as shown in Figure 52.

It is evident from Figure 50 and Figure 52 that *h* is independent of power input, as "*h*=12.5 W/m^2.K" (approx.), for both power input of 1.3 W and 5 W.

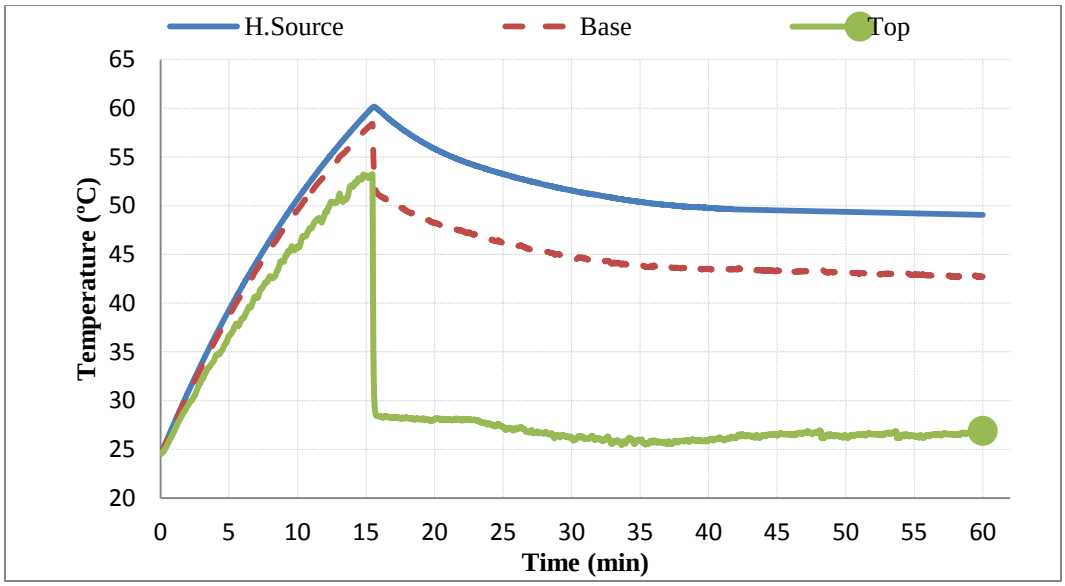

Figure 51 Temperature distribution of the heat sink at 3.6 m/s

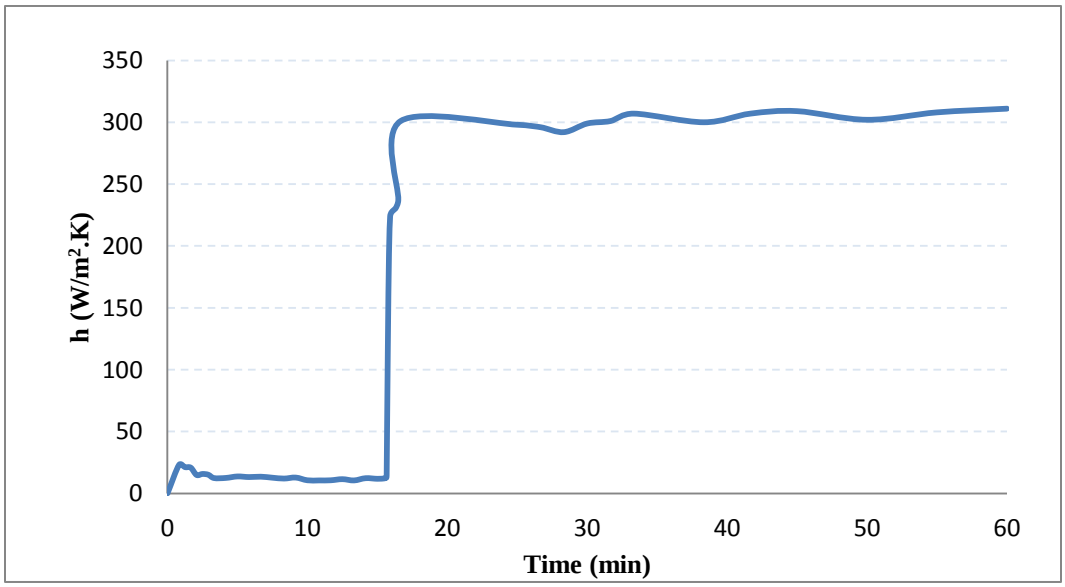

Figure 52 Heat transfer coefficient (h) for single fin metal foam –fan-off and fan-on conditions (4PPC with fan speed of 3.6 m/s)

7.2.2 Validation of FE Model

At this stage all the necessary parameters needed to run the simulation studies are available. Now we need to verify whether our model and technique is suitable for carrying out the numerical study with our claimed accuracy or not. For this we run one numerical study for single fin 4 PPC metal foam heat sink. Test conditions set for this simulation were kept to that of the experiment shown in Figure 19(c) (i.e. 4 PPC single fin heat sink with thermal spray coating). And the *h* values for fan-off and fan-on conditions were taken from Figure 52. The detail of this simulation study has been explained in the subsequent sub-section 7.2.3.

Figure 53 shows the comparison between the experimental findings and the numerical simulation. Numerical plot in the graph shows the transient analysis ran for the same time period as that of the experiment. It only shows the temperature variation of the heat sinks' base with time. This simulated result was compared to heat sinks' base temperature in that of experiment explained by Figure 19(c). It is visually apparent the remarkable similarity in pattern of both results. Though fan-off plot is slightly underestimated by the numerical simulation but fan-on (or forced convection) is in perfect harmony with the experimental data. Even for the underestimation the difference is not more than 8 percent at the maximum. This outcome ensures the reasonable accuracy of our model used in further simulation studies.

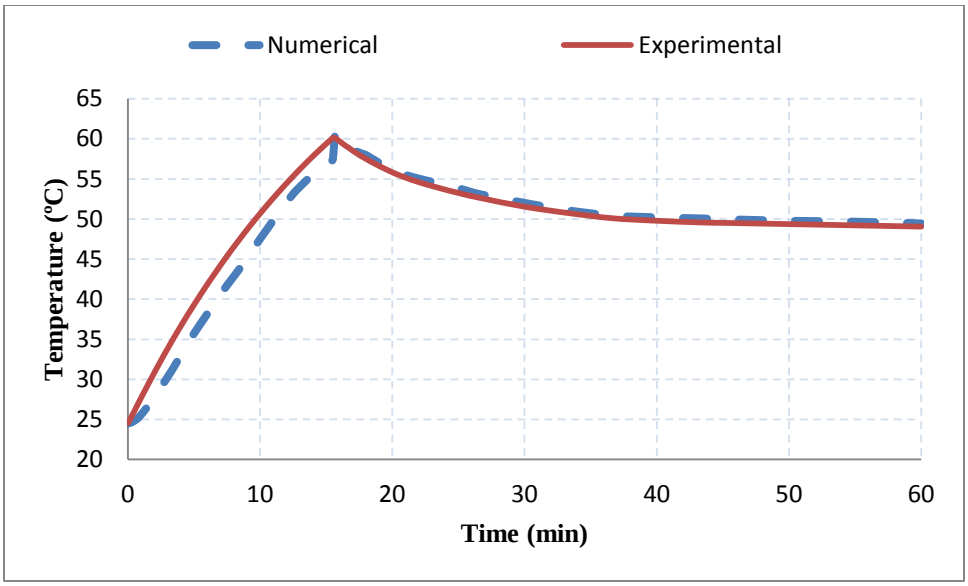

Figure 53 Comparison of experimental and simulation results

7.2.3 General procedure of FE simulations

Now having the confidence in our model and our technique, some general experiments for the sake of comparative study between CAD sample models of different pore density (PPC) and varying number of fins were run.

The particular experimental data in the section 7.2.1 above was only used to determine the value of "h" for our model. Mancin et al. [73] showed that "h" does not depend on imposed heat flux, therefore for sake of comparison only, for all 2 PPC and 4 PPC heat sink models, heat of 1W has been provided to the base. Other boundary conditions for both cases are also same. The simulations were run on the following models:

i. 2PPC__1 Fin

ii. 4PPC__1 Fin

iii. 4PPC__2 Fins

iv. 4PPC__3 Fins

For all the analysis discussed in this section, transient thermal and transient structural analyses were used for our simulations in ANSYS Workbench. As ANSYS Workbench does not has the ability to solve multi-physics problem with a coupled approach, so a sequential approach has been used instead. That is, first the transient thermal is solved and then its results are used as an input for transient structural. In the transient thermal we are interested only in the temperature distribution for each analysis over a certain span of time and in transient structural analysis stress distribution for respective time has been observed.

After starting ANSYS Workbench, transient thermal and then transient structural were chosen from the Analysis Systems. These are then coupled together sequentially. Engineering data, geometry and mesh are also shared for both of these models. The mesh especially is more important to share, as to make sure that when output temperature data of transient thermal is given as input to transient structural module there is no mismatch between the mesh of both these modules. Engineering data for both the metal foam fin and the base as shown in Table 7 are created as new materials separately and saved in the materials library for future simulations too.

In the geometry section of transient thermal, the geometry is directly imported in parasolid format created from SolidWorks. In the model section fins and bases appear as individual parts and are assigned the user specified particular material properties. Also

the contact region between the base and the fin is checked by connection properties to check that there did not arise any anomaly when importing the model in the FE package.

The mesh is then generated using the automatic default settings, as ANSYS Workbench creates an optimized number of mesh elements for each model without compromising the accuracy of the results. No special method was chosen for the meshing of these models in our analysis.

Then in the transient thermal analysis settings, the initial temperature is set same as that of the particular experiment. For the step control settings, the total simulation time of 1500 sec (or 25 min.) was chosen. For the first 900 sec (or 15 min.), *h* value of fan-off was used (i.e. 12.5 W/m.K) and from 900 to 1500 sec (or last 10 min.), *h* value of fan-on was used (i.e. 110 W/m.K).

Heat flow and convective heat transfer was applied on the surface of the model as shown in Figure 54. As depicted, the *h* was applied to complete outer surface metal foam fins as they are fully exposed to the surrounding, while for the base only top surface has been selected and the rest of base has been insulated. And the heat input flow was applied only to the base.

The simulations for thermal analysis were let to run till its completion. At the end of analysis, the temperature data for the complete simulation could be collected for any particular time in any of the following form:

a) Temperature vs. time plot.
b) Tabular data for each instant over complete time span.
c) Visually by color contours over the model.

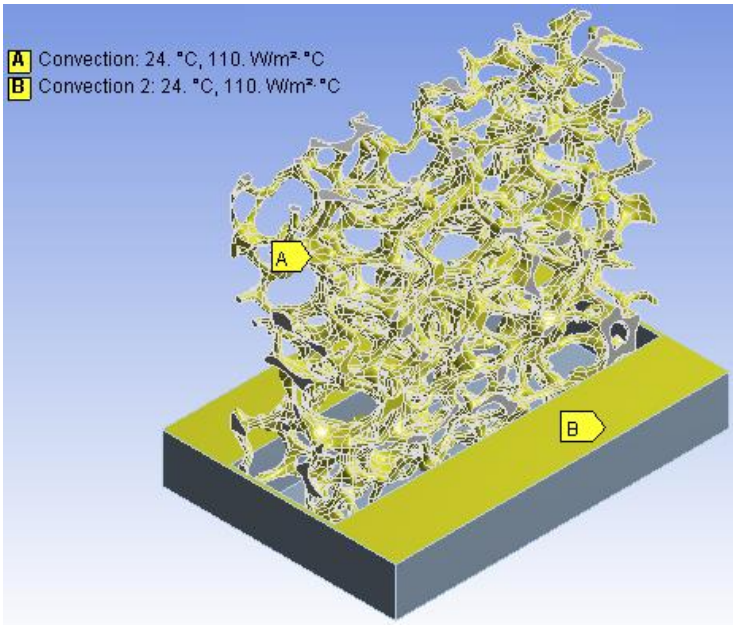

(a)

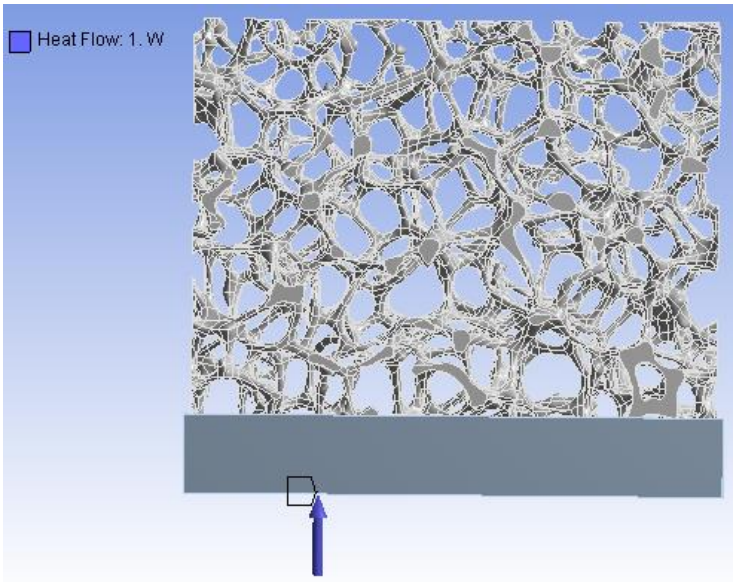

(b)

Figure 54 Boundary conditions: (a) Convective heat transfer and (b) Heat input

Once the transient thermal analysis is complete the transient structural analysis module is started. The engineering data, geometry and the mesh are automatically imported as both the thermal and structural modules have been coupled. In the transient analysis setting of the transient structural the exact same settings were applied as to that of thermal analysis over a span of again 1500 sec (or 25 min.).

For boundary conditions the temperature output from thermal analysis is applied as imported thermal load to generate the thermal stress in the body of the heat sink. The base on the other hand has been applied with roller supports to confine the rigid body motion.

The simulations for structural analysis were again let to run till its completion. At the end of analysis, the stress data for the complete simulation could be collected for any particular time in any of forms as in case of thermal analysis.

CHAPTER 8

NUMERICAL FINDINGS

The procedure carried out for each of the simulation study has been discussed in detail in the previous section 7.2.3. Here only the results and few unique aspects of each simulation analysis are highlighted.

8.1 Metal Foam Heat Sinks Simulation Results

As stated already, a comparative numerical study was carried out for following models only:

i. 2PPC__1 Fin
ii. 4PPC__1 Fin
iii. 4PPC__2 Fins
iv. 4PPC__3 Fins

All of the above studies were transient temperature and transient respective stresses for a complete span of 1500 sec (2 5min). For first 900 sec (15 min) the condition were applied that of fan-off (or natural convection) and for remaining 600 sec (10 min) the conditions were set to that of fan-on (or forced convection). Although the studies were transient, but Figure 55 to Figure 70 shows only the steady-state temperatures and steady-state stresses at fan-off and fan-on. Whereas, Figure 71 to Figure 74 shows the complete detailed

variation of temperatures and stresses for the whole run, but for minimum and maximum values only.

Roller supports were applied as boundary conditions at the base of all heat sink samples for all the simulation, as in the experiments carried out the heat sink was attached to the heating base with thermal grease only (no other physical constraints other than the strength of glue were applied to restrain the free movement when it was heated). For all the figures showing the stress distribution, as expected, it can be seen that the whole model has same blue color contour, which suggests that the stresses on the overall model are only meager. While some of the specific points are highly concentrated. But the stresses in the vicinity of those high stress regions again fall rapidly to an acceptable range. This can be explained due to point of singularities arising at these points during the solution, so these high concentrated stress values in reality are meaningless. And the minimum stress plots in Figure 71 to Figure 74 show that minimum stresses are almost zero throughout the run and appear at the top of fins, which makes a perfect sense.

But on the other hand, temperature distribution profiles make a lot more sense. And even by the plots of Figure 71 to Figure 74 it can be seen that they easily reach steady-state value at the end of both fan-off and fan-on.

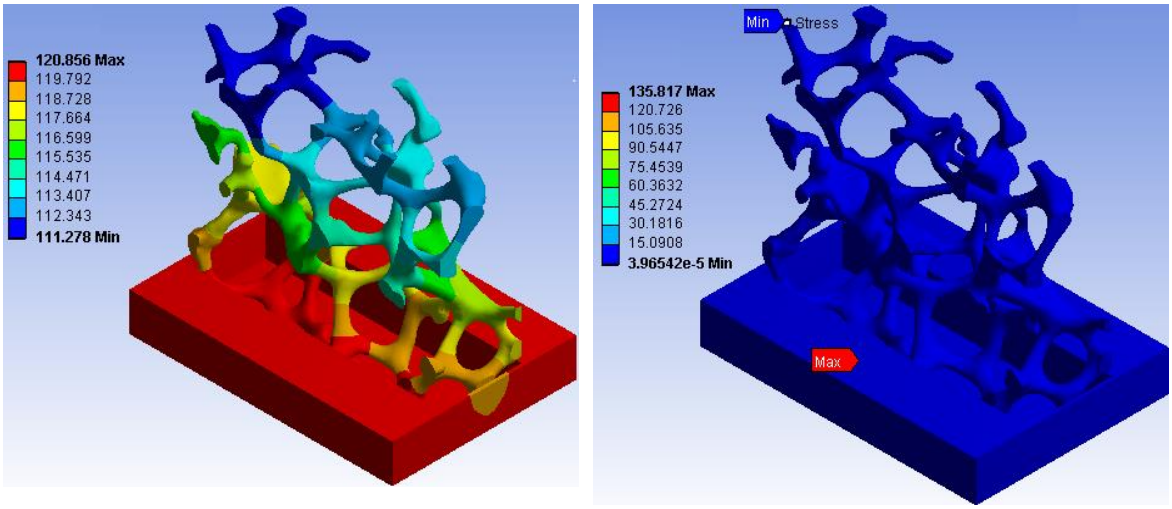

(a) **(b)**

Figure 55 2PPC-1 Fin Steady-state fan-off: (a) Temperature Distribution, (b) Stress Distribution

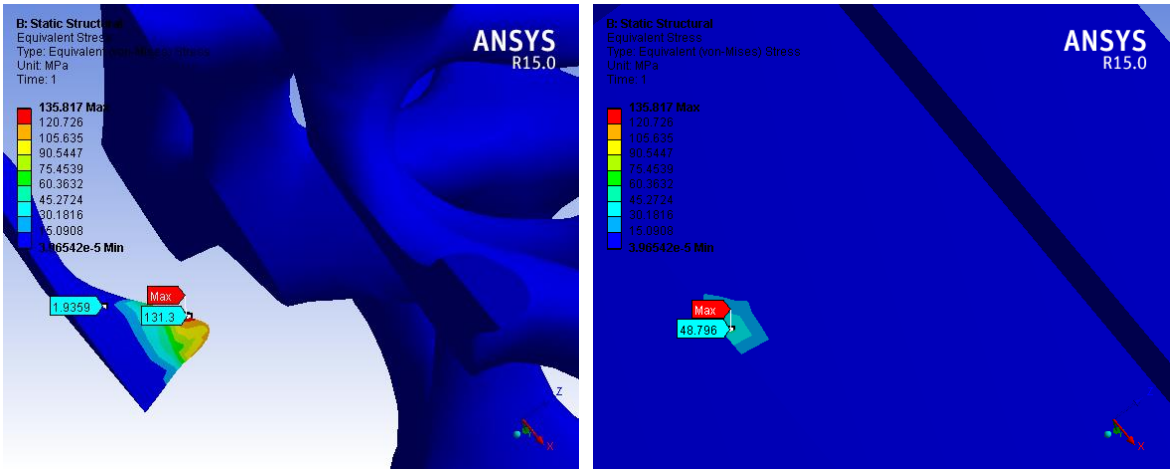

(a) **(b)**

Figure 56 2PPC-1 Fin Steady-state fan-off: (a) Point of maximum stress on metal foam and (b) Point of maximum stress on the base

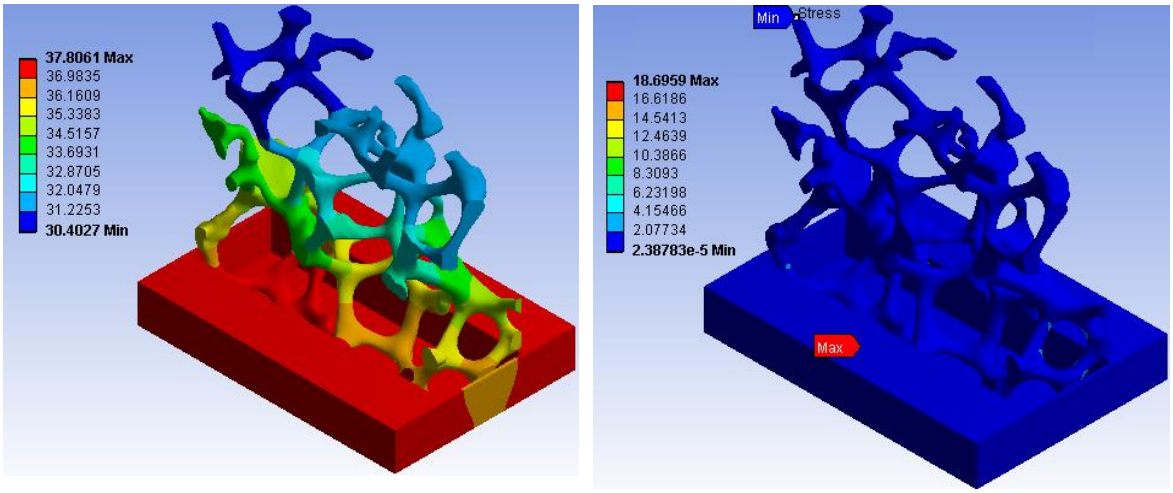

(a) **(b)**

Figure 57 2PPC-1 Fin Steady-state fan-on: (a) Temperature Distribution, (b) Stress Distribution

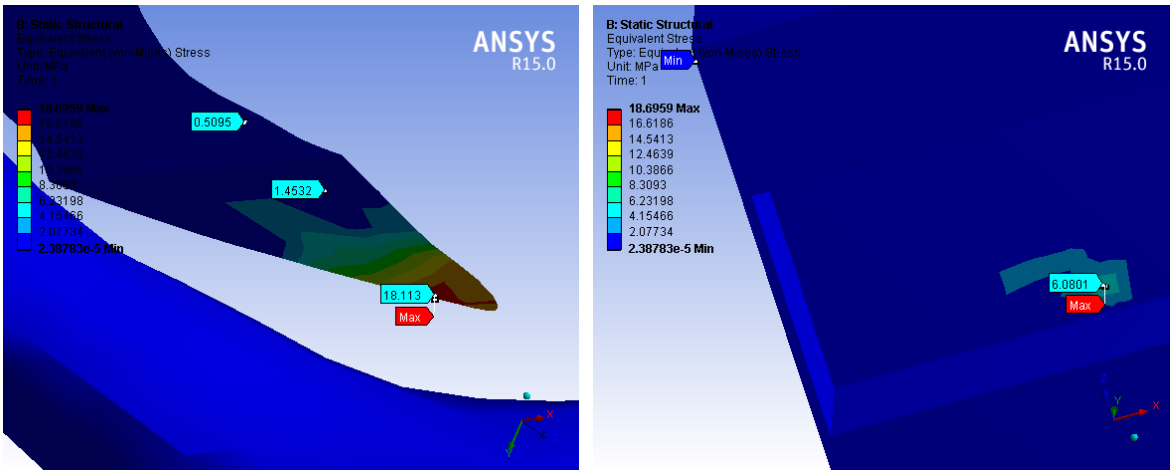

(a) **(b)**

Figure 58 2PPC-1 Fin Steady-state fan-on: (a) Point of maximum stress on metal foam and (b) Point of maximum stress on the base

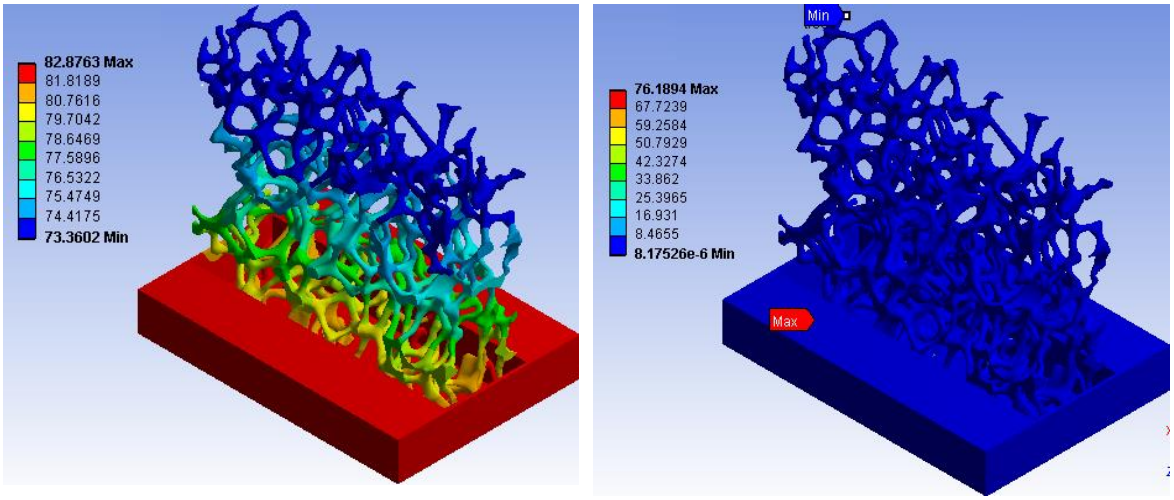

(a) **(b)**

Figure 59 4PPC-1 Fin Steady-state fan-off: (a) Temperature Distribution, (b) Stress Distribution

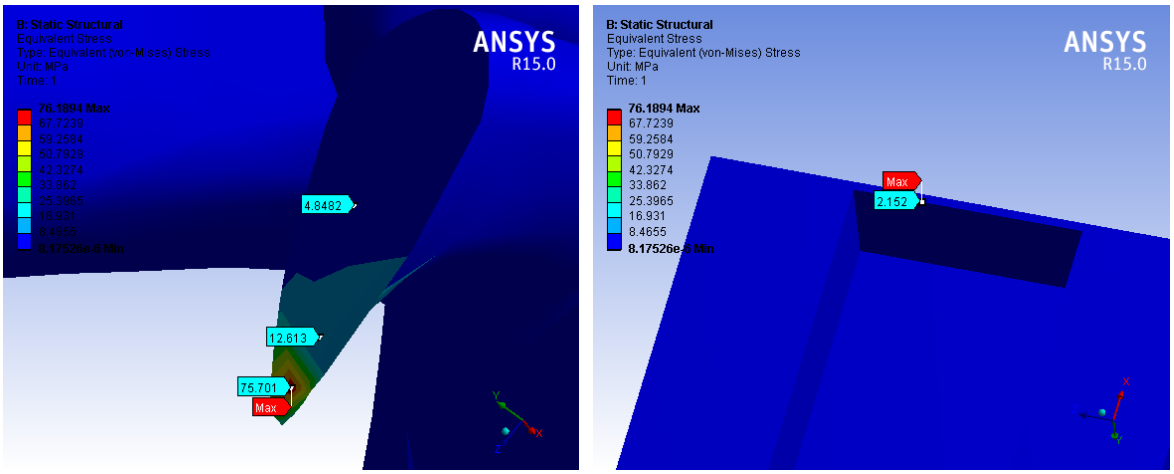

(a) **(b)**

Figure 60 4PPC-1 Fin Steady-state fan-off: (a) Point of maximum stress on metal foam and (b) Point of maximum stress on the base

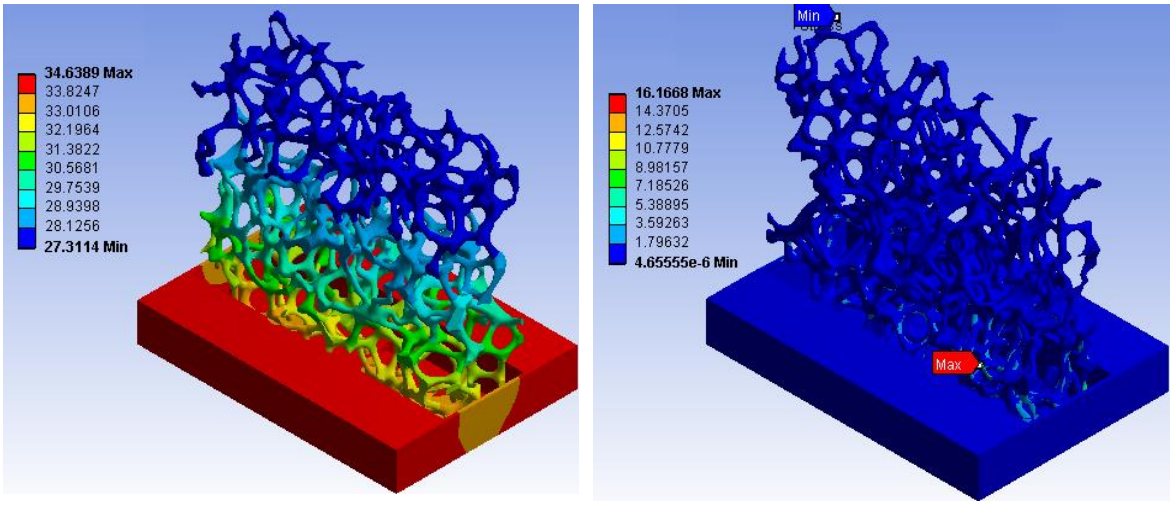

(a) **(b)**

Figure 61 4PPC-1 Fin Steady-state fan-on: (a) Temperature Distribution, (b) Stress Distribution

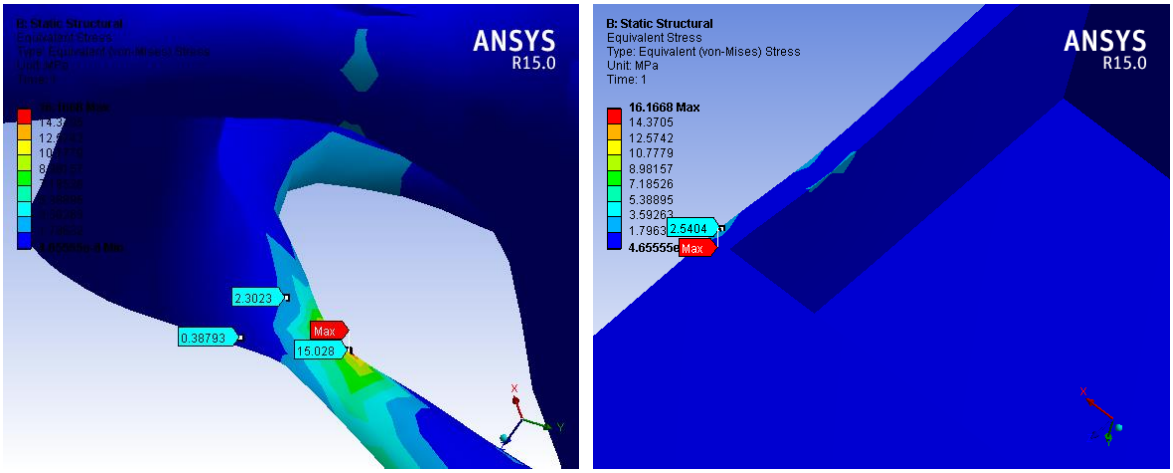

(a) **(b)**

Figure 62 4PPC-1 Fin Steady-state fan-on: (a) Point of maximum stress on metal foam and (b) Point of maximum stress on the base

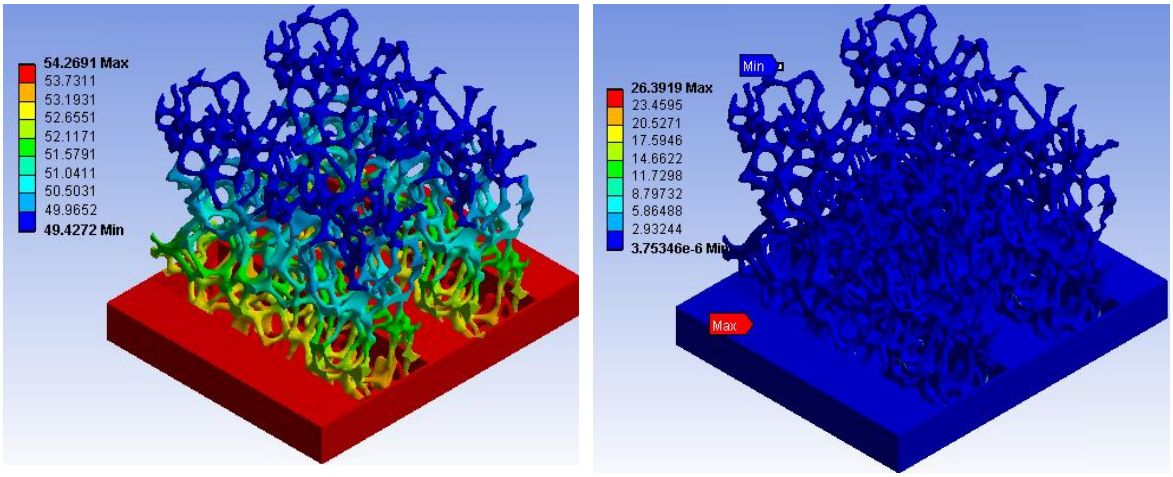

(a) **(b)**

Figure 63 4PPC-2 Fins Steady-state fan-off: (a) Temperature Distribution, (b) Stress Distribution

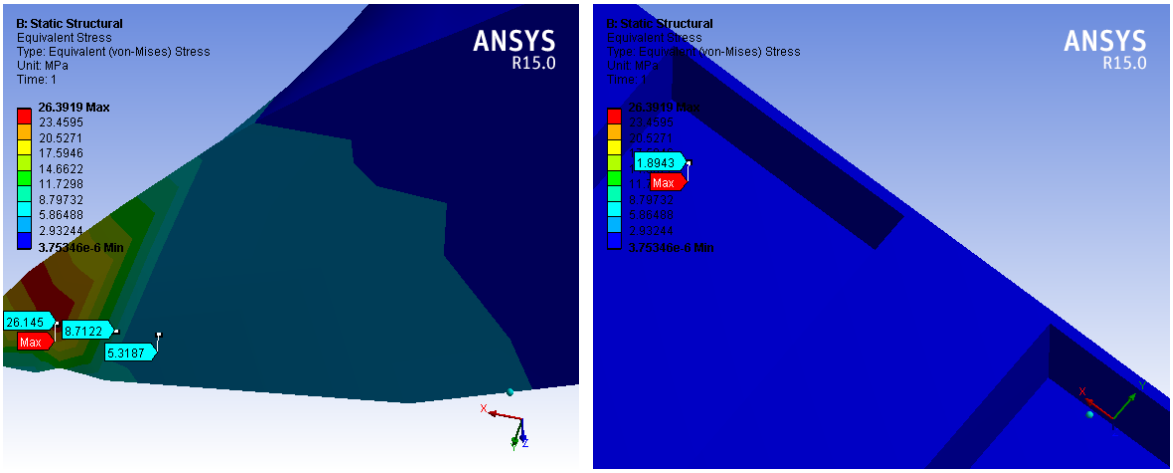

(a) **(b)**

Figure 64 4PPC-2 Fins Steady-state fan-off: (a) Point of maximum stress on metal foam and (b) Point of maximum stress on the base

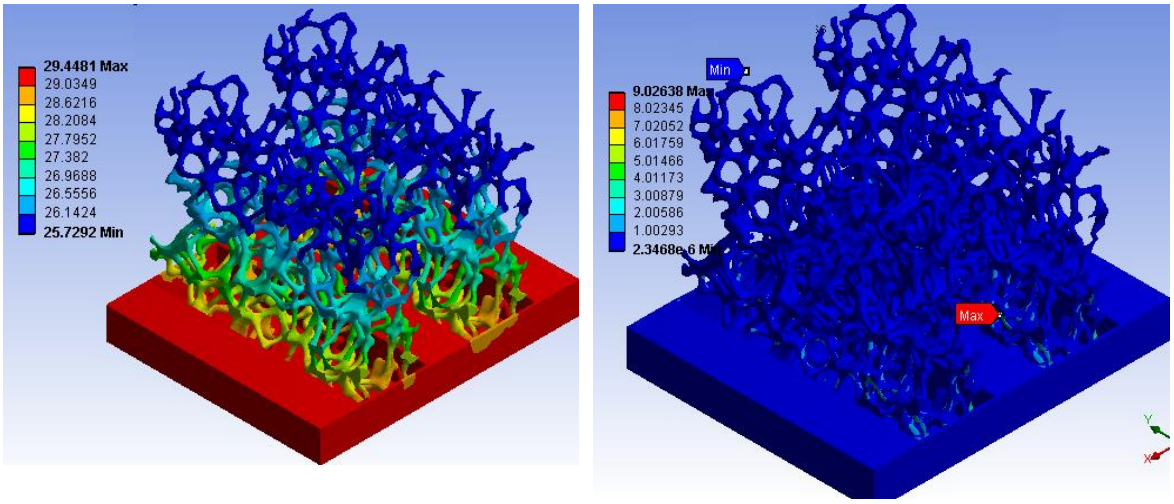

(a) **(b)**

Figure 65 4PPC-2 Fins Steady-state fan-on: (a) Temperature Distribution, (b) Stress Distribution

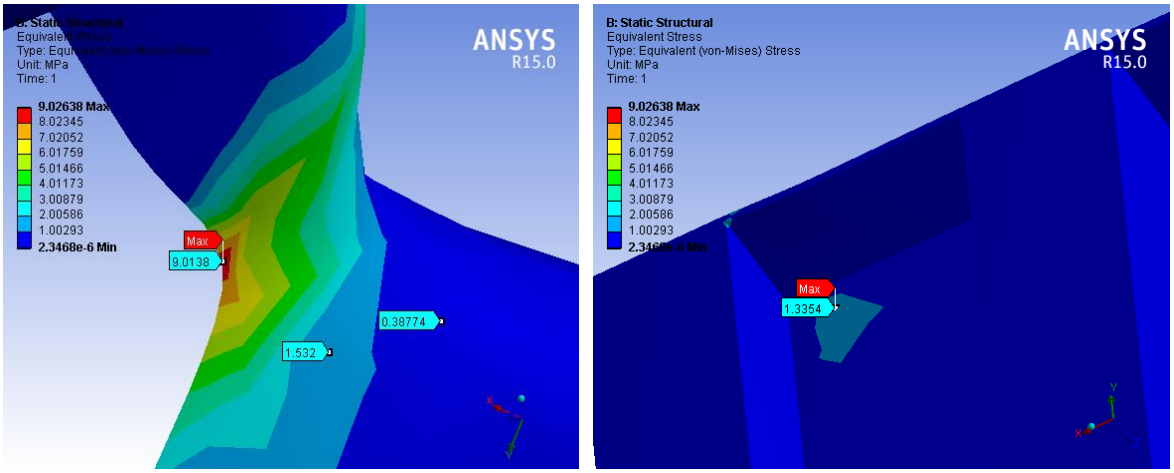

(a) **(b)**

Figure 66 4PPC-2 Fins Steady-state fan-on: (a) Point of maximum stress on metal foam and (b) Point of maximum stress on the base

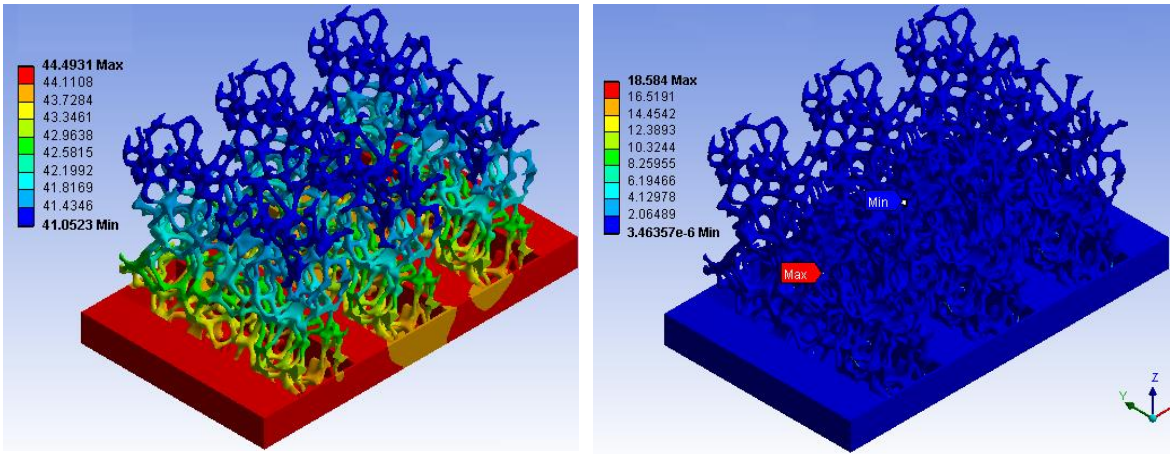

(a) **(b)**

Figure 67 4PPC-3 Fins Steady-state fan-off: (a) Temperature Distribution, (b) Stress Distribution

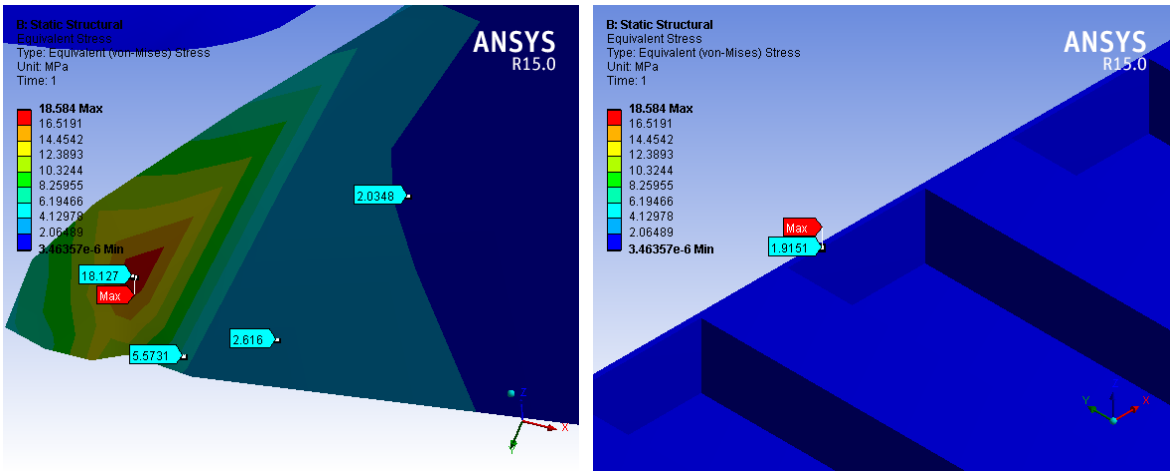

(a) **(b)**

Figure 68 4PPC-3 Fins Steady-state fan-off: (a) Point of maximum stress on metal foam and (b) Point of maximum stress on the base

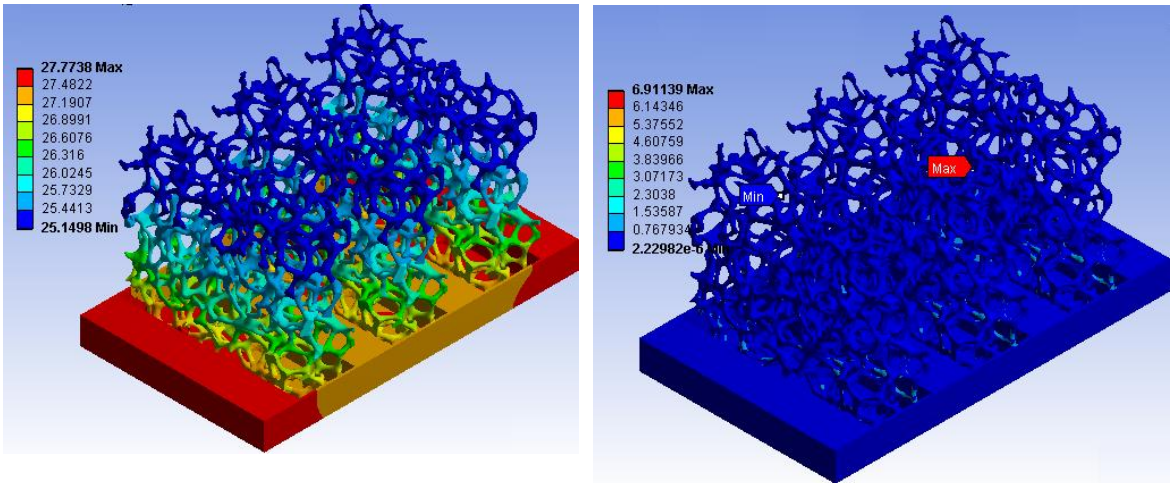

(a) **(b)**

Figure 69 4PPC-3 Fins Steady-state fan-on: (a) Temperature Distribution, (b) Stress Distribution

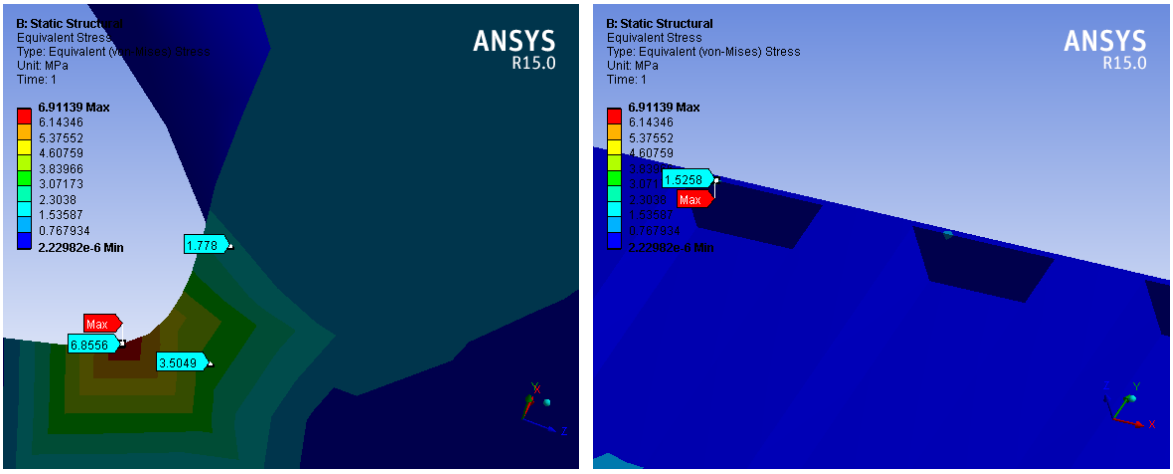

(a) **(b)**

Figure 70 4PPC-3 Fins Steady-state fan-on: (a) Point of maximum stress on metal foam and (b) Point of maximum stress on the base

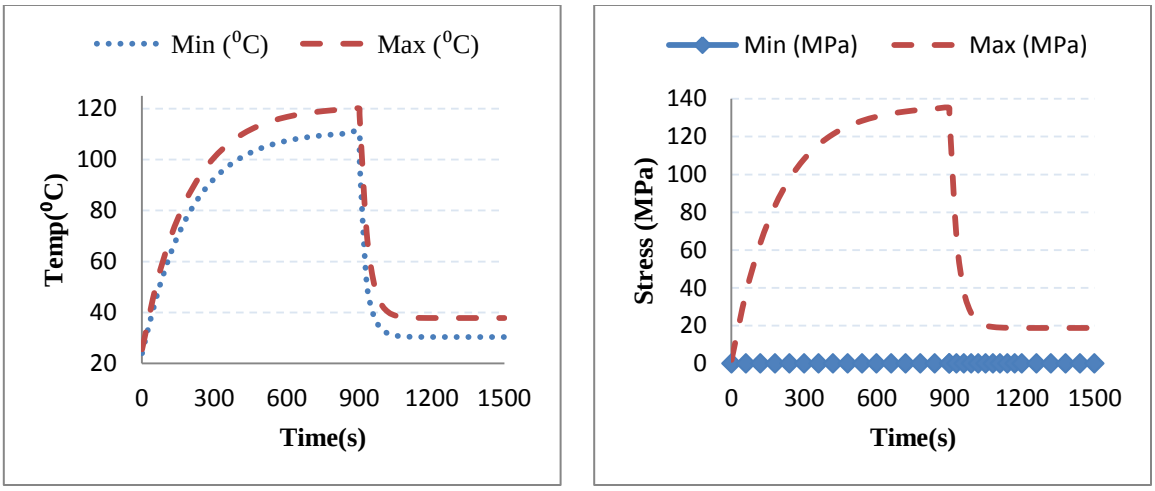

(a) **(b)**

Figure 71 2 PPC- 1 Fin: (a) Temperature variation and (b) Stress variation

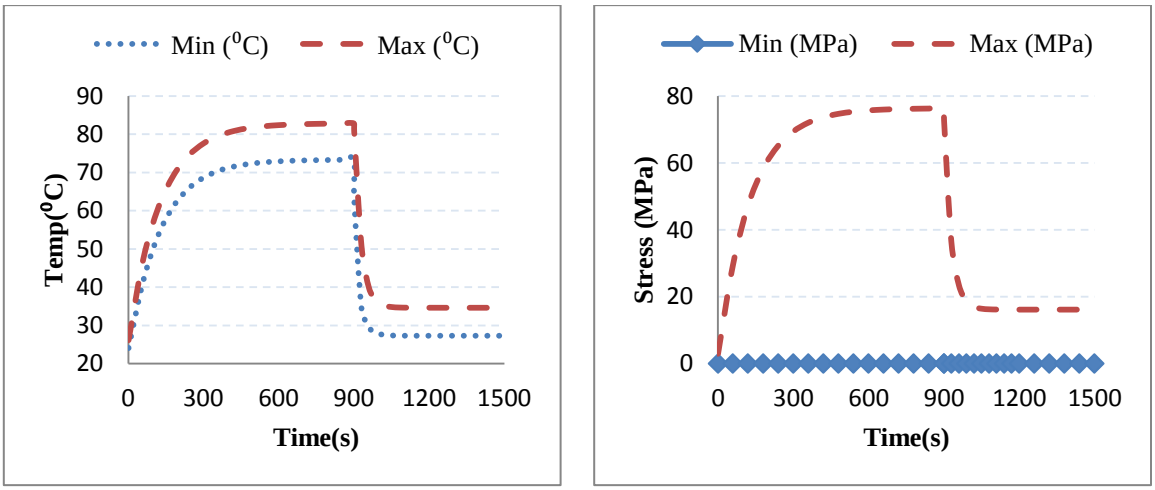

(a) **(b)**

Figure 72 4 PPC- 1 Fin: (a) Temperature variation and (b) Stress variation

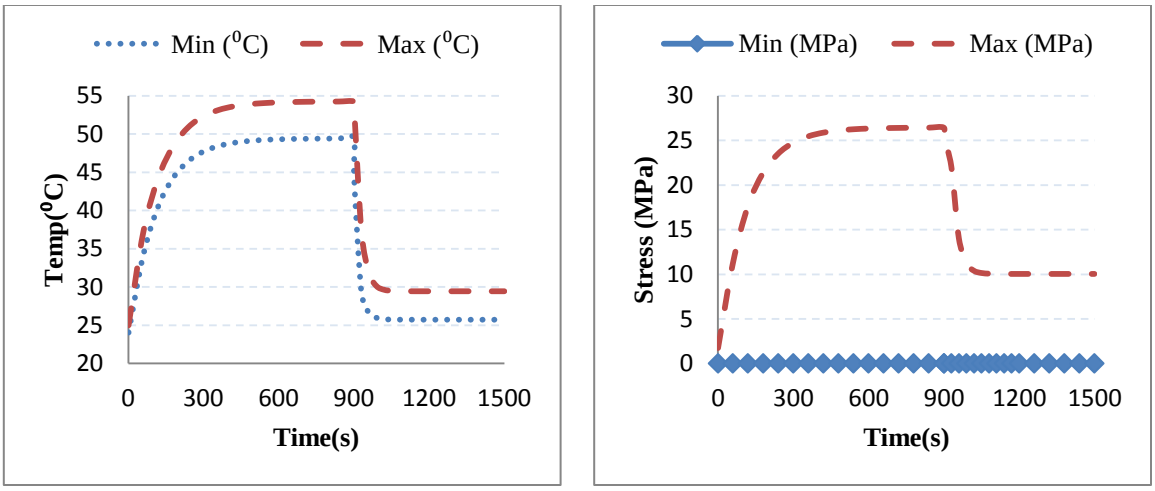

(a) **(b)**

Figure 73 4 PPC- 2 Fins: (a) Temperature variation and (b) Stress variation

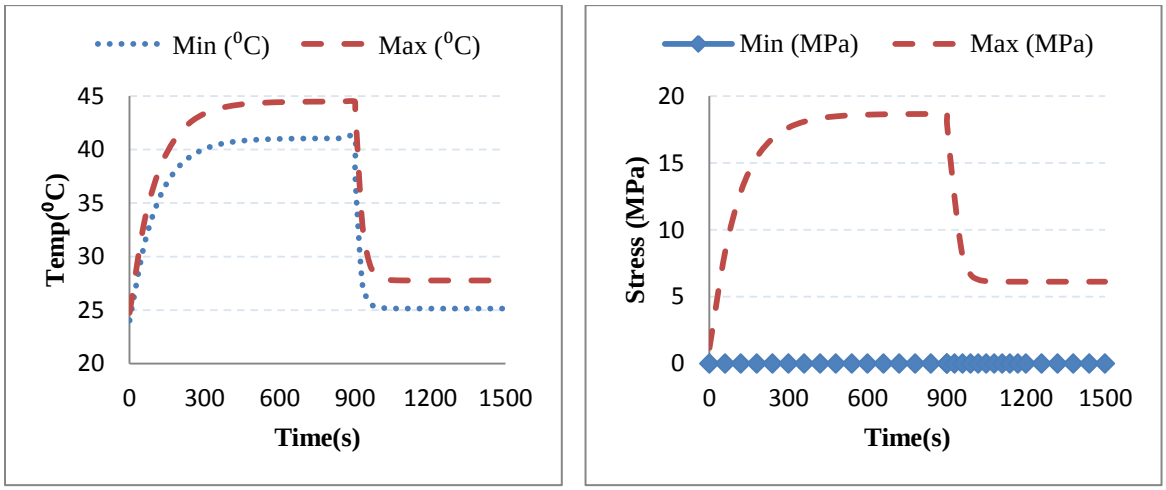

(a) **(b)**

Figure 74 4 PPC- 3 Fins: (a) Temperature variation and (b) Stress variation

8.2 Summary

Figure 75 gives the summary of simulation results from Figure 71 to Figure 74. The simulation results clearly show that under same test conditions, the maximum temperature reached both under natural and forced convection becomes less as the number of fins increase. Consequently with the decrease in temperature the thermal stresses inside the heat sinks also decrease. Also comparing Figure 71 and Figure 72 it can be seen that as the porosity is increased from 2 PPC to 4 PPC, the maximum steady-state temperature at fan-off decrease from 120 ºC to 82 ºC. While for fan-on it decreases from 34 ºC to 29 ºC.

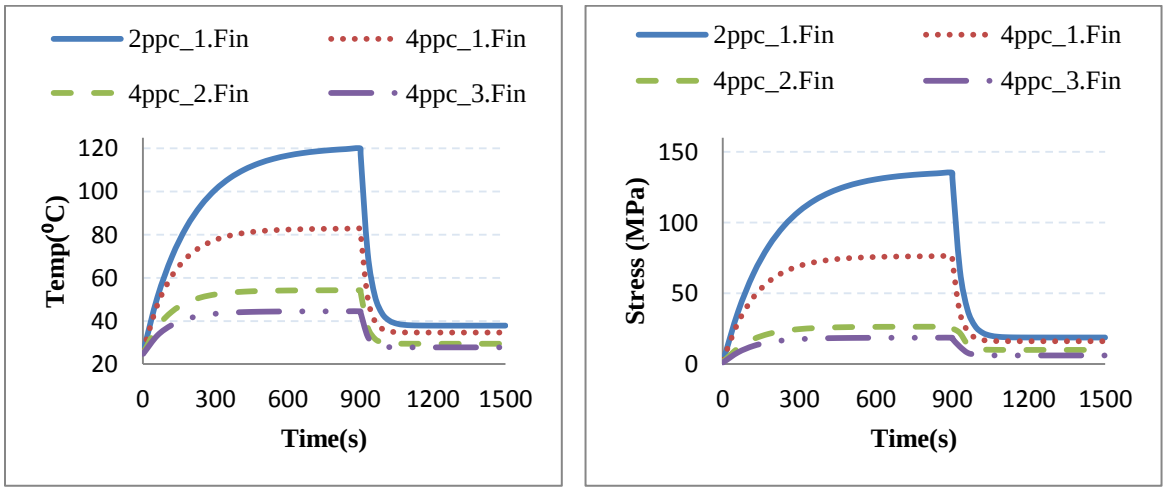

(a) **(b)**

Figure 75 Combined Plot for all Heat Sinks: (a) Temperature variation and (b) Stress variation

Also it is visually evident from Figure 55 to Figure 70 that the maximum stresses occur at the points of connection between the metal foam fin and the solid base. While the

minimum stresses are usually at the fins top where the temperature as expected is lowest and also that region is not physically constrained. These high stresses are just located at single nodes and are arising due to point singularity deformation.

These findings show that at natural convection (or fan-off), increase in porosity and number of fins the temperature drop and stresses decrement are more prominent, while compared to forced convection condition (or fan-on).

CHAPTER 9

CONCLUSIONS AND FUTURE WORK

Both experimental and numerical study have been carried out in order to thoroughly understand the thermo-mechanical behavior of metal foams especially in heat sink applications

The effect of thermal spray coating (along with various factors) on the performance of finned metal foam heat sinks has been analyzed experimentally, for their use in cooling of electronics. A comparative study was also conducted between thermally spray coated, glued and solid machined heat sinks.

The results in our experiments indicate that for single fin heat sink samples, the thermally spray coated metal foam heat sink outperformed the other two samples under same test conditions by proving to be almost 9.8% more efficient at dissipating heat. In fact remarkably, even the solid machined heat sink performed almost 2.7% better than the glued metal foam heat sink sample in our test conditions.

Experiments also showed that heat transfer increases with almost a linear trend with increase/decrease in air velocity, but with an expense of more power consumption. And also for single fin samples, 90º is the best orientation for highest rate of heat dissipation.

Two and three fins samples regardless of the pore density (PPC) show that for multiple fins the best orientation for most heat dissipation is 45º. This can be explained due to better thorough mixing of the air with the metal foam fins and also the turbulence caused

by the complicated structure further uplifts the heat transfer coefficient. Also with an enhancement in the number of fins, the total temperature drop increases.

This computational work presents a methodology for developing a realistic and accurate 3D computational model of open-cell metal foams. CT scan was used to capture the precise geometry of metal foam. This study also discussed the optimized process of obtaining a clean workable FE volume (solid) model. The resolution of our model is better than the known literature to us. This makes our model as close as possible to the real structure of metal foams. Techniques have been implanted to make the model smaller in terms of size, but without compromising the real shape and details of original model. This reduction in size makes the model easily run on even normal computers.

A novel method has been proposed to find heat transfer coefficient (h) values of complicated objects like metal foam. It has also been shown that value of h is independent of power input. This h value can then be used for FE simulations of different scenarios.

After checking the accuracy of our model and technique, in simulation study the effect of changing the number of fins and pore density (PPC) for same test conditions has been observed. Simulations results though theoretical, but are in conjunction with the experimental study.

Size scaling method of this very same model has been shown and used in the study. Thus it can be used for varying pore density (PPC) for different scenarios, without the need of taking scan for different samples. This model can further be used in CFD analysis for better understanding of fluid and metal foam interaction.

Thus keeping in mind the space and power constraints, number of fins, heat sink orientation and air velocity could be set to optimize the thermal performance of metal foam heat sink. If pressure drop is not of concern then metal foam heat sinks clearly outperform conventional heat sinks.

This work has a lot of potential for further detailed study of metal foams' thermo-mechanical behavior. Though certainly not limited to, but some of the suggested future work can be as follows:

- To utilize the 3D detailed metal foam heat sink model in a CFD analysis.
- To utilize the 3D detailed metal foam model in other applications of open-cell metal foams.
- To run simulation studies on different pore densities like 8 PPC and 16 PPC etc. as well.
- Find the value of contact resistance in thermally glued and thermally sprayed samples (both experimentally and numerically).
- Other related work in the literature can be utilized to further validate the use of the model as a credible source.
- Experimentation should be carried out on other variety of samples and test conditions too.
- Pressure drop measurements could also be made a part of these studies to enhance a better understanding of the metal foam behavior in thermal applications.

References

[1] Ashby, M. F., Evans, A. G., Fleck, N. A., Gibson, L. J., Hutchinson, J. W., and Wadley, H. N. G., 2000, Metal Foams, Elsevier.

[2] Banhart, J., 2001, "Manufacture, characterisation and application of cellular metals and metal foams," Prog. Mater. Sci., **46**, pp. 559–632.

[3] Ayyagari, R. S., and Vural, M., 2015, "Multiaxial yield surface of transversely isotropic foams: Part I—Modeling," J. Mech. Phys. Solids, **74**, pp. 49–67.

[4] Gong, L., Kyriakides, S., and Triantafyllidis, N., 2005, "On the stability of Kelvin cell foams under compressive loads," J. Mech. Phys. Solids, **53**, pp. 771–794.

[5] Khairul Alam, M., and Anghelescu, M. S., 2009, "Analysis of Deformation and Residual Stresses in Composites Processed on a Carbon Foam Tooling," J. Compos. Mater., **43**(19), pp. 2057–2070.

[6] Fernández, P., Cruz, L. J., and Coleto, J., 2008, "Manufacturing processes of cellular metals. Part I: Liquid route processes," Rev. Metal., **44**, p. 40055161.

[7] Fernández, P., Cruz, L. J., and Coleto, J., 2009, "Manufacturing processes of cellular metals. Part II: Solid route, metals deposition, other processes," Rev. Metal., **45**, p. 40086814.

[8] Ghosh, I., 2009, "How Good Is Open-Cell Metal Foam as Heat Transfer Surface?," J. Heat Transfer, **131**(10), p. 101004.

[9] Han, X.-H., Wang, Q., Park, Y.-G., T'Joen, C., Sommers, A., and Jacobi, A., 2012, "A Review of Metal Foam and Metal Matrix Composites for Heat Exchangers and Heat Sinks," Heat Transf. Eng., **33**(February), pp. 991–1009.

[10] Zhu, H. X., Knott, J. F., and Mills, N. J., 1997, "Analysis of the elastic properties of open-cell foams with tetrakaidecahedral cells," J. Mech. Phys. Solids, **45**(3), pp. 319–343.

[11] Warren, W. E., and Kraynik, A. M., 1988, "The Linear Elastic Properties of Open-Cell Foams," J. Appl. Mech., **55**(2), p. 341.

[12] Luxner, M. H., Stampfl, J., and Pettermann, H. E., 2007, "Numerical simulations of 3D open cell structures - influence of structural irregularities on elasto-plasticity and deformation localization," Int. J. Solids Struct., **44**, pp. 2990–3003.

[13] Boomsma, K., Poulikakos, D., and Ventikos, Y., 2003, "Simulations of flow through open cell metal foams using an idealized periodic cell structure," Int. J. Heat Fluid Flow, **24**, pp. 825–834.

[14] Kopanidis, a., Theodorakakos, a., Gavaises, E., and Bouris, D., 2010, "3D numerical simulation of flow and conjugate heat transfer through a pore scale model of high porosity open cell metal foam," Int. J. Heat Mass Transf., **53**(11-12), pp. 2539–2550.

[15] Kumar, P., Topin, F., and Vicente, J., 2014, "Determination of effective thermal conductivity from geometrical properties: Application to open cell foams," Int. J. Therm. Sci., **81**, pp. 13–28.

[16] Tsolas, N., and Chandra, S., 2012, "Forced Convection Heat Transfer in Spray Formed Copper and Nickel Foam Heat Exchanger Tubes," J. Heat Transfer, **134**(6), p. 062602.

[17] Kandlikar, S. G., 2013, "Review and Projections of Integrated Cooling Systems for 3D ICs," ASME J. Electron. Packag, **136**(June), pp. 1–11.

[18] Hajmohammadi, M. R., Poozesh, S., Salman Nourazar, S., and Manesh, A. H., 2013, "Optimal architecture of heat generating pieces in a fin," J. Mech. Sci. Technol., **27**(4), pp. 1143–1149.

[19] Dixit, T., and Ghosh, I., 2015, "Review of micro- and mini-channel heat sinks and heat exchangers for single phase fl uids," Renew. Sustain. Energy Rev., **41**, pp. 1298–1311.

[20] Chingulpitak, S., and Wongwises, S., 2015, "A review of the effect of flow directions and behaviors on the thermal performance of conventional heat sinks," Int. J. Heat Mass Transf., **81**, pp. 10–18.

[21] Kim, S. Y., Paek, J. W., and Kang, B. H., 2003, "Thermal performance of aluminum-foam heat sinks by forced air cooling," IEEE Trans. Components Packag. Technol., **26**(1), pp. 262–267.

[22] Kaviany, M., 2002, Principles of heat transfer.

[23] Leong, K. C., and Jin, L. W., 2006, "Effect of oscillatory frequency on heat transfer in metal foam heat sinks of various pore densities," Int. J. Heat Mass Transf., **49**(3-4), pp. 671–681.

[24] Mancin, S., Zilio, C., Cavallini, A., and Rossetto, L., 2010, "Heat transfer during air flow in aluminum foams," Int. J. Heat Mass Transf., **53**(21-22), pp. 4976–4984.

[25] Mancin, S., Zilio, C., Cavallini, A., and Rossetto, L., 2010, "Pressure drop during air flow in aluminum foams," Int. J. Heat Mass Transf., **53**(15-16), pp. 3121–3130.

[26] Cavallini, a., Mancin, S., Rossetto, L., and Zilio, C., 2009, "Air Flow in Aluminum Foam: Heat Transfer and Pressure Drops Measurements," Exp. Heat Transf., **23**(February), pp. 94–105.

[27] Liu, J. F., Wu, W. T., Chiu, W. C., and Hsieh, W. H., 2006, "Measurement and correlation of friction characteristic of flow through foam matrixes," Exp. Therm. Fluid Sci., **30**(4), pp. 329–336.

[28] Hsieh, W. H., Wu, J. Y., Shih, W. H., and Chiu, W. C., 2004, "Experimental investigation of heat-transfer characteristics of aluminum-foam heat sinks," Int. J. Heat Mass Transf., **47**, pp. 5149–5157.

[29] Dogan, A., and Tezel, T., 2013, "Experimental investigation of convection heat transfer from open-celled metal foam blocks," J. Enhanc. Heat Transf., **20**(3), pp. 267–275.

[30] Giani, L., Groppi, G., and Tronconi, E., 2005, "Heat Transfer Characterization of Metallic Foams," Ind. Eng. Chem. Res., **44**(24), pp. 9078–9085.

[31] Dukhan, N., Picón-Feliciano, R., and Álvarez-Hernández, A. R., 2006, "Air Flow Through Compressed and Uncompressed Aluminum Foam: Measurements and Correlations," J. Fluids Eng., **128**(5), p. 1004.

[32] Whitaker, S., 1996, "The Forchheimer equation: A theoretical development," Transp. Porous Media, **25**(3), pp. 27–61.

[33] Guarino, S., Rubino, G., Tagliaferri, V., and Ucciardello, N., 2015, "Thermal behavior of open cell aluminum foams in forced air: Experimental analysis," Measurement, **60**, pp. 97–103.

[34] Yang, Y., Ji, X., and Xu, J., 2010, "Pool boiling heat transfer on copper foam covers with water as working fluid," Int. J. Therm. Sci., **49**(7), pp. 1227–1237.

[35] Zhang, H. Y., Pinjala, D., Joshi, Y. K., Wong, T. N., Toh, K. C., and Iyer, M. K., 2005, "Fluid flow and heat transfer in liquid cooled foam heat sinks for electronic packages," IEEE Trans. Components Packag. Technol., **28**(2), pp. 272–280.

[36] Calmidi, V. V., and Mahajan, R. L., 2000, "Forced Convection in High Porosity Metal Foams," J. Heat Transfer, **122**(3), p. 557.

[37] Odabaee, M., Mancin, S., and Hooman, K., 2013, "Metal foam heat exchangers for thermal management of fuel cell systems - An experimental study," Exp. Therm. Fluid Sci., **51**, pp. 214–219.

[38] Lu, W., Zhao, C. Y., and Tassou, S. a., 2006, "Thermal analysis on metal-foam filled heat exchangers. Part I: Metal-foam filled pipes," Int. J. Heat Mass Transf., **49**(15-16), pp. 2751–2761.

[39] Chumpia, a., and Hooman, K., 2014, "Performance evaluation of single tubular aluminium foam heat exchangers," Appl. Therm. Eng., **66**(1-2), pp. 266–273.

[40] Kim, S. Y., Lee, M. H., and Lee, K. S., 2005, "Heat removal by aluminum-foam heat sinks in a multi-air jet impingement," IEEE Trans. Components Packag. Technol., **28**(1), pp. 142–148.

[41] Yang, K.-S., Chung, C.-H., Lee, M.-T., Chiang, S.-B., Wong, C.-C., and Wang, C.-C., 2013, "An experimental study on the heat dissipation of LED lighting module using metal/carbon foam," Int. Commun. Heat Mass Transf., **48**, pp. 73–79.

[42] Byon, C., 2015, "Heat transfer characteristics of aluminum foam heat sinks subject to an impinging jet under fixed pumping power," Int. J. Heat Mass Transf., **84**, pp. 1056–1060.

[43] Kim, S. J., and Kim, D., 1999, "Forced Convection in Microstructures for Electronic Equipment Cooling," J. Heat Transfer, **121**(3), p. 639.

[44] DeGroot, C. T., Gateman, D., and Straatman, A. G., 2010, "The Effect of Thermal Contact Resistance at Porous-Solid Interfaces in Finned Metal Foam Heat Sinks," J. Electron. Packag., **132**(4), p. 041007.

[45] Zhao, C. Y., 2012, "Review on thermal transport in high porosity cellular metal foams with open cells," Int. J. Heat Mass Transf., **55**(13-14), pp. 3618–3632.

[46] Sir Thomson, W., 1887, "On the division of space with minimum partitional area," Acta Math., **11**, pp. 121–134.

[47] Liquides, D. E. S., 1873, "Des liquides," Sci. York.

[48] MATZKE, E. B., 1946, "The three-dimensional shape of bubbles in foam; an analysis of the role of surface forces in three-dimensional cell shape determination.," Am. J. Bot., **33**(1), pp. 58–80.

[49] Gabbrielli, R., 2009, "A new counter-example to Kelvin's conjecture on minimal surfaces," **89**(8), pp. 483–491.

[50] Weaire, D., and Phelan, R., 1994, "A counter-example to Kelvin's conjecture on minimal surfaces," Philos. Mag. Lett., **69**(2), pp. 107–110.

[51] Krishnan, S., Murthy, J. Y., and Garimella, S. V., 2006, "Direct Simulation of Transport in Open-Cell Metal Foam," J. Heat Transfer, **128**(8), p. 793.

[52] Sihn, S., and Roy, A. K., 2004, "Modeling and prediction of bulk properties of open-cell carbon foam," J. Mech. Phys. Solids, **52**, pp. 167–191.

[53] Straatman, A. G., Gallego, N. C., Yu, Q., Betchen, L., and Thompson, B. E., 2007, "Forced Convection Heat Transfer and Hydraulic Losses in Graphitic Foam," J. Heat Transfer, **129**(9), p. 1237.

[54] Li, K., Gao, X.-L., and Roy, a. K., 2005, "Micromechanical modeling of three-dimensional open-cell foams using the matrix method for spatial frames," Compos. Part B Eng., **36**, pp. 249–262.

[55] Druma, A., Alam, M. K., Anghelescu, M., Druma, C., and Maruyama, B., 2005, "Three Dimensional Modeling of Carbon Foams," Heat Transfer, Part A, ASME, pp. 209–211.

[56] Warren, W. ., Neilsen, M. ., and Kraynik, a. ., 1997, "Torsional rigidity of a plateau border," Mech. Res. Commun., **24**, pp. 667–672.

[57] Roberts, a. P., and Garboczi, E. J., 2002, "Elastic properties of model random three-dimensional open-cell solids," J. Mech. Phys. Solids, **50**, pp. 33–55.

[58] Chiu, S. N., Stoyan, D., Kendall, W. S., and Mecke, J., 2013, Stochastic Geometry and Its Applications, John Wiley & Sons.

[59] Yuan, Z., Rayess, N., and Dukhan, N., 2014, "Modeling of the Mechanical Properties of a Polymer-metal Foam Hybrid," Procedia Mater. Sci., **4**(2009), pp. 207–211.

[60] Suleiman, A. S., and Dukhan, N., 2014, "Forced convection inside metal foam: Simulation over a long domain and analytical validation," Int. J. Therm. Sci., **86**, pp. 104–114.

[61] Baillis, D., and Coquard, R., 2008, Radiative and Conductive Thermal Properties of Foams.

[62] Rodrigues, F. P., Li, J., Silikas, N., Ballester, R. Y., and Watts, D. C., 2009, "Sequential software processing of micro-XCT dental-images for 3D-FE analysis," Dent. Mater., **25**, pp. 47–55.

[63] Langton, C. M., Pisharody, S., and Keyak, J. H., 2009, "Comparison of 3D finite element analysis derived stiffness and BMD to determine the failure load of the excised proximal femur," Med. Eng. Phys., **31**, pp. 668–672.

[64] Tie, Y., Wang, D. M., Ji, T., Wang, C. T., and Zhang, C. P., 2006, "Three-dimensional finite-element analysis investigating the biomechanical effects of human mandibular reconstruction with autogenous bone grafts," J. Cranio-Maxillofacial Surg., **34**, pp. 290–298.

[65] Li, M., Miller, K., Joldes, G. R., Doyle, B., Garlapati, R. R., Kikinis, R., and Wittek, A., 2015, "Patient-Specific biomechanical model as whole-body CT image registration tool," Med. Image Anal.

[66] Wulf, R., Mendes, M. a a, Skibina, V., Al-Zoubi, A., Trimis, D., Ray, S., and Gross, U., 2014, "Experimental and numerical determination of effective thermal conductivity of open cell FeCrAl-alloy metal foams," Int. J. Therm. Sci., **86**, pp. 95–103.

[67] Liebscher, a., Proppe, C., Redenbach, C., and Schwarzer, D., 2013, "Stochastic multiscale modeling of metal foams," Procedia IUTAM, **6**, pp. 87–96.

[68] Http://www.walmate-cn.com/Page/list/28.html, 2009, "http://www.walmate-cn.com/Page/list/28.html."

[69] Azar, a., and Al., E., 2009, "Heat sink testing methods and common oversights," Qpedia Therm. E-Magazine, **II**(Xii).

[70] "http://www.omega.com/."

[71] "http://www.mie.utoronto.ca/labs/cact/."

[72] "http://www.goodfellow.com/."

[73] Mancin, S., Zilio, C., Diani, A., and Rossetto, L., 2012, "Experimental air heat transfer and pressure drop through copper foams," Exp. Therm. Fluid Sci., **36**, pp. 224–232.

[74] Bhattacharya, a., and Mahajan, R. L., 2002, "Finned Metal Foam Heat Sinks for Electronics Cooling in Forced Convection," J. Electron. Packag., **124**(3), p. 155.

[75] Várady, T., Martin, R. R., and Cox, J., 1997, "Reverse engineering of geometric models—an introduction," Comput. Des., **29**(4), pp. 255–268.

Vitae

Name	**:**	Shahzada Pamir Aly
Nationality	**:**	Pakistani
Date of Birth	**:**	03/11/1988
Email	**:**	pamir254@hotmail.com
Permanent Address	**:**	8-D, Askari Apartments, Kakul Road, Abbottabad Pakistan
Academic Background	**:**	**M.S (Mechanical Engineering)** May, 2015 King Fahd University of Petroleum and Minerals Dhahran, Saudi Arabia **B.E (Mechatronics Engineering)** May, 2011 National University of Science and Technology Rawalpindi, Pakistan